On the Performance of Constrained Amplify-and-Forward Networks

Name :	David Edward Simmons
College :	Oriel
Supervisor :	Justin P. Coon
Department :	Engineering Science

A thesis submitted to the University of Oxford in accordance with the requirements of the degree of Doctor of Philosophy in the Department of Engineering Science.

233 pages

On the Performance of Constrained Amplify-and-Forward Networks

David Edward Simmons

August, 2016

On the Performance of Constrained Amplify-and-Forward Networks

Name: David Edward Simmons

College: Oriel

Degree: Doctor of Philosophy

Term and Year of Submission: Hilary 2016 (March 2016)

This thesis examines the effects of resource constraints on amplify-and-forward (AF) networks.

Chapters 3 and 4 are the first research chapters. Chapter 3 studies the outage probability performance of a two-hop two-way AF peak power constrained orthogonal frequency division multiplexing (OFDM) network. Its performance is then optimized. Chapter 4 focuses on the one-way special case of the system studied in Chapter 3. It begins with an analysis of the network when nonlinear distortion produced by signal clipping dominates the additive noise in the system. To conclude Chapter 4, the theoretical study performed throughout Chapters 3 and 4 is used to optimize the performance of a one-way real world test bed.

Chapter 5 studies the n-hop multiple-input multiple-output (MIMO) AF relay network. Novel techniques are developed using random dynamical system (RDS) theory and Lyapunov exponents to establish capacity and power scaling laws for the network as n grows large. One of the main conclusions is that the average transmit power must grow at an exponential rate if capacity decay across the network is to be avoided.

Chapter 6 constitutes the final research chapter. In it, the techniques used to study peak-power constrained OFDM-based networks are combined with those developed in Chapter 5, which were used to study capacity and power scaling for multihop AF networks. The conclusion of this is that incorporating OFDM into peak-power constrained multihop AF relay networks will cause the capacity along each of the network's eigenchannels to decay exponentially. Finally, we show that the effects of distortion can be circumvented by ensuring the number of antennas at each node scales at a super-linear rate with the number of hops within the network.

($<$ 300 words)

Acknowledgements

I would like to thank first and foremost my supervisor, Justin Coon, for believing in my ability as a student to carry this project through to its conclusions. I also thank him for the many many hours he has patiently devoted towards me and this project.

'Justin, thank you.'

I would like to thank David Halls for his effort designing and running a real world implementation of a particular relay network that was studied by us together during the second year of my DPhil. This was a great industry collaboration that resulted in us (Justin, David, and myself) collectively receiving a best paper award at the European Conference on Networks and Communications, 2014.

I would also like to thank Naqueeb Warsi for his help piecing my most significant publication together, and the interesting discussions that we have had relating to this and other work. On the subject of interesting discussions, I would like to thank Alex Giles, Dene Hedges, Hachem Yassine, Leo Laughlin, Nidhi Bhargav, and Shuping Dang (ordered alphabetically), for

the hours of academic discussions that we have had together.

To Steve Sheard and Dominic O'Brien, I thank you for handling my transition to the third year of my DPhil. Also, I believe I can speak on behalf of the entire communications lab at Oxford when I say thank you to Grahame Faulkner for all of the help that he offers us.

Thanks should also go to the academic staff at the University of Bristol. Without their help and support during my MSc, I would never have been exposed to the diverse field of communications. I would like to give particular credit to Joe McGeehan for supervising me during the first year of my DPhil and Mark Beach for introducing me to Justin.

Finally, to my Mum; Dad; brothers; friends; and my girlfriend, Nidhi, I thank you all for your unconditional support throughout this journey.

'Thank you.'

Acronyms

AF	Amplify-and-forward
AMPS	Advanced Mobile Phone Systems
AWGN	Additive white Gaussian noise
CDMA	Code division multiple access
CF	Compress-and-forward
CP	Cyclic prefix
CR	Conjugate-and-return
CSI	Channel state information
D2D	Device-to-device
DF	Decode-and-forward
FDMA	Frequency division multiple access
FFT	Fast Fourier Transform
FG	Fixed-gain
FM	Frequency modulation
GSM	Groupe Spécial Mobile
IMT-A	International Mobile Telecommunication-Advanced
IoT	Internet of things
IS	Interim Standard
ISI	Inter symbol interference

ITU	International Telecommunications Union
LAN	Local area network
LTE	Long term evolution
LTE-A	Long term evolution advanced
M2M	Machine-to-machine
MIMO	Multiple input multiple output
NLoS	Non-line-of-sight
NMT	Nordic Mobile Telephone
NTT	Nippon Telephone and Telegraph
OFDM	Orthogonal frequency division multiplexing
OFDMA	Orthogonal frequency division multiple access
PAPR	Peak-to-average power ratio
PDC	Pacific Digital Cellular
PNC	Physical-layer network coding
PSK	Phase shift keying
QPSK	Quadrature phase shift keying
RDS	Random dynamical system
SC	Single carrier
SEL	Soft envelope limiter
SER	Symbol error rate
SINDR	signal-to-interference noise and distortion ratio
SMS	Short message service
SNDR	signal-to-noise and distortion ratio
SNR	Signal-to-noise ratio
SSPA	Solid state power amplifier

TDD	Time division duplexing
TDMA	Time division multiple access
TWT	Traveling wave tube
UMTS	Universal Mobile Telecommunication System
USRP	Universal software radio peripheral
VG	Variable-gain
W-CDMA	Wideband code division multiple access
ZMCG	Zero-mean complex Gaussian

Notation

Matrices are always represented using uppercase boldface notation, vectors are always represented using uppercase non-boldface notation, and scalars are always represented using lowercase notation. We use $\overset{d}{=}$ to denote equality in distribution, $:=$ to denote equality by definition, logarithms are always base e unless otherwise specified, and $\log^+(x) := \max\{0, \log x\}$. We use $\angle(x)$ to denote the argument of $x \in \mathbb{C}$ and $\mathbf{0}$ is used to denote the column vector of zeros, where the dimension of $\mathbf{0}$ is implied from the context. $\mathcal{E}_i\{\mathbf{A}\}$ denotes the ith ordered eigenvalue of the matrix $\mathbf{A}$, where $\mathcal{E}_i(\mathbf{A}) \geq \mathcal{E}_j(\mathbf{A})$ implies $i \leq j$. a^* denotes the complex conjugate of $a \in \mathbb{C}$ and $\mathbf{A}^\dagger$ is used to denote the conjugate transpose of the matrix $\mathbf{A}$. Matrix products are defined in the following way $\prod_{i=j}^{n} \mathbf{A}_i := \mathbf{A}_n \cdots \mathbf{A}_j$, and when $j = 1$ we sometimes use the definition

$$\pi_n(\mathbf{A}) := \prod_{i=1}^{n} \mathbf{A}_i. \tag{1}$$

The standard 2-norm of a matrix $\mathbf{A}$ is denoted by $\|\mathbf{A}\|$, and its Frobenius norm is denoted by $\|\mathbf{A}\|_F$. The Landau notation $f(x) = o(g(x))$ is used to

imply $\lim_{x\to\infty} f(x)/g(x) = 0$. Also, we use the following notation:

$$\begin{aligned} f(n) &= O\left(g(n)\right) \Rightarrow \exists\ k_1, n' > 0 \text{ s.t. } k_1|g(n)| > |f(n)|, \forall n > n' \\ f(n) &= \Omega\left(g(n)\right) \Rightarrow \exists\ k_2, n' > 0 \text{ s.t. } k_2|g(n)| < |f(n)|, \forall n > n' \\ f(n) &= \Theta\left(g(n)\right) \text{ if } f(n) = O\left(g(n)\right) \text{ and } f(n) = \Omega\left(g(n)\right); \end{aligned}$$

and for a random variable $f(n) \geq 0$ depending on n, and $h(n) = |o(n)|$ [1]

$$\begin{aligned} f(n) &= O_{\mathbb{P}}\left(g(n)\right) \Rightarrow \lim_{n\to\infty} \mathbb{P}\left[f(n) \leq g(n)e^{h(n)}\right] = 1 \\ f(n) &= \Omega_{\mathbb{P}}\left(g(n)\right) \Rightarrow \lim_{n\to\infty} \mathbb{P}\left[f(n) \geq g(n)e^{-h(n)}\right] = 1 \\ f(n) &= \Theta_{\mathbb{P}}\left(g(n)\right) \text{ if } f(n) = O_{\mathbb{P}}\left(g(n)\right) \text{ and } f(n) = \Omega_{\mathbb{P}}\left(g(n)\right). \end{aligned}$$

Below, is a list of algebraic notation used in the thesis[1]

c	Channel capacity, (2.1)
$\mathbb{C}$	Set of complex numbers
d	Diversity gain, (2.9)
$\mathbb{E}\left[\cdot\right]$	Expectation operator
$\mathbf{F}_n$	n dimensional Fourier transform matrix
g	Relay amplification factor
h	Scalar frequency-domain channel coefficient
$\tilde{h}$	Scalar time-domain channel tap
$\mathbf{H}$	Frequency domain channel matrix
$\tilde{\mathbf{H}}$ or $\underline{\tilde{\mathbf{H}}}$	Time domain dispersive channel matrix
$\mathcal{H}_i$	ith Harmonic series, (5.51)

[1]Symbols may contain (extra) subscripts/superscripts denoting, e.g., node correspondence, antenna number, or the particular type of amplification that has been considered.

$\mathbf{i}$	$\sqrt{-1}$
$I(\cdot;\cdot)$	Mutual information, (2.2)
$\mathbf{I}_n$	n dimensional identity matrix
$\mathcal{I}_n$	Transmit information vector at nth node, (5.6)
$K_n(\cdot)$	Modified Bessel function of the second kind, [2]
l	Number of channel taps in channel impulse response
m	Number of antennas at a particular node
n_0	Noise power spectral density
$\mathbb{N}$	Set of natural numbers
$\mathcal{N}_n$	Transmit noise vector at nth node, (5.8)
p	Transmit power term
$p_{\log}$	Natural logarithm of p, (3.59)
$\underline{p}$	Normalized transmit power term, (4.5)
$p^\star$	Optimal transmit power, (3.50)
p_{max}	Maximum transmit power constraint
$P_o(\cdot)$	SNR version of outage probability function, (2.6)
$\mathbf{R}_{cp}$	Cyclic prefix removing matrix, (2.19)
$\mathbb{R}$	Real numbers
r	Gain numerator, (3.41) and (3.42)
s	Log power minus Lyapunov exponent, (6.14)
$\mathbf{T}_{cp}$	Cyclic prefix inserting matrix, (2.18)
$U(\cdot,\cdot,\cdot)$	Confluent hyper-geometric function of the second kind, (4.27)
v	Gaussian scalar noise term
V	Gaussian vector noise term
$\mathbb{V}[\cdot]$	Variance operator
w	Self interference term, (3.22)
$\underline{w}$	Self interference and distortion term, (3.32)

w_{avg}	Average normalized self-interference term, (3.43)
$\mathbb{Z}$	Set of integers
$W(\cdot)$	Lambert-W function, [2]

γ	Instantaneous SNR term
$\bar{\gamma}$	Average SNR term
γ_{th}	SNR threshold used as argument to $P_o(\cdot)$
$\gamma_{th,c}$	ϵ-critical value of γ_{th}, (4.18) and (4.19)
δ	Power delay profile exponent
ϵ	Ratio between n_0 and η, (3.21)
$\epsilon_\star$	Minimum (over all nodes) value of ϵ, (4.14)
ζ	Bussgang information attenuation factor, (2.29)
η	Bussgang average distortion power term, (2.28)
$\underline{\eta}$	Normalized Bussgang average distortion power term, (4.5)
λ	Lyapunov exponent, (5.26)
μ	Average channel gain, i.e., $\mathbb{E}[\lvert h\rvert^2]$
ν	Ratio between ith and jth eigenchannel capacity at nth node, (5.47)
ξ	Coding gain, (2.10)
ρ	Normalized (by n_0) input power to SEL, σ^2, (3.34)
ρ_{opt}	Optimal value of ρ
σ^2	Input power to SEL, (3.8) and (3.9)
$\underline{\sigma}^2$	Normalized SEL input power term, (4.5)
$\phi_{i,j}$	Difference between ith and jth Lyapunov exponent, (5.48)
$\bar{\phi}_{i,j}$	Upper bound on $\phi_{i,j}$
$\psi(\cdot)$	Digamma function, [2]

Manuscripts Since Beginning of DPhil

Below is a complete list in reverse chronological order of manuscripts that have been published, are currently under review, or are currently being prepared for submission.

Under Review	**David Simmons** and Justin P. Coon, Random Fibonacci Sequences and Capacity/Power Scaling in Cooperative Multihop Networks. In the international conference n communicaitons (ICC), 2017.
Under Review	**David Simmons** and Justin P. Coon. Scaling Power Constrained Amplify-and-Forward OFDM-Based MIMO Relay Networks. In the international conference n communicaitons (ICC), 2017.
Under Review	**David Simmons** and Justin P. Coon. Distortion Limited Amplify-and-Forward Relay Networks. In the international conference n communicaitons (ICC), 2017.
Under Review	**David Simmons**, Hachem Yassine, and Justin P. Coon. Applying Bussgang's Theorem to Fixed-gain OFDM-based Relay Networks: A Profile Decay Analysis. In the international conference n communicaitons (ICC), 2017.
Published	Nidhi Bhargav, Simon Cotton, and **David Simmons**. On the Secrecy Capacity of $\kappa - \mu$, $\kappa - \mu$

Fading Channels. In *IEEE Transactions on Wireless Communications*, 2016.

Published — Shuping Dang, Justin P. Coon, **David Simmons**. Combined Bulk/Per-Subcarrier Relay Selection in Two-Hop OFDM Systems. In *82nd Edition of VTC Spring, IEEE,* 2016.

Published — **David Simmons**, Justin P. Coon, and Naqueeb Warsi. Capacity and Power Scaling Laws for Finite Antenna Amplify-and-Forward Relay Networks. In *the International Symposium on Information Theory (ISIT), IEEE*, 2016.

Published — **David Simmons**, Justin P. Coon, and Naqueeb Warsi. Capacity and Power Scaling Laws for Finite Antenna MIMO Amplify-and-Forward Relay Networks. In *IEEE Transactions on Informations Theory*, 2016.

Published — Shuping Dang, Justin P. Coon, **David Simmons**. Comparison of multicarrier relay selection schemes in super dense networks. In *20th International Workshop on Computer Aided Modeling and Design of Communication Links and Networks, IEEE*, 2015.

Published — Justin P. Coon, **David Simmons,** and Marco Di Renzo. On the Outage Probability of Parallel Fading Channels. In *IEEE Communications Letters,* 2015.

Published	**David Simmons** and Justin P. Coon. Two-way OFDM-based Nonlinear Amplify-and-Forward Relay Systems: Power Allocation. In *24rd Edition of the European Conference on Networks and Communications, IEEE,* 2015.
Published	Shuping Dang, Justin P. Coon, **David Simmons**. Combined Bulk and Per-Tone Relay Selection in Super Dense Wireless Networks. In *International Conference on Communications, IEEE*, 2015.
Published	**David Simmons,** Nidhi Bhargav, Justin P. Coon, and Simon L. Cotton. Physical Layer Security Over OFDM-Based Links: Conjugate-and-Return. In *81st Edition of VTC Spring, IEEE,* 2015.
Published	**David Simmons** and Justin P. Coon. Two-way OFDM based Nonlinear Amplify-and-Forward Relay Systems. In *IEEE Transactions on Vehicular Technology,* 2015.
Published and recipient of best paper award	**David Simmons,** David Hall, and Justin P. Coon. OFDM-based Nonlinear Fixed-Gain Amplify and Forward Relay Systems: SER Optimization and Experimental Testing. In *23rd Edition of the European Conference on Networks and Communications,* 2014.
Published	**David Simmons,** Justin Coon, and Joe McGeehan. Analyzing the Scalability of Linear Amplify-and-Forward Relay Networks. In *14th Annual Post*

Graduate Symposium on the Convergence of Telecommunications, Networking and Broadcasting, 2013.

Contents

Abstract i

Acknowledgements iii

Acronyms v

Notation ix

Manuscripts Since Beginning of DPhil xvi

1 Introduction **1**

1.1 Key Research Contributions of this Thesis 3

1.2 Thesis Overview and Related Manuscripts 5

2 An Introduction to Wireless Communications **9**

2.1 A Brief Introduction to Modern Wireless Communication Systems 10

2.1.1 First, Second and Third Generation Cellular Networks 10

2.1.2 Fourth and Fifth Generation Cellular Networks . . . 12

2.1.3 Non-Cellular Network Architectures 16

2.2 Modern Communication Techniques: Spatial multiplexing, OFDM, and Relaying 17

2.2.1 Fundamentals 17

2.2.2 Multiple Antennas and Spatial Multiplexing 23

2.2.3 OFDM 25
2.2.4 Peak-power Constrained OFDM-based Systems . . . 29
2.2.5 Relaying 35
2.3 Summary 43

3 Two-way Networks: Outage Probability Analysis and Optimization 45

3.1 Introduction 46
3.2 System Model 48
3.2.1 First Time Slot 50
3.2.2 Relay Amplification Model 53
3.2.3 Second Time Slot 57
3.3 Outage Probability for Two-way Network with Imperfect Interference Removal 58
3.3.1 Fixed-gain Outage Probability 59
3.3.2 Variable-gain Outage Probability 60
3.3.3 A Brief Discussion of Fixed-gain and Variable-gain Results 62
3.3.4 Extending Results to Distortion at the Sources 65
3.4 Gain Optimization and Interference Removal Assessment . . 66
3.4.1 Gain Optimization 66
3.4.2 Interference Removal Assessment 69
3.5 Power Allocation Strategies with Perfect Self-interference Removal 72
3.5.1 Power Allocation when Relay is not Considered in Power Budget 73

3.5.2 Power Allocation when Relay is Considered in Power Budget . . . 77
3.5.3 Discussion and Further Results . . . 82
3.6 Summary . . . 83

4 One-way Networks: Distortion Limitation, Symbol Error Rate and Experimental Testing 85
4.1 Introduction . . . 86
4.2 Distortion Limited Networks . . . 87
4.2.1 Distortion Limited Performance . . . 88
4.2.2 The ϵ-critical Phase Transition . . . 91
4.2.3 A Discussion of the ϵ-critical Phase Transition . . . 97
4.3 Fixed-gain Performance Analysis and Gain Optimization . . . 98
4.3.1 Symbol Error Rate Calculation . . . 98
4.3.2 Optimal Relay Gain . . . 99
4.4 Physical Universal Software Radio Peripheral Relay Testbed and Results . . . 101
4.4.1 Implementation . . . 102
4.4.2 Testbed Results . . . 105
4.5 Summary . . . 106

5 Multihop MIMO Networks: Capacity and Power Scaling Laws 109
5.1 Introduction . . . 110
5.2 System Model . . . 115
5.3 Key Results . . . 119
5.4 Random Dynamical Systems . . . 122

5.4.1 Preliminary Random Dynamical Systems Results . . 122
5.4.2 On the Lyapunov Exponents of Affine Random Dynamical Systems 126
5.5 Capacity and Power Scaling 128
5.5.1 A Brief Discussion of Theorem 2 and Lemma 6 . . . 130
5.6 Applications of Theorem 2 and Lemma 6 133
5.6.1 Preliminary Definitions and Lemmas 134
5.6.2 Growth of $\nu_{i,j,n}^{(\alpha)}$ and $\|X_n\|^2$ 135
5.7 Numerical Illustration 141
5.8 Summary 144

6 Multihop OFDM-based MIMO Networks: Peak-power Constraints 149

6.1 Introduction 150
6.2 System Model 152
6.2.1 Power Constraints 155
6.3 Scaling OFDM-based Amplify-and-forward Relay Networks . 157
6.3.1 Combating Issues of Distortion in OFDM-based Networks 159
6.4 Numerical Results and Discussion 161
6.5 Summary 163

7 Conclusions and Future Work 167

A Chapter 3 Proofs 171

A.1 Outage Probability for FG System 171
A.2 Outage Probability for VG System 173

B Chapter 5 Proofs **175**

B.1 Proof of Theorem 1 175

B.2 Proof of Lemma 5 178

B.3 Proof of Theorem 2 180

B.3.1 First Statement 180

B.3.2 Second Statement 185

B.4 Proof of Lemma 6 186

B.4.1 First Statement 186

B.4.2 Second Statement 186

B.5 Proof of Lemma 7 187

B.6 Lemma 11 and Proof 188

Bibliography **189**

Chapter 1

Introduction

> *'The fundamental problem of communication is that of reproducing at one point either exactly or approximately a message selected at another point.'*
>
> Claude E. Shannon, A Mathematical Theory of Communication, [3].

The mathematical framework used to study communication is called *information theory*, and was introduced by Claude E. Shannon in his groundbreaking seminal paper, A Mathematical Theory of Communication, [3]. This theory has been of utmost importance to the development of modern communication systems. Crucially, it has allowed scientists and engineers to establish the fundamental limits of performance (data transmission and data compression) that can be achieved in such systems. These limits are invariably governed by the resources offered to the system, e.g., in a wireless system the transmitter may have a peak transmit power that it must operate below or a limited number of antennas to transmit with. Naturally, the performance of a system will improve as it is offered more resources.

This thesis examines the effects of limited resources (peak and average power constraints, and a restricted number of antennas) on the theoretical performance of a certain class of wireless network: the amplify-and-forward (AF) relay network. As they become large, AF networks are notorious for their high level of mathematical complexity. Owing to this notoriety, our examination begins with the study of a bare-bones example of such a network: the two-hop (three node) AF network, where each node is restricted to using a single antenna and limited by a peak transmit power constraint. This initial study is performed through the lens of elementary information theory and makes use of a result originally developed in 1952, Bussgang's theorem [4], which can be used to describe the nonlinear distortion that occurs in peak-power constrained systems. Following this, we move to study a more advanced network topology: the multihop AF network, where each node possesses an arbitrary finite number of antennas and is limited by an average or peak transmit power constraint. The classical tools offered by elementary information theory prove insufficient when studying such networks, and recent attempts to analyze related systems have invariably leveraged results from Random Matrix theory [5]. While Random Matrix theory represents a well developed branch of mathematics, the tools that it offers are limited in their ability to study wireless networks with a strictly finite number of antennas, particularly when this number is small. Owing to these limitations, our advanced study involves developing a novel technique that provides a bridge from information theory to a seemingly disconnected branch of mathematics, Random Dynamical Systems (RDS) theory [6]. It is this bridging that represents one of the main contributions of this thesis.

1.1 Key Research Contributions of this Thesis

In the following, we outline the key research contributions of this thesis:

1. We develop a novel technique, based on RDSs and Lyapunov exponents (key observables studied in RDS theory), that is used to study multihop AF networks when each node possesses a finite number of antennas. Our technique contrasts with those previously used to study similar multihop networks, where it was always assumed that the number of antennas at each node grew without bound. Crucially, our approach provides a much richer level of detail about how the capacity of such networks behaves on each of the network's eigenchannels.

2. We determine novel expressions that describe system performance for two types of AF network topology:

   (a) For two-hop *two-way* single antenna fixed-gain (FG) and variable-gain (VG) networks, we establish outage probability results when each of the nodes is subject to a peak-power constraint. For the *one-way* special case, we establish diversity results for both FG and VG networks, and symbol error rate (SER) results for FG networks. With our analysis, we determine

      i. how transmit power should be allocated among the nodes of the two-way network,

      ii. how the relay's amplifier should be set (we successfully test this in hardware for the one-way FG network),

      iii. that different amplification strategies ((FG) or (VG)) may provide vastly different system performance: relay peak-

power constraints will induce a diversity order of zero for FG; for VG, it will be one. Analogous results *do not* occur if peak-power constraints are removed.

(b) For multihop multi-antenna networks with a fixed number of antennas at each node, we establish capacity and power scaling laws. With these, we discover that

i. when increasing the number of hops in single-carrier (SC) AF networks, if the peak transmit power is not permitted to grow exponentially with the number of hops, *all but the first* eigenchannel capacity will decay exponentially to zero;

ii. when increasing the number of hops in orthogonal frequency division multiplexing (OFDM) AF networks, if the peak transmit power is not permitted to grow exponentially with the number of hops, *all* the eigenchannel capacities will decay exponentially to zero;

iii. for both SC and OFDM based systems, we can circumvent the capacity decay by allowing the number of antennas at each node to grow at least linearly with the number of hops in the network.

In the next section, we will give a detailed overview to the thesis structure, its contents, and the author's publications that relate to the thesis.

1.2 Thesis Overview and Related Manuscripts

In **Chapter 2**, we briefly summarize the history of contemporary wireless communications systems. We then provide pertinent details of modern communications fundementals *(capacity, outage probability, and diversity)* and techniques *(spatial multiplexing across eigenchannels and MIMO, OFDM, one-way and two-way relay networks, and different relay forwarding strategies)*, which will be called upon throughout the remainder of the thesis. In this chapter, we will also build upon the basic OFDM ideas that we present. In more detail, we will discuss a fundamental problem - nonlinear amplifier distortion - that will arise when peak-power constraints are imposed on OFDM-based systems. We then proceed to present previously developed theory ([7], the extension of Bussgang's theorem to memoryless nonlinear amplifiers with complex Gaussian inputs) that can be used to characterize how this problem affects the performance of such systems.

Chapter 3 is the first of four research chapters. In it, we begin by determining novel expressions for the outage probability of the two-way OFDM-based peak-power constrained relay network. We then proceed to determine criteria that will allow (approximate) optimal network performance to be achieved. We focus on two criteria for our optimization: optimization of the relay's power amplifier and optimization of power allocation among the nodes of the network when subject to a total network average power constraint.

This chapter is joint work with Justin Coon. The research has been published in one journal, Transactions on Vehicular Technology, IEEE, 2015, [8], and in the 24th Edition of the European Conference on Networks and Commu-

nications, 2015, [9].

In **Chapter 4**, we consider a special case of the system studied in Chapter 3. In particular, we consider the network when it becomes one-way. We begin by considering the scenario in which the nonlinear distortion power dominates the noise power. With this specialization, we identify a peculiar effect of nonlinear distortion in the system. In more detail, the log-log decay of the outage probability with the source/relay transmit power is shown to be (asymptotically) 0 for FG and 1 for VG if distortion occurs at the relay; if distortion occurs only at the source, this decay will be 1 for both schemes. Finally, by utilizing the outage probability results derived in the previous chapter, we calculate the SER performance of the one-way system. With this calculation, we are able to optimize the SER of the network by appropriately selecting the amplification factor at the relay so that the derivative of the SER expression is zero. We then proceed to demonstrate the system performance improvement that is achieved when this theoretically derived optimal gain is applied on a real world test-bed.
This chapter is joint work with Justin Coon and David Halls. The research has been published in the 23th Edition of the European Conference on Networks and Communications, 2014, [10], and has been submitted for possible publication in the journal Transactions on Vehicular Technology, IEEE, 2016, [11].

In **Chapter 5**, we focus our effort on a new AF relay network topology: the multihop m antenna MIMO AF relay network. For this, we establish capacity and power scaling laws for the network as the number of hops grows large. This is done by studying the network as a RDS and calculating its Lyapunov exponents. We show that 1) the exponential decay rate of the

capacity along each of the eigenchannels of the network can be determined using the network's Lyapunov exponents and 2) the exponential growth rate of the transmit power across the network can be determined using the network's largest Lyapunov exponent. With these results, one of our main conclusions is that the average transmit power across the network must necessarily grow at an exponential rate if we are to avoid exponential capacity decay on the network's dominant eigenchannel. Among other things, we are also able to assign a transmit power cost to each extra eigenchannel that is multiplexed across the network.

This chapter is joint work with Justin Coon and Naqueeb Warsi. The research has been published in the journal Transactions on Information Theory, IEEE, 2016, [12], and has been published in the Proceedings of the International Symposium on Information Theory, IEEE, 2016.

Chapter 6 constitutes our final research chapter. In it, we combine the techniques used to study peak-power constrained OFDM-based networks with those that were developed to study the capacity and power scaling properties of multihop AF networks in Chapter 5. With this combination, we conclude that incorporating OFDM into a peak-power constrained multihop AF relay network will necessarily degrade the capacity along each of the network's eigenchannels as the network grows large.

This chapter is joint work with Justin Coon. The research has been submitted for possible publication in Wireless Communications Letters, IEEE, 2016.

The Thesis finishes with **Chapter 7**, which provides a conclusion and some potential options for future work.

Chapter 2

An Introduction to Wireless Communications

In this chapter, we will discuss the development of modern wireless communication systems, giving focus to salient modern day performance metrics (channel capacity, outage probability, and diversity) and techniques (spatial multiplexing, OFDM, and relaying) from an information-theoretic viewpoint. We will also provide pertinent details regarding a result that Chapters 3 and 4 will rely heavily on [7] (the extension of Bussgang's theorem to memoryless nonlinear devices with complex Gaussian inputs). This result provides a framework for studying the theoretical characteristics of nonlinear distortion in peak-power constrained OFDM-based systems and will be given immediately after the discussion of OFDM-based systems.

2.1 A Brief Introduction to Modern Wireless Communication Systems

The idea that wireless communications could be offered to an entire population was conceived in the 1960s and 1970s at Bell Laboratories, when the concept of cellular networks was introduced, [13–16]. The evolution of modern cellular networks has been remarkable in the last three decades. From a user perspective, this has been observed most predominately through the successive mobile cellular generations that have been rolled out (approximately) each decade. We will discuss this development in the next two subsections. Following this, we will discuss other pertinent (non-cellular) network architectures.

2.1.1 First, Second and Third Generation Cellular Networks

Much of the research that would subsequently be used in the first generation (1G) cellular network was performed in the 1960s and 1970s. For a highlight of state of the art work at that time, see [17]. It was not until 1979 that Nippon Telephone and Telegraph (NTT) would establish the first commercial cellphone system in Tokyo. However, it was Erricson AB that were the first to build a cellular network with a large coverage area, establishing the Nordic Mobile Telephone (NMT) system in 1981 [18]. Other countries would later follow suit in the development of their own cellular systems. Developed by Bell Labs, the USA system was called Advanced Mobile Phone Systems (AMPS) and was introduced in 1983, [16]. These

1G networks were voice-only analog networks, relying exclusively on frequency division multiple access (FDMA) and analog frequency-modulation (FM), which prevented the use of modern encryption and channel coding techniques. Consequently, eavesdropping and poor service quality were common problems for them, [16].

As with 1G, it was the Europeans who led the way for second generation (2G) technology, developing the European Telecommunications Standards Institute, which was eventually adopted in most parts of the world, and came to be known as Groupe Spécial Mobile (GSM). Deployment of GSM began in the early 1990s, [19]. The main differentiation between 1G and 2G networks is that 2G can support digital modulation [16], and employs time-division or code-division multiple access techniques (TDMA or CDMA, respectively). There were four main competing 2G standards to be deployed, three operated using TDMA (GSM, Interim Standard (IS) 136, and Pacific Digital Cellular (PDC)), while the fourth operated using CDMA (Interim Standard 95 (IS-95)). More information on these standards can be found in [16, 20]. Because of its digital modulation, the 2G network was able to support encryption of voice calls, channel coding for improved error resilience, and the transmission of more abstract forms of data (e.g., Short Messaging Service (SMS)). Most crucially, the 2G network was able to provide at least a factor of three improvement in the spectral efficiency (bits/s/Hz) of the network [16], which was necessary for the rapidly growing consumer base that was to ensue.

Although the 2G network provided an increase in network capacity compared to the 1G network, it was still limited to a per user data rate of approximately 10 Kbits/s. Such data rates could only offer limited support

for modern Internet applications (e.g., email, Internet browsing). To resolve the issues of limited data rates, new standards[1] were developed that could be overlaid on top of the 2G network. These new standards came to be known as 2.5G, allowing for an increased user throughput of approximately 56Kbits/s that could support, among other things, email and web browsing, [16].

Then, not too long ago (1998, [21]), the third generation (3G) of cellular networks was released. The specifications for 3G are called the International Mobile Telecommunications-2000, and were defined by the International Telecommunications Union (ITU), [21]. The focus of this generation was to allow users to access data intensive services such as video streaming, and multi-megabit Internet. These high data rates (up to 2Mbits/s) were achieved by operating over much wider bandwidths[2] than was previously performed by using the wideband CDMA (W-CDMA) system, which came to be known as the Universal Mobile Telecommunication System (UMTS).

2.1.2 Fourth and Fifth Generation Cellular Networks

We are currently in the midst of a fourth generation (4G) network roll out, which began with the release of two candidate systems: WiMAX (2007) and the Long Term Evolution (LTE) standard (2009), [22]. As defined by the ITU in the International Mobile Telecommunication-Advanced (IMT-A) standard, the 4G network should be able to support peak data rates of 1Gbit/s, and allow users to access gaming services, high-definition mobile

[1] The four most commonly deployed standards were IS-95B, High Speed Circuit Switched Data (HSCSD), General packet Radio Service (GPRS), and Enhanced Data Rates for GSM Evolution (EDGE). More details of these can be found in [16].

[2] 3G networks allocated 5MHz of bandwidth to each user, while 2.5G allocated only 200KHz.

TV, 3D television, and cloud computing services [23]. There has been significant debate in the community as to whether LTE and WiMAX should themselves be considered 4G systems, owing to the fact that they do not quite meet the capacity requirements as defined by ITU. However, because of marketing pressure, it was eventually accepted (2012) that LTE and WiMAX can be referred to as 4G technologies [24], but it was not until the release of LTE-Advanced (LTE-A) and WiMAX-Advanced, that the requirements (as originally defined by ITU) would be formally met. LTE-A and WiMAX-Advanced are now known as *true* 4G, [25].

For 4G, the spread spectrum based CDMA technology was abandoned in favor of orthogonal frequency division multiple-access[3] (OFDMA) techniques for the downlink and single-carrier frequency division multiple access (SC-FDMA) for the uplink. The main driving factor for this choice was that OFDM was better suited to the advanced multiple antenna techniques that would also come to fruition in 4G. From this perspective, LTE-A and LTE are effectively the same technologies; however, LTE-A allows for the aggregation of a greater number of carriers to achieve wider bandwidths, as well as the ability to employ MIMO techniques[4], [26]. Another state-of-the-art feature that has been migrated into LTE-A is cooperative communications in the form of relaying[5] [27]. Cooperative communications will offer benefits to wireless networks. As an example, single antenna users will be able to cooperate with each other (acting as relays for one another), allowing

[3]OFDM will be discussed in detail in section.

[4]MIMO systems are able to perform spatial multiplexing, which provides significant capacity improvements. This will be discussed in more detail in section 2.2.2. MIMO systems also offer diversity gains. Diversity will be discussed in section 2.2.1.3, while the diversity gains offered by MIMO will be discussed in more detail in section 2.2.5.2.

[5]Relaying will be discussed in more detail in section 2.2.5.

them to obtain similar gains as those offered by MIMO systems. They are also effective at providing improved cell edge performance and reducing infrastructure deployment costs, [28].

There has been a lot of discussion in the research community as to what the fifth generation (5G) of wireless networks will encompass, but up until now there is no industry-wide consensus on what this will be [29]. The move to 5G is envisaged to occur at the turn of the next decade (2020), and it is thought that, along with improved data rates[6] and higher energy efficiency, 5G will amalgamate many different technologies to support future network requirements. The following is a list of some of the technologies that 5G will likely support [29]:

1. small (femto/pico) cells,
2. massive MIMO,
3. millimeter wave,
4. device-to-device (D2D) communications,
5. machine-to-machine (M2M) ('The Internet of Things (IoT)').

Small cell sizes allow spectrum to be re-allocated more frequently, which improves spectral efficiency. Massive MIMO will introduce large arrays of antenna elements to increase diversity[7], provide large spatial multiplexing gains[8], and improve beamforming resolution. Millimeter wave will tackle problems of spectrum scarcity, and is also attractive for use in massive

[6] Qualcomm and Nokia Siemens Networks have been looking at technologies capable of coping with 1000 times more traffic than 4G, [29, 30].

[7] Diversity will be discussed in more detail in section 2.2.1.3.

[8] Capacity gains from massive MIMO may be several orders greater than what is currently achieved, [29].

MIMO systems. This is because millimeter wave antennas are smaller and can be packed much more closely together. For D2D communications, it is thought that each terminal within a cell will be able to communicate directly with other terminals within that cell, allowing them to share spectrum and exchange information with each other. They may also act as relays for one another. Note, this is not to be confused with communication in unlicensed spectrum as per Bluetooth or Wireless local area networks (LAN). Instead, this will be communication between devices within the licensed spectrum. Finally, and most significantly, IoT is often purported to be the coming of a new era in human history, [31–35], one in which all 'things'[9] will be uniquely identifiable[10]; have access to electronics, software, sensors, and wireless connectivity; and whose role will be to perform tasks for the good of human kind. The following gives a few examples for IoT applications:

1. Environmental monitoring: sensors may be deployed to monitor atmospheric conditions, water quality, wildlife habitats, tsunami warning signs, etc.

2. Energy management: smart grids will correctly deploy power to where it is needed based on feedback from 'things' within the environment.

3. Health care systems: sensors may detect anomalies in blood measurements in real time to aid better health plans.

4. Home automation: lighting, heating, ventilation, and other aspects of comfort may be controlled by "things".

[9]'Things' may include any device or object (e.g., chairs, doors, street lights, or biochips within pets, etc.).
[10]Things will be identified through an IP-like address.

5. Transportation: 'things' may be deployed to control traffic more intelligently/efficiently.

The list could go on, and crucially, there may exist brilliant future applications that have not yet been conceived. One thing that is certain, the wireless network research that is being performed today will play a significant role in the development of future technologies.

2.1.3 Non-Cellular Network Architectures

In the previous two subsections, we outlined the development of modern cellular networks. It was mentioned that 5G cellular systems will likely support D2D and M2M communications. Although cellular infrastructure *may* support these technologies, it is believed non-cellular networks will be their biggest enablers, [36]. This is because not every device is required to be cellular-connected over expensive licensed spectrum. Instead, they will connect over unlicensed spectrum forming personal area/LAN, using open standards such as WiFi, Bluetooth and ZigBee, [36]. These networks may also aggregate over a common Internet protocol (IP) based node that provides an egress point to the wider world.

An interesting class of non-cellular based networks are wireless ad hoc/mesh networks, [37]. These are decentralized networks that do not rely on pre-existing infrastructure. Instead, nodes cooperate with each other, forming a network in which packets of information are dynamically routed/relayed from source to destination, potentially traversing multiple hops. According to [38] the number of nodes deployed in such a network may be in the order of hundreds, thousands or even millions, depending on the application.

Nodes within these networks may be static or mobile, and are allowed to enter and exit the network as they wish. Naturally then, understanding the theoretical characteristics of relay networks will be vital if wireless ad hoc/mesh networks are to proliferate.

2.2 Modern Communication Techniques: Spatial multiplexing, OFDM, and Relaying

In the previous section, we gave a brief introduction to the development - as well as the future - of wireless communications. We briefly hinted at certain modern techniques that have been developed and will be deployed in current and next generation systems. Most important to the work contained within this thesis are 1) spatial multiplexing, 2) OFDM, and 3) relaying. In this subsection, we will provide a detailed information theoretic overview of these techniques, but first we will introduce some fundamental ideas: channel capacity, outage probability, and diversity.

2.2.1 Fundamentals

2.2.1.1 Channel Capacity

In this thesis, we define a channel to be a system that consists of an input alphabet $\mathcal{X}$, an output alphabet $\mathcal{Y}$, and a probability transition function $f(\beta|\alpha)$ that describes the probability of observing channel output $\beta \in \mathcal{Y}$ given channel input $\alpha \in \mathcal{X}$. Fig. 2.1 shows an example of such a channel. The input in this figure is a *random variable* x which is drawn from $\mathcal{X}$ according to the probability mass function $f_x(\alpha)$. The output is the random

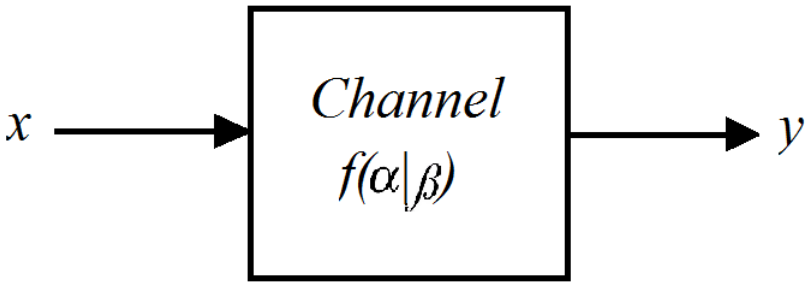

Figure 2.1: Block diagram of OFDM system.

variable y, which has a conditional probability mass function $f(\beta|\alpha)$.

The end-to-end capacity, c bits/channel use, of a channel is defined to be the mutual information (to be described in (2.2)) between the source and destination, maximized over all input signal distributions [39, Eq. (7.1)]; i.e., with channel input x and channel output y

$$c := \max_{f_x(\alpha)} I(x;y), \tag{2.1}$$

where $I(x,y)$ denotes the mutual information (discussed next) between x and y, [39, Eq. (2.30)]. For two random variables a and b with joint probability mass function $f_{a,b}(\alpha,\beta)$, marginal probability mass functions $f_a(\alpha)$ and $f_b(\beta)$, and supports $\mathcal{A}$ and $\mathcal{B}$, the mutual information is given by

$$I(a;b) := \sum_{\alpha\in\mathcal{A}}\sum_{\beta\in\mathcal{B}} f_{a,b}(\alpha,\beta)\log\frac{f_{a,b}(\alpha,\beta)}{f_a(\alpha)f_b(\beta)}. \tag{2.2}$$

The cornerstone of modern information theory, *the channel coding theorem* [39, Theorem 7.7.1], provides an operational meaning for c. Specifically, it tells us that c is the maximum rate at which information can be transmitted over the channel whilst being able to attain an arbitrarily small prob-

ability of error. This is achieved by employing powerful capacity achieving error correction codes, [40].

As an example of channel capacity, consider the Gaussian channel with input x and output y:

$$y = x + v, \tag{2.3}$$

where $\mathbb{E}[|x|^2] = p$ is the average transmit power, and v is a zero-mean complex Gaussian (ZMCG) noise term with total variance n_0. It is well known that the complex Gaussian distribution maximizes the mutual information [39], and the end-to-end (bandwidth normalized) capacity of the channel is given by the capacity formula [39]

$$c = \log_2\left(1 + \frac{p}{n_0}\right). \tag{2.4}$$

Fig. 2.2 shows a plot of (2.4) as a function of p/n_0. From this figure, the channel coding theorem [39, Theorem 7.7.1] tells us that we can split the plot up into two regions: rates than can be achieved with arbitrarily small error probabilities (using capacity achieving error correction codes) and rates that cannot be achieved with arbitrarily small error probabilities.

2.2.1.2 Outage Probability

For a slow fading environment[11] where there is a non-zero probability that the channel will drop into a deep fade, it is not possible to drive the probability of error to zero. This is because the deep fade will cause the SNR of

[11]Slow fading refers to the scenario in which the channel's coherence time is greater than the period of a code word.

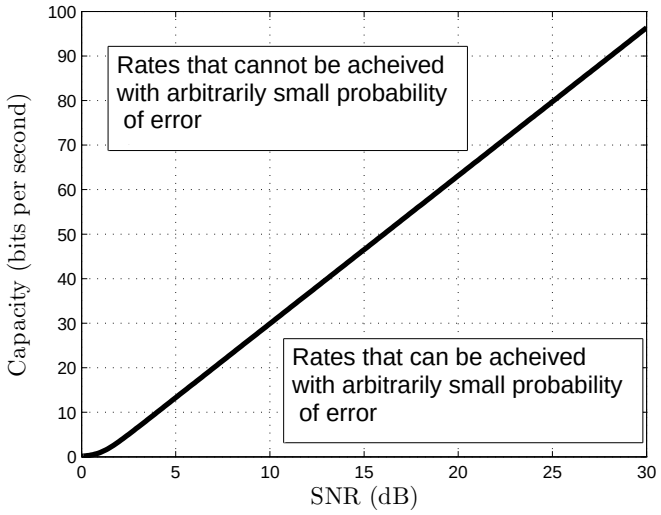

Figure 2.2: Capacity as a function of SNR (p/n_0) for a Gaussian channel, (2.4). Plot is generated by fixing $n_0 = 1$ and varying p.

the link to drop dramatically. In the strict sense then, the capacity of a slow fading channel is 0, and we must take into account the probability that the channel has dropped into a deep fade and is unable to support the desired rate, c_{th}, of the link. This probability is called the outage probability, and is defined to be [41]

$$P_{o,c}\left(c_{th}\right) := \mathbb{P}\left[c \leq c_{th}\right]. \tag{2.5}$$

In the context of slow fading channels - instead of capacity - one may refer to the ϵ-outage capacity, c_ϵ. This is the largest rate that can be transmitted at whilst achieving an outage probability of less than ϵ, [42].

As capacity is a monotonically increasing function of signal-to-noise ratio (SNR), (2.5) is often modified to

$$P_o\left(\gamma_{th}\right) := \mathbb{P}\left[\gamma \leq \gamma_{th}\right], \tag{2.6}$$

for scalar channels, where γ is the end-to-end instantaneous SNR and γ_{th} is an instantaneous SNR threshold. For a Gaussian channel [39], the relationship between c and γ, and c_{th} and γ_{th} is given by $c = \log_2(1+\gamma)$ and $c_{th} = \log_2(1+\gamma_{th})$, which implies that

$$P_o(\gamma_{th}) = P_{o,c}(\log(1+\gamma_{th})). \tag{2.7}$$

Fig. 2.3 shows a plot of the outage probability for a basic single antenna Rayleigh fading source-destination link, given by

$$P_o(1) = \mathbb{P}\left[\frac{p|h|^2}{n_0} \leq 1\right], \tag{2.8}$$

where $|h|$ is a Rayleigh distributed channel coefficient and the target rate is given by $c_{th} = \log_2(2) = 1$. As one might naturally expect, the probability of outage decays as the SNR grows.

2.2.1.3 Diversity

Once outage probability has been defined, we can consider another performance metric: diversity order. The diversity order of a network is defined to be

$$d := -\lim_{\mathbb{E}[\gamma]\to\infty} \frac{\log P_o(\gamma_{th})}{\log \mathbb{E}[\gamma]}, \tag{2.9}$$

where γ denotes the instantaneous SNR of the link. In words, the diversity order gives the limiting log-log decay rate of the outage probability with respect to the average SNR. Provided the outage probability function is analytic in the average SNR (i.e., can be expressed as a formal power series

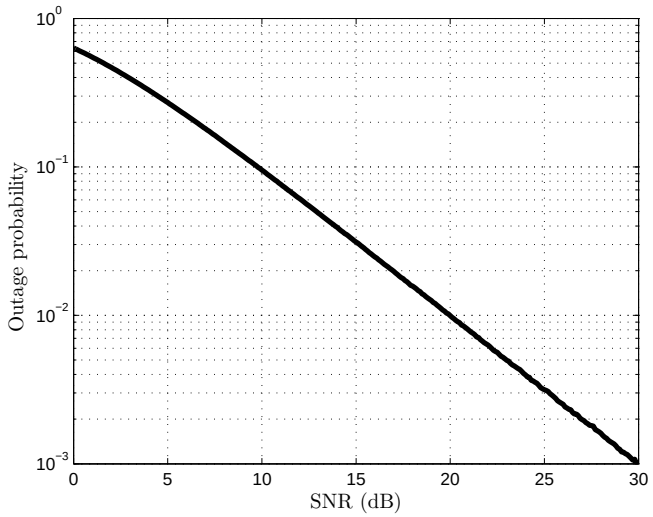

Figure 2.3: Figure showing the Monte Carlo generated (5000000 trials) simulation of outage probability for a basic single antenna Rayleigh fading link as a function of average SNR ($\mathbb{E}\left[|h|^2\right] p/n_0$), (2.8). The desired rate of the link is given by $c_{th} = \log_2(2)$.

of the average SNR), this is known to imply

$$P_o\left(\gamma_{th}\right) \sim \left(\xi \mathbb{E}\left[\gamma\right]\right)^{-d}. \tag{2.10}$$

The pre-factor ξ of (2.10) is usually called the coding gain and, on a log-log scale, describes the vertical shift associated with the outage probability curve.

Diversity is a very powerful observable, as it gives us an intuitive/simplistic understanding of how a system's performance changes at high SNR. As an example, the diversity order of a single antenna Rayleigh fading link is known to be 1 [42]. This result can be observed heuristically in Fig. 2.3, which shows the outage probability of a Rayleigh fading link. By inspecting this figure at high SNR, we can see that the (log-log) gradient is approximately -1, which suggests that the diversity order of the system is 1,

agreeing with the theory.

2.2.2 Multiple Antennas and Spatial Multiplexing

One solution to improve a network's capacity is to increase the number of antennas at the source and receiver. In particular, if the source is deployed with m_S antennas and subject to a total average power constraint p, the destination is deployed with m_D antennas (see Fig. 2.4), and each destination antenna receives complex Gaussian noise with total variance n_0, the channel capacity will be given by [42, 43]

$$c = \sum_{i=1}^{\min\{m_S, m_D\}} \log\left(1 + \frac{p_i^\star \omega_i^2}{n_0}\right), \tag{2.11}$$

where $\{p_i^\star\}$ is the power allocation set that maximizes (2.11) subject to the total power constraint $p = \sum_i p_i^\star$, and ω_i is the ith ordered singular value of the $m_S \times m_D$ channel matrix $\mathbf{H}$ between the source and destination. Using the Lagrangian method [44], it can be shown that

$$p_i^\star = \max\left\{\left(\mu - \frac{n_0}{\omega_i^2}\right), 0\right\}, \tag{2.12}$$

where μ is chosen to satisfy the total power constraint p. This is known as water-filling.

To provide intuition to (2.11), observe the MIMO signaling model:

$$Y = \mathbf{H}X + V, \tag{2.13}$$

which mathematically describes the system depicted in Fig. 2.4, where

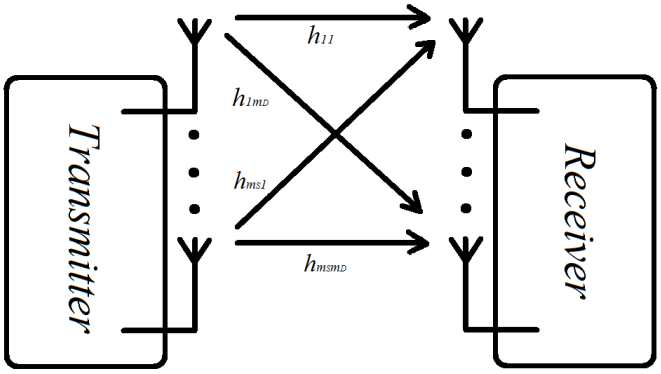

Figure 2.4: Illustration of MIMO system, where transmitter has m_S transmit antennas and receiver has m_D receive antennas. The links between the i,jth antenna pair are described by the channel coefficient h_{ij}. The channel between the transmitter and receiver can then be described by the channel matrix $\mathbf{H} \in \mathbb{C}^{m_S \times m_D}$, where h_{ij} is the i,jth element of $\mathbf{H}$.

$X \in \mathbb{C}^{m_S}$ is the transmit signal vector; $Y \in \mathbb{C}^{m_D}$ is the received signal vector; $\mathbf{H}$ is the channel matrix; and $V \in \mathbb{C}^{m_D}$ is the received noise vector at the destination, the elements of which are complex Gaussian with total variance n_0. Note that $\mathbf{H}$ can be decomposed into $\mathbf{H} = \mathbf{U}\mathbf{\Lambda}\mathbf{V}^\dagger$, where $\mathbf{U}$ and $\mathbf{V}$ are unitary matrices, and $\mathbf{\Lambda}$ is a diagonal matrix whose diagonal entries are the singular values of $\mathbf{H}$. This decomposition is known as the singular value decomposition (SVD), [45]. By pre and post coding[12] by $\mathbf{V}$ and $\mathbf{U}^\dagger$, respectively, the signaling model becomes

$$\underline{Y} = \mathbf{\Lambda} X + \underline{V}, \tag{2.14}$$

where $\underline{Y} = \mathbf{U}^\dagger Y$ and $\underline{V} = \mathbf{U}^\dagger V$. From (2.14), the channel has been diagonalized into $\min\{m_S, m_D\}$ parallel subchannels[13], one for each non-zero singular value. More specifically, letting x_i, $\underline{y}_i$ and $\underline{v}_i$ be the ith elements of

[12]This would require full channel state information (CSI) at the source and destination.

[13]Note, the subchannels are often referred to as eigenchannels, and the transmission of separate data streams over these is referred to as spatial multiplexing.

X, $\underline{Y}$ and $\underline{V}$, respectively, and assuming that $\mathbb{E}|x_i|^2 = p_i^\star$, we can write the signaling model for the ith eigenchannel as

$$\underline{y}_i = \omega_i x_i + \underline{v}_i, \tag{2.15}$$

and because $\mathbf{U}$ and $\mathbf{V}$ are unitary, pre and post coding does not affect the total average transmit power or noise statistic. Consequently, the network's capacity is given by the sum of the capacities on each eigenchannel, which, from (2.4), gives us (2.11). Thus, provided the channel matrix is well conditioned the capacity will *almost surely* scale linearly with $\min\{m_S, m_D\}$ [43] - the number of non-zero singular values of $\mathbf{H}$ - and employing more source and destination antennas can dramatically improve the performance of a wireless link. This is in stark contrast to SISO systems, for which linear capacity gains require exponential SNR growth when SNR is large (see (2.4)).

2.2.3 OFDM

Another solution to increase the network's capacity is to allow users to operate over larger bandwidths[14]. This is because larger bandwidths allow the source to transmit a signal that has been sampled at a higher rate[15], and consequently transmit at a larger symbol rate. However, in wireless channels, if the symbol period becomes too short with respect to the delay spread, inter-symbol interference (ISI) will occur. If not properly countered, ISI can be extremely detrimental to system performance. ISI is canonically

[14]It is important to note that, for a fixed average transmit power, the capacity cannot be increased arbitrarily by appropriately selecting the bandwidth. This is because system noise scales linearly with bandwidth.

[15]The Nyquist sampling theorem tells us that to perfectly reconstruct a sampled signal, we must sample at no less than twice the highest frequency contained within the signal.

a time domain observation. The frequency domain dual of ISI is that the bandwidth of operation is *wider* than the coherence bandwidth of the channel so that it appears frequency selective. In this scenario, the channel is referred to as *wideband*. Interestingly, if ISI is properly dealt with, frequency selectivity can improve the diversity order of the channel.

An incredibly efficient method for countering ISI in wideband wireless channels is to employ OFDM [46], which we will now describe in detail. Consider a wireless channel with end-to-end[16] impulse response $\tilde{h}(t)$. Furthermore, assume that the memory of the impulse response is l times the sample period. Suppose the source packages time-domain samples into blocks of n' before transmission. At baseband, the ith transmit OFDM symbol can then be written as $\tilde{X}(i) = [\tilde{x}_1(i) \ \cdots \ \tilde{x}_{n'}(i)]^T \in \mathbb{C}^{n'}$, so that the ith received OFDM symbol, $\tilde{Y}(i) = [\tilde{y}_1(i) \ \cdots \ \tilde{y}_{n'}(i)]^T \in \mathbb{C}^{n'}$, observed at the destination is given by

$$\tilde{Y}(i) = \tilde{\mathbf{H}}_0 \tilde{X}(i) + \tilde{\mathbf{H}}_1 \tilde{X}(i-1) + \tilde{V}(i), \tag{2.16}$$

where

$$\tilde{\mathbf{H}}_0 = \begin{bmatrix} \tilde{h}(0) & 0 & 0 & \cdots & 0 \\ \vdots & \tilde{h}(0) & 0 & \cdots & 0 \\ \tilde{h}(l) & \cdots & \ddots & \cdots & \vdots \\ \vdots & \ddots & \cdots & \ddots & \vdots \\ 0 & \cdots & \tilde{h}(l) & \cdots & \tilde{h}(0) \end{bmatrix}, \tilde{\mathbf{H}}_1 = \begin{bmatrix} 0 & \cdots & \tilde{h}(l) & \cdots & \tilde{h}(1) \\ \vdots & \ddots & 0 & \ddots & \vdots \\ 0 & \cdots & \ddots & \cdots & \tilde{h}(l) \\ \vdots & \ddots & \vdots & \ddots & \vdots \\ 0 & \cdots & 0 & \cdots & 0 \end{bmatrix} \tag{2.17}$$

are $n' \times n'$ complex random matrices. From (2.16), it can be seen that, if not properly countered, inter-block interference (IBI) will occur. To circumvent

[16]Here, the end-to-end impulse response is the cascade of the transmit filter, the time dispersive channel, and the receiver filter.

IBI, guard chips are inserted into the transmitted block. This is done by taking the vector $\underline{\tilde{X}}(i) \in \mathbb{C}^n$ of intended transmit information symbols, and constructing $\tilde{X}(i) = \mathbf{T}_{cp}\underline{\tilde{X}}(i)$, where

$$\mathbf{T}_{cp} = \left[\mathbf{I}_{cp}^T \;\; \mathbf{I}_n^T\right]^T \in \mathbb{C}^{n' \times n} \tag{2.18}$$

($\mathbf{I}_{cp}$ is formed from the final l rows of $\mathbf{I}_n$) is a cyclic-prefix (CP) inserting matrix that takes a copy of the final l elements from $\underline{\tilde{X}}(i)$ and appends them to its beginning, so that $n' = l + n$ symbols are used to transmit $n = n' - l$ information symbols. IBI is then removed by ignoring the first l samples of $\tilde{Y}(i)$, which is achieved by post multiplying $\tilde{Y}(i)$ by the CP removal matrix

$$\mathbf{R}_{cp} = [\mathbf{0}_{n \times l} \; \mathbf{I}_n] \in \mathbb{C}^{n \times (n+n')} \tag{2.19}$$

to give $\underline{\tilde{Y}}(i) \in \mathbb{C}^n$. After all these steps have been performed, it can be shown that

$$\underline{\tilde{Y}}(i) := \mathbf{R}_{cp}\tilde{Y}(i) = [\tilde{y}_{l+1}(i) \; \cdots \; \tilde{y}_{n'}(i)]^T = \underline{\tilde{\mathbf{H}}}_0\underline{\tilde{X}}(i) + \mathbf{R}_{cp}\tilde{V}(i), \tag{2.20}$$

where $\underline{\tilde{\mathbf{H}}}_0 = \mathbf{R}_{cp}\tilde{\mathbf{H}}_0\mathbf{T}_{cp}$. Thus, by inserting and removing sufficiently long CPs, IBI can be removed. Furthermore, it can be shown that $\underline{\tilde{\mathbf{H}}}_0$ is a circulant matrix. Consequently, the following eigendecomposition holds: $\underline{\tilde{\mathbf{H}}}_0 = \mathbf{F}_n^{-1}\mathbf{\Lambda}\mathbf{F}_n$ [47], where $\mathbf{F}_n$ is the $n \times n$ fast fourier transform (FFT) matrix whose (j,k)th element is given by $e^{-\frac{\mathrm{i}2\pi(j-1)(k-1))}{n}}/\sqrt{n}$ and $\mathbf{\Lambda}$ is a diagonal matrix. This property allows for low-complexity equalization: The source constructs a frequency domain block $\underline{X}(i) = [\underline{x}_1(i) \; \cdots \; \underline{x}_n(i)]^T \in \mathbb{C}^n$

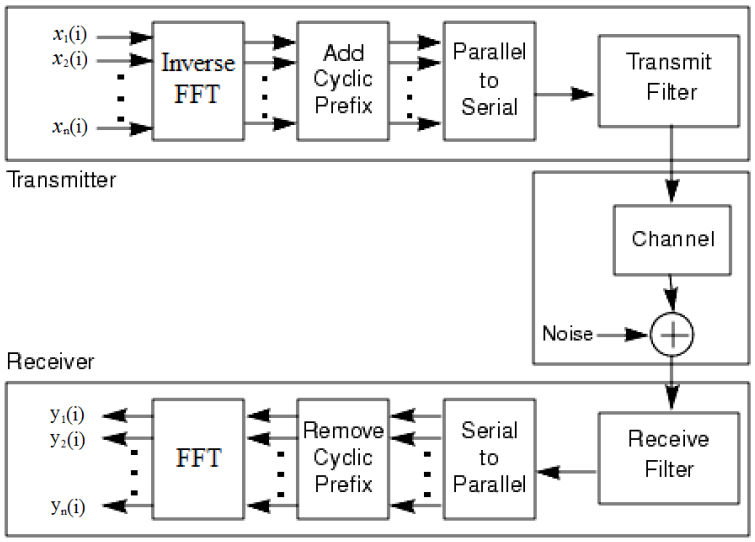

Figure 2.5: Block diagram of OFDM system.

and performs an inverse FFT to obtain

$$\underline{\tilde{X}}(i) = \mathbf{F}_n^{-1}\underline{X}(i). \tag{2.21}$$

The CP is then inserted at the transmitter. After the OFDM block has traversed the channel, the destination removes the CP, and then takes the FFT of the received block to obtain

$$\mathbf{F}_n\underline{\tilde{Y}}(i) = \mathbf{\Lambda}\underline{X}(i) + \mathbf{F}_n\mathbf{R}_{cp}\tilde{V}(i), \tag{2.22}$$

allowing the channel to be diagonalized. Equalization can then be performed by inverting $\mathbf{\Lambda}$, which is trivially achieved by inverting the elements along its leading diagonal. Fig. 2.5 shows a block diagram describing the OFDM system discussed above.

2.2.3.1 Multicarrier interpretation of OFDM

At present, we have provided a sufficient amount of detail to how OFDM can be employed to mitigate the effects of IBI, but we have not yet revealed the interpretation of OFDM as a multicarrier system. To reveal this, consider (2.21). From this, we can see that the kth column of $\mathbf{F}_n^{-1}$, given by

$$\mathbf{f}_k := \frac{1}{\sqrt{N}} \left[e^{\mathbf{i}\times 0} \;\; e^{\mathbf{i}2\pi k/n} \;\; e^{\mathbf{i}2\pi k2/n} \;\; \cdots \;\; e^{\mathbf{i}2\pi k(n-1)/n} \right]^T, \tag{2.23}$$

can be viewed as representing a kth carrier wave (in the time domain at base-band) that is being modulated by the kth element of $\underline{X}(i)$ to form a modulated transmit subcarrier. This is where the interpretation of OFDM as a multicarrier system comes from. In Fig. 2.6 we show the real part of $\mathbf{f}_k$ for a 128 subcarrier system when $k = 1, 2, 3$. In the frequency domain, the $\mathbf{f}_k$'s become sinc functions. Fig. 2.7 shows a plot of these sinc functions for an 8 subcarrier system. The crucial point to acknowledge about Fig. 2.7 is that each of the sinc functions are orthogonal in the sense that the peak of one coincides exactly with the zeros of all the others. This explains where 'Orthogonal' comes from in the abbreviation 'OFDM'.

2.2.4 Peak-power Constrained OFDM-based Systems

We now discuss a fundamental issue that arises when amplifying OFDM waveforms. Consider an n subcarrier OFDM transmitter, β, as described in section 2.2.3. The time-domain waveform at β is given by

$$\tilde{X}_\beta(t) = \frac{1}{\sqrt{n}} \sum_{k=1}^{n} e^{\frac{\mathbf{i}2\pi kt}{n}} X_\beta(k), \tag{2.24}$$

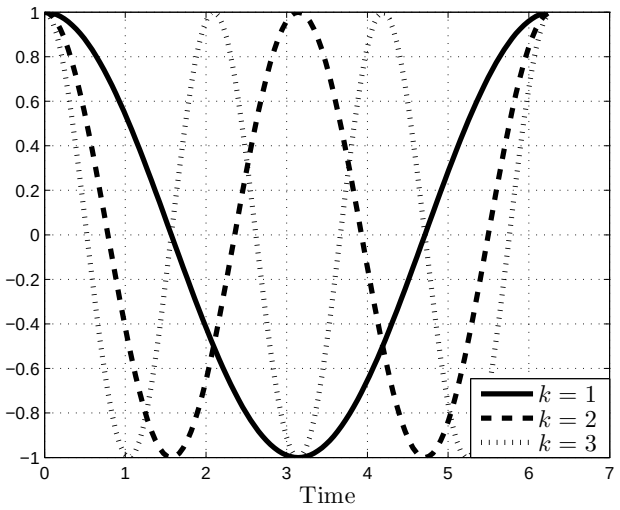

Figure 2.6: Plot showing the real part of $\mathbf{f}_k$ (2.23) for a 128 subcarrier system when $k = 1, 2, 3$.

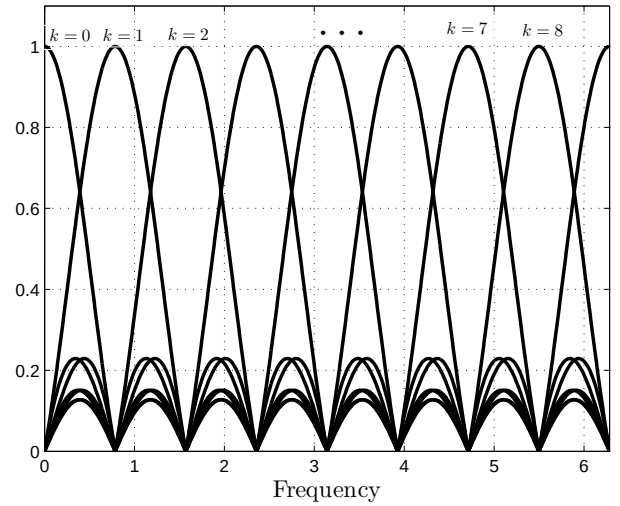

Figure 2.7: Plot showing the absolute value of the FFT of $\mathbf{f}_k$ (2.23) for an 8 subcarrier system.

where $X_\beta \in \mathbb{C}^n$ represents the frequency-domain block of symbols, and $\tilde{X}_\beta \in \mathbb{C}^n$ represents the OFDM block in the time-domain. Suppose that the frequency domain symbols are zero-mean, constant amplitude, independent and identically distributed (i.i.d.), and without loss of generality (w.l.o.g.) normalized such that the entire block has unit average power, then it is easy to see from (2.24) that the peak-power of the time-domain symbol is n. In a more general setting, we find that the peak-to-average power ratio (PAPR) of OFDM waveforms scale like $O(n)$.

This $O(n)$ scaling poses an immediate problem when amplifying such signals because the amplifier will require a large linear region (with respect to the average power) - to cope with the large peaks - if nonlinear distortion[17] is to be avoided. Amplifiers with large linear regions are expensive (both economically and in power efficiency); while amplifiers with smaller linear regions tend to be less expensive, but suffer more greatly from the effects of nonlinear distortion, [49,50]. For these reasons, OFDM-based terminals will often have to deal with the effects of nonlinear distortion, and a thorough understanding of the corresponding performance degradation is necessary.

In [7], the theoretical characteristics of OFDM-based systems operating with band-pass filters[18] over memoryless nonlinear channels were studied. In particular, with the input to the OFDM-based nonlinear channel given by a stationary random process

$$\tilde{X}_\beta(t) = a(t) + ib(t) = \theta(t)e^{\mathbf{i}\phi(t)}, \tag{2.25}$$

[17]Nonlinear amplifier distortion occurs when the output power of the amplifier does not scale linearly with its input power. The distortion can be partitioned into two categories: signal amplitude inducing amplitude distortion (AM-AM) and/or signal amplitude inducing phase distortion (AM-PM), [48].

[18]It is well known [51] that OFDM systems generally require root-raised cosine filters with extremely steep roll-off factors that closely resemble band-pass filters.

where $\theta_A(t)$ is the amplitude response and $\theta_P(t)$ is the phase response, it is shown that as the number of subcarriers grows large the output of the nonlinear channel

$$\tilde{Y}_\beta(t) = F_A\left[\theta_A(t)\right] e^{\mathbf{i}F_P[\theta_A(t)]} e^{\mathbf{i}\theta_P(t)} = F\left[a(t), b(t)\right], \tag{2.26}$$

where F_A is the channel's amplitude response and F_P is its phase response, can be written as

$$\tilde{Y}_\beta(t) = \zeta_\beta \tilde{X}_\beta(t) + \tilde{\varrho}_\beta(t), \tag{2.27}$$

where $\varrho(t)$ is an in-band ZMCG nonlinear distortion artifact uncorrelated with $\tilde{X}_\beta(t)$, having variance

$$\eta_\beta := \mathbb{E}\left[|\tilde{\varrho}(t)|^2\right] = \mathbb{E}\left[F_A\left[\theta(t)\right]^2\right] - |\zeta_\beta|^2\, \mathbb{E}\left[\theta(t)^2\right]; \tag{2.28}$$

and

$$\zeta_\beta = \frac{1}{2}\mathbb{E}\left[\frac{\partial F\left[a,b\right]}{\partial a} - \mathbf{i}\frac{\partial F\left[a,b\right]}{\partial b}\right] \tag{2.29}$$

is a complex scaling term, independent of time, which acts as an attenuation factor to the input of the memoryless nonlinear device. Because of the linearity of the Fourier transform, (2.27) can be expressed in the frequency domain as

$$Y_\beta(k) = \zeta_\beta X_\beta(k) + \varrho_\beta(k). \tag{2.30}$$

Eqs. (2.27) and (2.30) can be thought of as an extension of Bussgang's theorem [4] to memoryless nonlinear devices with complex Gaussian inputs; for, as an immediate consequence of the central limit theorem, the time-domain OFDM waveform converges to a complex Gaussian distribution as

the number of subcarriers grows large (see (2.24)). Throughout this thesis, the terms η_β and ζ_β are often referred to as *Bussgang parameters*.

Different nonlinear amplifier models exist, for example, the traveling-wave tube (TWT), solid-state power amplifier (SSPA) and the soft envelope limiter (SEL). The amplitude, $F_A(\cdot)$, and phase response, $F_P(\cdot)$, for each of these are given, respectively, below [7]:

$$F_A\left(\theta_A, p_{max\beta}\right) = \frac{p_{max\beta}\theta_A}{\theta^2 + p_{max\beta}}, \qquad F_P\left(\theta_A, p_{max\beta}\right) = \frac{\pi}{3}\left(\frac{\theta_A}{\theta_A^2 + p_{max\beta}}\right) \tag{2.31}$$

$$F_A\left(\theta_A, p_{max\beta}\right) = \frac{\theta_A}{\sqrt{1 + \frac{\theta_A^2}{p_{0\beta}}}}, \qquad F_P\left(\theta_A, p_{max\beta}\right) = 0 \tag{2.32}$$

$$F_A\left(\theta_A, p_{max\beta}\right) = \begin{cases} \theta_A, & \theta_A^2 \leq p_{max\beta} \\ p_{max\beta}, & \theta_A^2 > p_{max\beta} \end{cases}, \quad F_P\left(\theta_A, p_{max\beta}\right) = 0, \tag{2.33}$$

where θ_A is the input amplitude, $p_{max\beta}$ is the amplifier input saturation power and $p_{0\beta}$ is the output power at the saturation point. Fig. 2.8 shows plots of the amplitude responses for each of these models. From this figure, it can be seen that the SEL provides a reasonable approximation to the SSPA.

For TWT and SSPA, the Bussgang parameters require numerical calculation; for the SEL, it can be shown that

$$\zeta_\beta = 1 - e^{-\frac{p_{max\beta}}{\sigma_\beta^2}} + \sqrt{\frac{\pi p_{max\beta}}{4\sigma_\beta^2}}\operatorname{erfc}\left(\frac{p_{max\beta}}{\sigma_\beta^2}\right) \tag{2.34}$$

$$\eta_\beta = \sigma_\beta^2\left(1 - e^{-\frac{p_{max\beta}}{\sigma_\beta^2}}\right) - \zeta_\beta^2\sigma_\beta^2, \tag{2.35}$$

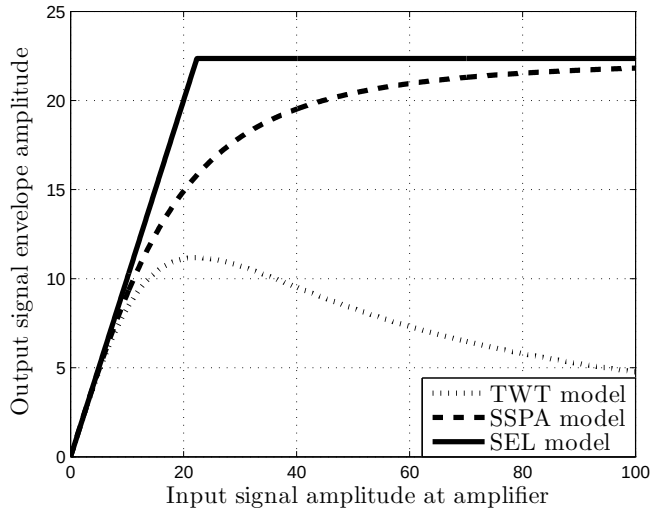

Figure 2.8: Figure showing the amplitude responses, $F_A(\theta, p_{max\beta})$, given for the TWT (2.31), SSPA (2.32), and SEL (2.33).

where $\sigma_\beta^2 = \mathbb{E}\left[|X_\beta(t)|^2\right]$, and the average transmit power is given by

$$p_\beta = \int_0^{p_{max,\beta}} \frac{e^{-\frac{x}{\sigma_\beta^2}}}{\sigma_\beta^2} dx + \int_{p_{max,\beta}}^{\infty} p_{max,\beta} \frac{e^{-\frac{x}{\sigma_\beta^2}}}{\sigma_\beta^2} dx = \sigma_\beta^2 \left(1 - e^{-\frac{p_{max\beta}}{\sigma_\beta^2}}\right). \quad (2.36)$$

Nonlinear distortion can be countered to a certain degree by employing predistortion techniques. These techniques predistort the input so that the cascade of the predistorter and the power amplifier response are (approximately) linear, [52]. Note, the SEL is of particularly important theoretical interest as it is known to model the entire transmit-side chain when ideal predistortion is implemented, [53]. Thus, not only does the SEL provide a reasonable approximation for the SSPA, performance results obtained for the SEL will also upper bound those for more general nonlinearities.

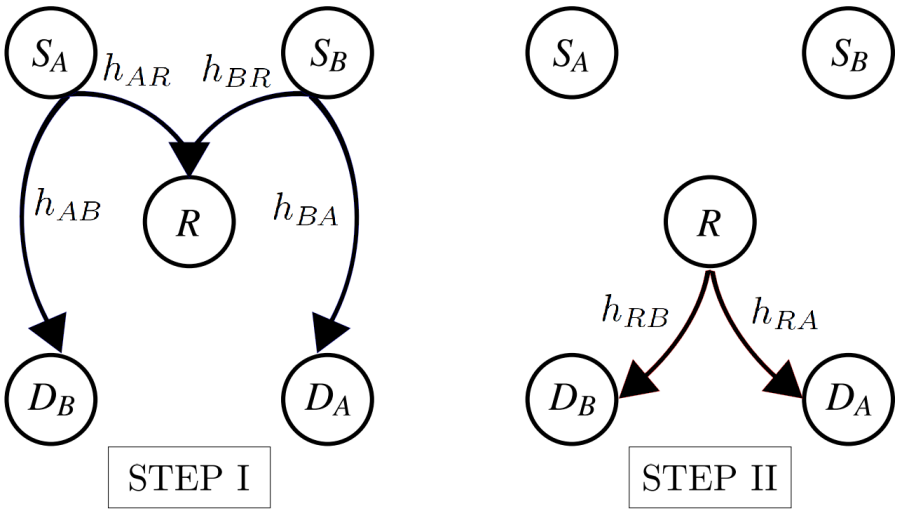

Figure 2.9: Basic illustration of a relay network, where one relay node aids communication between two source nodes and two destination nodes. The channel coefficients are given by h_{ij}, $i, j \in \{A, B, R\}$.

2.2.5 Relaying

In sections 2.1.2 and 2.1.3 relaying was discussed as a key technology for current and next generation communication systems. For this reason, over the last 15 years relaying has captured significant attention in the research community. The relay network was first introduced by Van der Meulen in his seminal work, [54]. In general, a relay network - in the context of wireless networks - is a wireless network consisting of a source or multiple source node(s), a destination or multiple destination node(s), and an arbitrary number of intermediary relay nodes. The nodes in the network must necessarily cooperate, and the relay nodes are responsible for relaying packets of information from the source(s) to the destination(s). Fig. 2.9 shows an example of a relay network.

Apart from their ability to facilitate adhoc networks, relays are deployed because they allow for an improved quality of service for the users of a

network. These improvements can be summarized as:

1. increased capacity,

2. increased diversity,

3. increased physical layer security.

We will now discuss each of these points in-turn.

2.2.5.1 Increased Capacity

An alternative to (or in combination with) embedding multiple antennas at the source and destination nodes of a network is to distribute antennas among the network as relay nodes. In [55], it is demonstrated that deploying a single relay can provide capacity improvements for a network. Capacity scaling laws are studied in [56] for two-hop relay networks when the source and destination have m antennas, and there are k single or multiple antenna relays aiding the communication. In this paper, it is shown that $c = (m/2)\log(k) + O(1)$ for large k. It is also shown in [56] that relays can be deployed to act as active scatterers, helping improve the condition number of the source-destination channel matrix. Similar results are reported in [57], where it is shown that relays can be deployed to mitigate keyhole effects[19] in MIMO systems. Other attempts to demonstrate the capacity improvements that relays provide can be found in [59–61].

[19] A MIMO keyhole is any environment that causes the channel matrix to have rank one, irrespective of the number of antennas at each node, [58].

2.2.5.2 Increased Diversity

A typical single-hop SISO Rayleigh fading channel will achieve a diversity order of one. By deploying more antennas at the nodes of such a network (i.e., transforming it into a MISO/SIMO/MIMO network), greater levels of diversity can be achieved, [62]. Under the assumption that channel fading is independent between each antenna pair, single-hop MIMO networks can achieve a maximum diversity order of mn, where m and n are the number of antennas at the source and destination, respectively[20]. In a similar fashion, relays can be deployed within a SISO network. Because they are spatially separated, the relays perform a similar role as the extra antennas in the MIMO example above, allowing for increased diversity.

The diversity order offered by relaying was originally studied by Laneman et al in their seminal work [63–65]. In particular, it was shown that deploying a single relay between two nodes subject to Rayleigh fading could double the diversity order of the network. Naturally, the diversity order can be increased further by introducing more relay nodes. In [66], a cooperative relaying scheme was proposed that would allow the network's diversity order to scale linearly with the number of relaying nodes. The scheme operated by having only the 'best' relay out of a cluster to perform forwarding. This scheme is now referred to as relay selection. Other efforts to understand the diversity order of relay networks can be found in [28,67,68].

[20]It should be noted that there exists a trade-off between the spatial multiplexing gains (discussed in section 2.2.2) and the diversity gain offered by MIMO systems, [62].

2.2.5.3 Relaying Strategies

Different relaying strategies have been proposed in the literature; e.g., AF, decode-and-forward (DF), compress-and-forward (CF) and others. We will now briefly discuss each of these, providing particular focus on the most common strategies (AF and DF).

Amplify-and-forward Relaying The AF strategy [69, 70] operates by having the relay apply an amplification factor to its received signal before subsequent (re)transmission. In more detail, suppose a single information source transmits the symbol x to a relay so that the relay receives $hx + v$, where h denotes the scalar channel coefficient between the source and relay and $v \sim \mathcal{CN}(0, n_0)$ denotes the channel noise, then the relay will transmit

$$y = g_\alpha \left(hx + v \right), \tag{2.37}$$

where g_α is given by [71]

$$g_{FG} = \sqrt{\frac{p_R}{p_S \mathbb{E}|h|^2 + n_0}} \tag{2.38}$$

for FG amplification and [72]

$$g_{VG} = \sqrt{\frac{p_R}{p_S |h|^2 + n_0}} \tag{2.39}$$

for VG amplification. The terms p_S and p_R denote the average transmit power at the information source and the relay, respectively.

The benefits of employing AF relaying are:

1. lower complexity;

2. lower latency;

3. takes place at the physical layer.

Each of these points are closely linked. The lower latency is an immediate consequence of the lower complexity, which results from the minimal signal processing performed by the relay. Similarly, because forwarding takes place at the physical layer, the relay has fewer overheads and will be able to more easily offer forwarding services to a wider range of devices, which may make it particularly attractive for the IoT. The main drawbacks of AF relaying are:

1. amplification of noise at the relay,

2. more difficult to study analytically,

3. increased signal variance as number of hops grows.

For the first point, clearly amplification of noise will degrade the channel quality. The second point occurs because the AF relay (by its nature) concatenates sequential channels. This results in a more mathematically complex end-to-end signaling distribution. The final point is also due to the concatenation of sequential channels and may result in power control issues, the symptoms of which may be, e.g., nonlinear amplifier distortion.

Decode-and-forward Relaying The DF strategy operates by having the relay decode its received signal and, provided correct decoding has been performed, (re)encoding and (re)transmitting to the next node. The benefits of DF relaying are:

1. provided decoding has been performed correctly, noise is removed at the relay;

2. more easy to study analytically.

The first point follows from the fact that the DF relay can employ error correction codes to remove errors in received information blocks. The main concern with this is that, if incorrect decoding has been performed at the relay without detection, instead of removing noise, the relay will forward an erroneous information block. If this occurs, the relay will hinder the performance of the network. Thus, it is important that DF relays only forward if non-erroneous decoding has been performed. The second point occurs because at each relay the signal is effectively 'reset' by the decoding operation. Consequently, the analysis of DF networks can often by reduced to studying each hop individually. The main drawbacks of DF relaying are

1. greater complexity;

2. greater latency;

3. requires, at the very least, demodulation and decoding followed by re-encoding, modulation and amplification;

4. erroneous decoding can further degrade the network performance.

All of these points are immediate consequences of the decoding operation. The third point implies that DF relays will require more overheads if they are to serve a wide range of devices. The final point was discussed above, and can cause severe performance degradation if not properly countered, [65].

Other Relaying Strategies For AF and DF, the relay forwards a copy[21] of the source's transmission. In CF [73], the relay quantizes and compresses the received message from the source before forwarding the message to the destination. The destination then uses the message from the source as side information when decoding the message from the relay.

There have been other efforts to extend the AF and DF schemes. For example, [74] proposes a scheme called decode-amplify-forward (DAF), which has the relay perform soft decoding to obtain the log-likelihood ratios, and then performs AF on these log-likelihood ratios. It was shown in [74] that DAF could provide capacity improvements for channels with binary inputs when compared to AF and DF. In [75], a hybrid AF-DF scheme was proposed, where the relay performs DF if correct decoding is performed, otherwise AF is performed.

2.2.5.4 Two-way Relaying and Network Coding

In certain scenarios, the relay may be aiding bi-directional communication. When this occurs, the relay channel is said to be two-way, see Fig. 2.10. Consider such a two-way two-hop network. Two nodes, A and B, communicate bidirectionally with the aid of a relay, node R. For this, a rudimentary approach to relaying is to partition the channel into four time-slots. Node A transmits to the relay in the first time-slot. The relay forwards this in the second time-slot. Node B transmits to the relay in the third time-slot. The relay forwards this in the fourth time-slot.

By employing standard network coding at the relay, the number of time-slots required can be reduced from four to three. This is achieved as follows:

[21] Either a noisy amplified version, or an (attempted) exact copy.

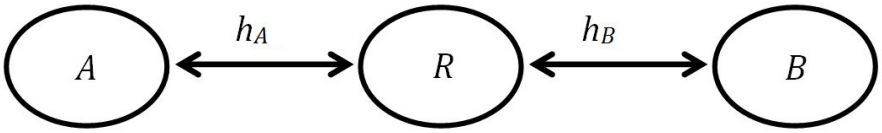

Figure 2.10: Topological illustration of a basic two-way relay network. The channel coefficients between nodes A and the relay and B and the relay are denoted h_A and h_B, respectively.

in the first time-slot, node A transmits the symbol a to the relay; in the second time-slot, node B transmits the symbol b to the relay; in the third time-slot, the relay transmits $a \oplus b$, where $\oplus$ is some predefined associative binary operation. Node A then obtains b by calculating $a^{-1} \oplus a \oplus b$, while node B obtains a by calculating $a \oplus b \oplus b^{-1}$. Note, here we have implicitly assumed that x^{-1} denotes the inverse of x with respect to the binary operation $\oplus$. Consequently, the network throughput can be increased by a factor of 4/3.

Although performance is improved by performing network coding at the relay, it is possible to further reduce the number of time-slots required from 3 to 2 by allowing the network coding to take place at the physical layer; i.e., perform PNC [76–79]. In this scenario, both source nodes transmit at the same time to the relay so that the relay receives a superposition of their transmissions. After processing[22] this superimposed signal, the relay then forwards the processed signal back to the source nodes in the second time-slot. The source nodes then remove their own symbols from the relay's transmission to obtain the other's symbol. This methodology can be applied to both AF and DF systems. In what follows, we will describe the technical details of PNC for AF relaying - details of PNC for DF relaying can be

[22]Processing may refer to amplification, or some other more complex process; e.g., mapping the superimposed signal to a particular set of symbols.

found in [79].

Physical Layer Network Coding for AF Suppose the first source transmits a and the second source transmits b. The relay then receives $(h_A a + h_B b + v_R)$ and transmits

$$x = g_\alpha(h_A a + h_B b + v_R), \tag{2.40}$$

where h_A and h_B are the respective channel coefficients between nodes A and R, and B and R; and v_i, $i \in \{A, B, R\}$, is the noise at node i. Assuming channel reciprocity, and that the entire protocol has taken place within the channel's coherence time, nodes A and B respectively receive

$$y_A = h_A g_\alpha(h_A a + h_B b + v_R) + v_A \text{ and } y_B = h_B g_\alpha(h_A a + h_B b + v_R) + v_B. \tag{2.41}$$

Each of the source nodes can remove its own self-interference by performing a simple subtraction of its symbol, phase shifted and scaled by the relevant channel coefficient and relay gain; e.g., node A removes self-interference by calculating $y_A - g_\alpha h_A^2 a$. We will return to this model in section 3.2.

2.3 Summary

In this chapter, we discussed the development of modern wireless networks. We then focused on modern communication techniques that are being considered for current and future systems: spatial multiplexing, OFDM, and relaying. These fundamental concepts will form the building blocks for the novel research presented in this thesis.

Chapter 3

Two-way Networks: Outage Probability Analysis and Optimization

This is the first of our research chapters. In this chapter, we derive closed form outage probability expressions for the FG and VG two-way AF relay network when a nonlinear transmission occurs only at the relay. We show how this result can be extended trivially to the scenario in which distortion also occurs at the source. We then derive an explicit expression for the relay gain that optimizes the network's performance. Following this, we show that if the source nodes have no access to the distortion characteristics of the relay's amplifier, which inhibits self-interference removal, the network's performance will change negligibly. Finally, we consider the problem of allocating power among the nodes of the network. Two power allocation problems are considered: 1) the transmit power budget of the communicating nodes is independent of the relay's transmit power, 2) the

relay's transmit power is included within the total power budget of the network. For the former, a closed form solution is obtained. For the latter, the problem is shown to be non-convex in its standard form. By applying a substitution, we show that it can be converted into a convex problem. Numerical results are provided to demonstrate the efficacy of our methods. Finally, a discussion is included to give further insight into how our power allocation scheme behaves as a function of the network's asymmetry.

3.1 Introduction

As discussed in section 2.2.4, OFDM systems exhibit a large PAPR in their transmit envelopes and are thus susceptible to the effects of nonlinear amplifier distortion. When combined with the effects of channel fading, even larger PAPR will be produced at the relay of OFDM-based networks. It is thus particularly important to understand how nonlinear amplification might affect the performance of OFDM-based relaying systems.

In [71], the effect of relay saturation on the outage probability of a single-carrier (SC) link is considered. However, the model adopted in that work does not include distortion (or OFDM), but instead opts to create an adaptive FG / VG system that changes state based upon whether or not the relay amplifier is saturated. In [80], closed form expressions are obtained for the complementary cumulative density function (CCDF) of the output power at the relay of an AF and DF relay, where it is shown that DF has a significantly lower probability of exceeding a predefined power constraint compared to AF. In [81], the outage probability of a two-hop OFDM VG relay system with a direct source-destination link in the presence of relay

nonlinearities is approximated, whereas [82] focuses on the SER of such a system without a source-destination link when a nonlinear transmission occurs at the source. The work of [83] considers an FG relay system with direct source-destination link, and nonlinear distortion at the relay. A nonlinear distortion aware maximal ratio combining strategy is proposed that is shown to improve the performance of the system significantly. In [84], a power allocation scheme is proposed over a cluster of relays that are subject to nonlinear transmissions and are aiding a two-hop network, which is shown to maximize the signal-to-noise and distortion ratio (SNDR) across the network. In [85], closed form expressions for the outage probability and ergodic capacity are established for an FG network when a nonlinear amplifier is present at the source, and in-phase and quadrature-phase imbalances are present at the destination.

To the best of the author's knowledge, in the previous literature no attempt has been made to study two-way relay networks in which the network's nodes are subject to nonlinear amplifier transmissions. The focus of this chapter is to provide such a study. We begin by:

1. establishing outage probability expressions for FG and VG networks in the general two-way relaying scenario (this work has been published in [8]),

2. we then determine optimal power allocation strategies for the two-way network (this work has been published in [9]).

To clarify the discussion in the previous two paragraphs, we present Table 3.1, which contains a corresponding high level overview of previous literature and our own contributions. Note, for completeness this table also

contains details of the contributions of this thesis that are presented in Chapter 4. This is because the system model considered in Chapter 4 can be viewed as a special case of that considered in this chapter.

3.2 System Model

The aim of this section is to present the general two-hop two-way AF relaying system model that will be studied throughout this and the next chapter. This chapter will study this general system model, while Chapter 4 will consider the one-way special case.

Consider a two-hop, two-way, time-division duplexing (TDD) AF OFDM relay network operating over a total of n subcarriers (Fig. 3.1). We consider an l tap quasi-static linear time-invariant channel impulse response for links A-R and B-R, respectively. We further assume that these impulse responses have exponentially decaying profiles, [86]. It is important to note that delay profiles are not in general limited to those that exponentially decay (see, for example, [87]). After time-domain sampling, the impulse response for hop $\beta \in \{A, B\}$ to the relay can be represented as the time-domain vector

$$\tilde{H}_\beta = \frac{\sqrt{n}\left[\delta(0)\tilde{h}_{\beta 0} \;\; \delta(1)\tilde{h}_{\beta 1} \;\; \cdots \;\; \delta(l-1)\tilde{h}_{\beta,l-1}\right]}{\sqrt{\sum_{i=0}^{l-1}\delta(i)^2}}, \tag{3.1}$$

where the ith entry of $\tilde{H}_\beta$ corresponds to ith tap of the channel, δ is the exponent of the delay profile, and $\tilde{h}_{\beta i}$, $i \in \{0, \ldots, l-1\}$, is an i.i.d. ZMCG random variable with total variance μ_β. The prefactor $\sqrt{n/\sum_{i=0}^{l-1}\delta(i)^2}$ is a normalization term. After taking the unitary FFT of the channel's l tap impulse response, the frequency response for the kth subcarrier between

System Model Studied	Main Result	Reference
SC FG relay with peak-power limit.	Relay saturation negligibly affects the performance of the system.	[71]
SC FG, VG, DF with peak-power limit.	Expressions for CCDF of relay's output power are obtained. DF shown to outperform AF.	[80]
Direct source-destination link and distortion at VG relay.	Outage probability approximated.	[81]
Distortion at source of VG network.	SER calculated.	[82]
Direct source-destination link and distortion at FG relay.	Nonlinear distortion aware maximal ratio combing strategy is proposed.	[83]
Distortion at cluster of FG relays.	Power allocation scheme determined that maximizes end-to-end SNR.	[84]
Distortion at FG relay and inphase/quadrature imbalances at source/destination in Nakagami-m fading.	Outage probability calculated and ergodic capacity approximated.	[85]
Two-way system with source and relay distortion.	Outage probability, optimal gains and power allocation strategies calculated.	[8, 9] (Ch. 3)
Distortion at FG relay.	SER calculated, and gain optimization on real-world test-bed.	[10] (Ch. 4)
Distortion at source and relay.	VG shown to significantly outperform FG in distortion limited regime.	[11] (Ch. 4)

Table 3.1: Table outlining previous power constrained relaying contribution in the literature, and our contributions. The base system model is an OFDM based one-way AF network with no power constraints at any of the nodes and Rayleigh fading between each of the links. The details in the "System Model Studied" column are modifications to this base model.

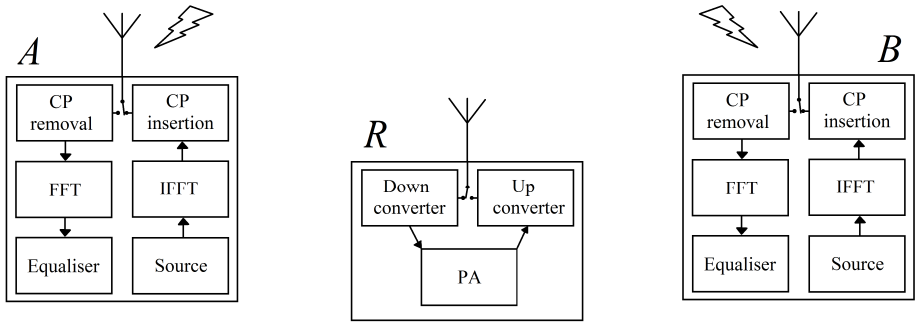

Figure 3.1: Nodes A and B wish to communicate with each other via the relay, node R. The figure represents the state of the half-duplex system in its first time slot.

links A-R and B-R are given by $h_{Ak} \sim \mathcal{CN}(0, \mu_A)$ and $h_{Bk} \sim \mathcal{CN}(0, \mu_B)$, $k \in \{1, \ldots, n\}$, respectively. Note, within our system model, individual subcarriers of the same hop are necessarily correlated with each other.

We will now describe the relaying protocol from transmission to reception. This takes place over two time slots and is detailed in the following subsections.

3.2.1 First Time Slot

Nodes A and B construct OFDM symbol vectors comprised of n symbols, which we denote by the frequency-domain vectors $X_A = [x_{A1}, \ldots, x_{An}]^T$ and $X_B = [x_{B1}, \ldots, x_{Bn}]^T$, where $\sigma_A^2 := \mathbb{E}[|x_{Ak}|^2]$ and $\sigma_B^2 := \mathbb{E}[|x_{Bk}|^2]$. It is assumed that the symbols $\{x_{Ak}\}$ and $\{x_{Bk}\}$ are chosen uniformly and independently from a quadrature phase-shift keying (QPSK) constellation.

3.2.1.1 Cyclic Prefix Insertion and Removal

Vectors X_A and X_B are processed with an inverse FFT, after which a CP of suitable length is appended to mitigate IBI. CP insertion and removal can

be performed in different ways for the relay network, [88]:

1. the relay may remove the CP so that it can locally mitigate IBI, and then insert a new CP for the second hop;

2. the CP insertion and removal may be performed entirely at the sources and destinations.

For the former, the CP for the first hop should be as long as the impulse response of the first hop, while the CP for the second hop should be as long as the impulse response of the second hop. For the latter, the length of the relay channel's impulse response is given by the convolution of the per-hop impulse responses. Consequently, the length of the entire channel impulse response is given by the sum of the lengths of the per-hop impulse responses. In this system model, we assume that CP insertion and removal is performed as per point 2; i.e., entirely at the sources and destinations. Consequently, the CP must be more than $2l$ sample periods in length to mitigate IBI. Before being passed through an SEL, the time-domain transmit vector at node β is given by

$$\tilde{X}_{\beta,cp} = [\tilde{x}_{\beta,n-2l-1} \quad \tilde{x}_{\beta,n-2l} \quad \cdots \quad \tilde{x}_{\beta,n-1} \quad \tilde{x}_{\beta,0} \quad \tilde{x}_{\beta,1} \cdots \quad \tilde{x}_{\beta,n-1}]^T, \quad (3.2)$$

where $\tilde{x}_{\beta,i}$ is the ith entry of $\tilde{X}_\beta := \mathbf{F}^{-1}X_\beta$. With this CP insertion and removal model, the channel can be considered at a subcarrier level.

3.2.1.2 Source Transmission

The sources are subject to maximum transmit power constraints, $p_{max,\beta}$, $\beta \in \{A, B\}$. To ensure that these constraints are not exceeded, nodes A

and B, respectively, pass their time-domain waveforms through SELs (see (2.33)). The output of the SEL in the time-domain given that the input is the kth element of (3.2) is

$$\tilde{y}_{\beta k} = \min\left\{\sqrt{p_{max\beta}}, |\tilde{x}_{\beta k}|\right\} \exp\left(\mathbf{i} \arg \tilde{x}_{\beta k}\right), \qquad \beta \in \{A, B\}. \tag{3.3}$$

By considering the theory presented in Chapter 2.2.4, and provided the number of subcarriers is sufficiently large, the frequency domain output of the SEL on each subcarrier can be written as

$$y_{\beta k} = \zeta_\beta x_{\beta k} + \varrho_{\beta k}, \qquad \beta \in \{A, B\}, \tag{3.4}$$

where ζ_β is given by (2.34), and $\varrho_{\beta k}$ is uncorrelated with $x_{\beta k}$ and well approximated by a ZMCG random variable with total variance η_β given by (2.35). The average transmit power, p_β, on each subcarrier at node β is given by (2.36). Note, since good codes commonly form stationary ZMCG processes [89], Bussgang's theorem will still apply when these are used.

The received signal at the relay on the kth subcarrier is then given by

$$y_{Rk} = h_{Ak}\zeta_A x_{Ak} + h_{Bk}\zeta_B x_{Bk} + v_{Rk} + h_{Ak}\varrho_{Ak} + h_{Bk}\varrho_{Bk}, \tag{3.5}$$

where $v_{Rk} \sim \mathcal{CN}(0, n_0)$ is the noise term on the kth subcarrier at the relay. We can write the average SNRs from nodes A and B to R, and total average SNR at the relay, as

$$\bar{\gamma}_{AR} = \frac{p_A \mu_A}{n_0}, \quad \bar{\gamma}_{BR} = \frac{p_B \mu_B}{n_0}, \quad \bar{\gamma}_R = \bar{\gamma}_{AR} + \bar{\gamma}_{BR}; \tag{3.6}$$

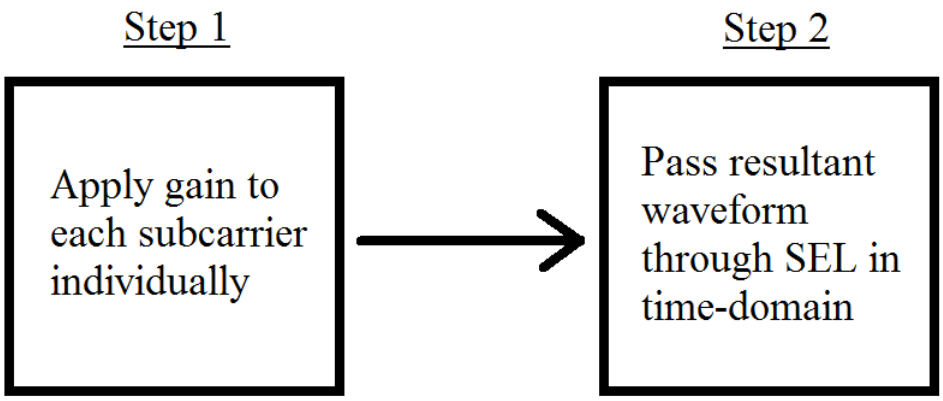

Figure 3.2: Figure illustrating the two step process used to model the amplification at the relay before transmission.

and the kth subcarrier instantaneous SNRs from nodes A and B to R, and total instantaneous SNR at the relay, as

$$\gamma_{ARk} = \frac{p_A |h_{Ak}|^2}{n_0}, \ \gamma_{BRk} = \frac{p_B |h_{Bk}|^2}{n_0}, \ \gamma_{Rk} = \gamma_{ARk} + \gamma_{BRk}. \tag{3.7}$$

3.2.2 Relay Amplification Model

Once y_{Rk}, (3.5), has been received at the relay, the relay performs the amplification process and then transmits the resultant signal. This process takes place over two distinct steps, see Fig. 3.2.

Step One The relay applies the amplification factor $g_{\alpha k}$ to its received signal, where $\alpha \in \{FG, VG\}$ denotes whether FG or VG has been considered. For the FG scenario, the amplification factor for the kth subcarrier is given by

$$g_{FGk} = \sqrt{\frac{\sigma_R^2}{p_A \mu_A + p_B \mu_B + n_0}}; \tag{3.8}$$

where σ_R^2 is the average input power to the SEL at the relay. For the VG scenario, we assume the gain for the kth subcarrier takes the form

$$g_{VGk} = \sqrt{\frac{\sigma_R^2}{p_A|h_{Ak}|^2 + p_B|h_{Bk}|^2 + n_0}}. \tag{3.9}$$

Note, (3.8) is independent of k. However, to aid exposition, we refrain from removing the subscript k.

Step Two Before transmission, the relay passes the amplified time-domain waveform through an SEL to limit its maximum transmit power to p_{maxR}. As an immediate consequence of the central limit theorem, this time-domain signal converges in distribution to a stationary ZMCG variable with variance σ_R^2 as the number of subcarriers grows large.

It is important that we discuss a particular subtlety that occurs when applying Bussgang's theorem to FG relaying. For the Bussgang parameters at the relay to be completely determined by the average input power to the SEL[1] (see σ_R^2 in (3.8) and (3.9)), the input to the relay's SEL should be stationary. For FG, this stationarity is contingent on there being a sufficient number of *significant* taps within the channel. This is *not* the case for VG. To understand why a sufficient number of taps is required for FG, consider the extreme scenario in which the channels are flat across all the subcarriers; i.e., the channels have a single tap impulse response. Furthermore, note that a quasi-static fading model has been considered, so the channel coefficients are considered to be fixed for a single OFDM time-domain block. For this, the subcarrier responses will be independent of their indices, i.e., $h_{\beta i} = h_{\beta j}$

[1] When this is the case, analytic calculations become tractable.

$\forall\ i, j$. With $h_{\beta i} = h_\beta \sim \mathcal{CN}(0, \mu_\beta)$ for all i, this allows us to write the time-domain waveform at the relay's SEL as

$$\tilde{Y}_R(t) = \frac{1}{\sqrt{n}} \sum_{k=1}^{n} e^{\frac{\mathrm{i}2\pi kt}{n}} g_{FGk} \left(h_A \zeta_A x_{Ak} + h_B \zeta_B x_{Bk} + v_{Rk} + h_A \varrho_{Ak} + h_B \varrho_{Bk} \right). \tag{3.10}$$

Because the gains are fixed and independent of k, and the channel coefficients are assumed to be quasi-static, $\tilde{Y}_R(t)$ will approach a ZMCG variable with conditional variance

$$\mathbb{V}\left[\tilde{Y}_R(t) \,|\{h_A, h_B\} \right] = \left(\frac{\sigma_R^2}{p_A \mu_A + p_B \mu_B + n_0} \right) \left(p_A |h_A|^2 + p_B |h_B|^2 + n_0 \right). \tag{3.11}$$

Note conditioning on the channel coefficients is performed to account for the quasi-static nature of the channel. Thus, we will not have the requirement for the Bussgang parameters that the input to the SEL be a stationary ZMCG variable with variance σ_R^2. In particular, this will be a function of the quasi-static random variables[2] h_A and h_B. The Bussgang parameters will then become functions of these instantaneous parameters, varying from one fading block to next. However, as the number of channel taps grows, h_{1i} and h_{1j}, $i \neq j$, will become increasingly decorrelated and the averaging performed by the inverse FFT in (3.10) will tend to remove the dependence of $\tilde{Y}_R(t)$'s conditional variance on the instantaneous realizations of h_{Ak} and h_{Bk}. Concretely, $\tilde{Y}_R(t)$ will approach a stationary ZMCG random variable with conditional variance σ_R^2 as the number of channel taps grows large. To

[2]Equation (3.11) also illustrates why a sufficient number of taps is not required for VG: for VG, the denominator of the first bracketed term will be identical to the second bracketed term, and therefore cancel with it.

see this, observe the following:

$$\begin{aligned}
&\mathbb{V}\left[\tilde{Y}_R(t) \,|\, \{h_{A1},\ldots,h_{An},h_{B1},\ldots,h_{Bn}\}\right] \\
=&\frac{1}{n}\sum_{k=1}^{n}\mathbb{V}\left[e^{\frac{i2\pi kt}{n}} g_{FGk}\left(h_{Ak}\zeta_A x_{Ak} + h_{Bk}\zeta_B x_{Bk} + v_{Rk} + h_{1k}d_{Sk}\right)|h_{1k}\right] \\
=&\left(\frac{\sigma_R^2}{p_A\mu_A + p_B\mu_B + n_0}\right)\frac{1}{n}\sum_{k=1}^{n}\left(p_A\left|h_{Ak}\right|^2 + p_B\left|h_{Bk}\right|^2 + n_0\right). \qquad (3.12)
\end{aligned}$$

In the limit as the number of channel taps and subcarriers grow large, $|h_{\beta i}|^2$ becomes independent of $|h_{\beta j}|^2$ for all $i \neq j$ and $\beta \in \{A, B\}$, and from (3.12) and the law of large numbers

$$\mathbb{V}\left[\tilde{Y}_R(t) \,|\, \{h_{A1},\ldots,h_{An},h_{B1},\ldots,h_{Bn}\}\right] \longrightarrow \sigma_R^2.$$

This shows us that $\tilde{Y}_R(t)$ approaches a stationary random variable as the number of channel taps grows large. Of course, in practice the number of channel taps will be finite. However, from heuristic observations, we find that 16 or more channel taps allows for very accurate analytical modeling of FG systems using Bussgang's theorem. We will demonstrate this in section 3.3.3. Note, in [90] it was shown that a particular 20MHz bandwidth non-line-of-sight micro cellular environment would have as many as 40 significant taps in its channel impulse response.

Similar to before (3.4), we can now write the frequency-domain output of the relay's SEL as

$$x_{Rk} = \zeta_R g_{\alpha k} y_{Rk} + \varrho_{Rk}, \qquad (3.13)$$

where ζ_R is given by (2.34) and ϱ_{Rk} is uncorrelated with y_{Rk} and well approximated by a ZMCG random variable with variance η_R given by (2.35).

The average transmit power on each subcarrier at the relay is given by p_R (see (2.36)).

3.2.3 Second Time Slot

By assuming channel reciprocity, which follows from the TDD nature of the channel, and that the entire relaying process has taken place within the coherence time of the channel, the received signal on the kth subcarrier at node $\beta \in \{A, B\}$ is

$$y_{\beta k} = h_{\beta k} x_{Rk} + v_{\beta k}, \tag{3.14}$$

where $v_{\beta k} \sim \mathcal{CN}(0, n_0)$ is the additive noise term on the kth carrier at node β. Note, to obtain (3.14), node β must first remove the CP from the received time-domain block and then perform an FFT on this block. The kth element of the output vector of the FFT will then be given by (3.14).

To perfectly remove all self-interference from the network, A and B should calculate

$$\underline{y}_{Ak} = y_{Ak} - \zeta_A \zeta_R g_{\alpha k} h_{Ak}^2 x_{Ak}, \qquad \underline{y}_{Bk} = y_{Bk} - \zeta_B \zeta_R g_{\alpha k} h_{Bk}^2 x_{Bk}. \tag{3.15}$$

However, in some scenarios the destination nodes may be unaware of the relay's amplifier distortion characteristics. In this scenario, they calculate

$$\underline{y}_{Ak} = y_{Ak} - \zeta_A g_{\alpha k} h_{Ak}^2 x_{Ak}, \; \underline{y}_{Bk} = y_{Bk} - \zeta_B g_{\alpha k} h_{Bk}^2 x_{Bk}. \tag{3.16}$$

Thus, there will be self-interference at A and B given, respectively, by

$$g_{\alpha k}(\zeta_R - 1) h_{Ak}^2 x_{Ak} \qquad \text{and} \qquad g_{\alpha k}(\zeta_R - 1) h_{Bk}^2 x_{Bk}. \tag{3.17}$$

The average SNRs from nodes R to A and B are given by

$$\bar{\gamma}_{RA} = \frac{p_R \mu_A}{n_0}, \quad \bar{\gamma}_{RB} = \frac{p_R \mu_B}{n_0}; \tag{3.18}$$

and the kth subcarrier instantaneous SNRs from nodes R to A and B are given by

$$\gamma_{RAk} = \frac{p_R |h_{Ak}|^2}{n_0}, \ \gamma_{RBk} = \frac{p_R |h_{Bk}|^2}{n_0}. \tag{3.19}$$

Note, in (3.18) and (3.19) we have assumed signal power to be the total power of the signal transmitted by the relay. This includes the self interference term and nonlinear distortion.

3.3 Outage Probability for Two-way Network with Imperfect Interference Removal

Consider the system model presented in section 3.2. Let us consider the per-direction outage probability of this network at node B when imperfect interference removal is performed as per (3.16) and no distortion occurs at the sources[3]. This is defined to be

$$P_{oB}^{(\alpha)} := \mathbb{P}[\gamma_{Bk}^{(\alpha)} < \gamma_{thB}], \tag{3.20}$$

where γ_{thB} is an appropriately selected signal-to-interference, noise and distortion ratio (SINDR) protection threshold and $\gamma_{Bk}^{(\alpha)}$ is the kth subcarrier

[3]Following this, we will show that the outage probability can be trivially extended to the source distortion scenario by applying a particular substitution.

instantaneous SINDR at B given by

$$\gamma_{Bk}^{(\alpha)} = \frac{\zeta_R^2 g_{\alpha k}^2 |h_{Ak}|^2 |h_{Bk}|^2 p_A}{|h_{Bk}|^2(\zeta_R^2 g_{\alpha k}^2 n_0 + \eta_R) + g_{\alpha k}^2 |h_{Bk}|^4 \; w + n_0}, \tag{3.21}$$

with $g_{\alpha k}$, $\alpha \in \{FG, VG\}$, given by (3.8) or (3.9) dependent upon whether FG or VG has been implemented and

$$w = p_B(\zeta_R - 1)^2 \tag{3.22}$$

denoting the self-interference. This definition of outage probability corresponds to the scenario where users are assigned a contiguous block of subcarriers within the coherence bandwidth. The outage probability on one subcarrier is then equal to that of the contiguous block. However, it was also shown in [91] that, for parallel fading channels, the outage probability of the entire channel could be written as a functional of the subchannel outage probabilities. Thus, the results in [91] extend the utility of per subcarrier outage probability expressions to the scenario in which a contiguous block of subcarriers exceeds the coherence bandwidth of the channel.

3.3.1 Fixed-gain Outage Probability

The outage probability of our FG system at node B is calculated by writing (3.21) in terms of the instantaneous and average per-hop SNRs γ_{ARk}, γ_{RBk} and $\bar{\gamma}_R$ (see (3.6), (3.7), (3.18) and (3.19)). This is done by defining

$$u_1 := \frac{p_A \mu_A + p_B \mu_B}{n_0} \Big/ \frac{\zeta_R^2 g_{FGk}^2 (p_A \mu_A + p_B \mu_B)}{\zeta_R^2 g_{FGk}^2 n_0 + \eta_R}, \tag{3.23}$$

$$u_2 := \frac{w}{p_R \zeta_R^2} = \frac{\bar{\gamma}_{BR} \left(\zeta_R - 1\right)^2}{\bar{\gamma}_{RB} \zeta_R^2}, \tag{3.24}$$

so that we can rewrite (3.21) as

$$\gamma_{Bk}^{(\alpha)} = \frac{\gamma_{ARk}\gamma_{RBk}}{u_1\left(\gamma_{RBk}+1\right)+\gamma_{RBk}^2 u_2+\bar{\gamma}_R}. \tag{3.25}$$

Here, u_1 is the ratio between the received SNR at the relay before amplification to output SNDR at the relay's SEL; u_2 relates to the self-interference.

Since γ_{ARk} and γ_{RBk} are exponentially distributed, the outage probability on a given subcarrier at node B can be calculated to be

$$P_{oB}^{(FG)} = 1 - 2\sqrt{\frac{\gamma_{thB}\left(u_1+\bar{\gamma}_R\right)}{\bar{\gamma}_{RB}(u_2\bar{\gamma}_{RB}\gamma_{thB}+\bar{\gamma}_{AR})}}e^{-\frac{u_1\gamma_{thB}}{\bar{\gamma}_{AR}}} \times K_1\left(2\sqrt{\frac{\gamma_{thB}\left(u_1+\bar{\gamma}_R\right)\left(u_2\bar{\gamma}_{RB}\gamma_{thB}+\bar{\gamma}_{AR}\right)}{\bar{\gamma}_{AR}^2\bar{\gamma}_{RB}}}\right), \tag{3.26}$$

where $K_v(\cdot)$ is the vth order modified Bessel function of the second kind. The proof of this can be found in Appendix A.1. It can be seen that (3.26) reduces to [71, eq. (10)]

$$P_{oB}^{(FG)} = 1 - 2\sqrt{\frac{\gamma_{thB}\left(1+\bar{\gamma}_{AR}\right)}{\bar{\gamma}_{RB}\bar{\gamma}_{AR}}}e^{-\frac{\gamma_{thB}}{\bar{\gamma}_{AR}}}K_1\left(2\sqrt{\frac{\gamma_{thB}\left(1+\bar{\gamma}_{AR}\right)}{\bar{\gamma}_{AR}\bar{\gamma}_{RB}}}\right) \tag{3.27}$$

as $p_{max,R} \to \infty \Rightarrow \eta_R \to 0$ ($\Rightarrow u_1 \to 1, u_2 \to 0$), and $p_B \to 0$; i.e., as distortion goes to zero and the network becomes one-way. Thus, (3.26) provides a generalization of this one-way distortionless result, (3.27).

3.3.2 Variable-gain Outage Probability

Focusing on VG, we use (3.6) and (3.7) to write the instantaneous SINDR, (3.21), at B as

$$\gamma_{Bk}^{(VG)} = \frac{\zeta_R^2 \rho \gamma_{ARk} \gamma_{BRk}}{p_B/n_0 \left(\gamma_{ARk}+1\right) + \gamma_{BRk}\left(b + \gamma_{ARk}\eta_R/n_0\right) + a\gamma_{BRk}^2}, \tag{3.28}$$

where $\rho = \sigma_R^2/n_0, a = \frac{w\rho + p_B\eta_R/n_0}{p_B}, b = \left(p_R + p_B\right)/n_0$. The outage probability can then be calculated to be

$$P_{oB}^{(VG)} = \begin{cases} 1 - \frac{2q_3}{q_1\bar{\gamma}_{BR}\sqrt{q_2 q_3}} e^{-k} K_1\left(2\sqrt{q_2 q_3}\right), & q_1 > 0 \\ 1, & q_1 \leq 0 \end{cases}, \tag{3.29}$$

where

$$\begin{aligned} q_1 &= \zeta_R^2\rho - \gamma_{thB}\bar{\eta}_R, \qquad q_2 = \frac{\gamma_{thB}a}{q_1^2\bar{\gamma}_{AR}} + \frac{1}{q_1\bar{\gamma}_{BR}}, \\ q_3 &= \frac{1}{\bar{\gamma}_{AR}}\left(\frac{p_B\gamma_{thB}}{n_0} + \frac{bp_B\gamma_{thB}^2}{n_0 q_1} + \frac{ap_B^2\gamma_{thB}^3}{{n_0}^2 q_1^2}\right), \\ q_4 &= \frac{p_B\gamma_{thB}}{n_0 q_1\bar{\gamma}_{BR}} + \frac{1}{\bar{\gamma}_{AR}}\left(\frac{b\gamma_{thB}}{q_1} + \frac{2ap_B\gamma_{thB}^2}{n_0 q_1^2}\right). \end{aligned}$$

The proof of this can be found in Appendix A.2. It can be shown that (3.29) reduces to the expression when no distortion is considered, [77, Theorem 1], as $p_{max,R} \to \infty$:

$$\begin{aligned} P_{oB}^{(VG)} = 1 - \frac{2\sqrt{\gamma_{th,B}\left(\gamma_{th,B}\left(\bar{\gamma}_{BR}+\bar{\gamma}_{RB}\right)\bar{\gamma}_{AR} + \bar{\gamma}_{AR}\bar{\gamma}_{RB}\right)}}{\bar{\gamma}_{AR}\bar{\gamma}_{RB}} \times \\ e^{-\frac{\gamma_{th,B}\left(\bar{\gamma}_{BR}+\bar{\gamma}_{RB}+\bar{\gamma}_{AR}\right)}{\bar{\gamma}_{AR}\bar{\gamma}_{RB}}} K_1\left(\frac{2\sqrt{\gamma_{th,B}\left(\gamma_{th,B}\left(\bar{\gamma}_{BR}+\bar{\gamma}_{RB}\right)\bar{\gamma}_{AR} + \bar{\gamma}_{AR}\bar{\gamma}_{RB}\right)}}{\bar{\gamma}_{AR}\bar{\gamma}_{RB}}\right). \end{aligned} \tag{3.30}$$

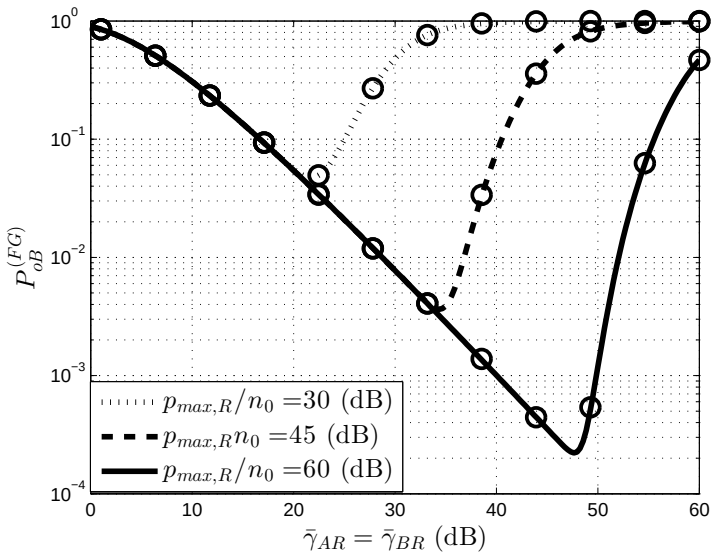

Figure 3.3: Theoretical (lines) vs Monte Carlo (circle marker, 100000 trials) outage probability for FG system with different values of $p_{max,R}/n_0$. We set $g_{FGk} = \mu_A = \mu_B = \gamma_{thB} = n_0 = 1$, $l = 32$ taps, $n = 256$ subcarriers, and vary $p_A = p_B$. The delay profile exponent, δ, was set to 0.

3.3.3 A Brief Discussion of Fixed-gain and Variable-gain Results

A plot of (3.26), the FG outage probability expression, is shown in Fig. 3.3 to demonstrate its accuracy when compared to Monte Carlo simulations. A similar plot is shown for (3.29), the VG outage probability exression, in Fig. 3.4. These simulations were performed for a 256 subcarrier system. The channels were generated from a 32 tap time-domain impulse response with an exponentially decaying profile (see (3.1)). The delay profile exponent, δ, was set to 0.2.

From Figs. 3.3 and 3.4, both systems can be characterized as being in one of two regions: a noise limited region, a distortion limited region.

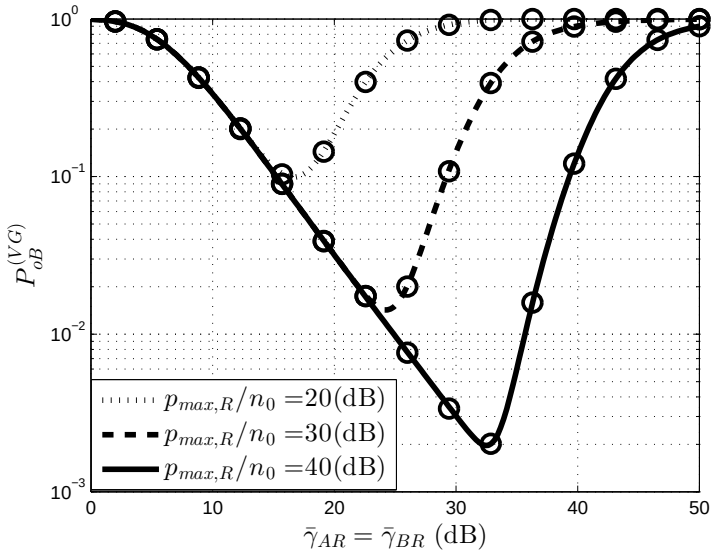

Figure 3.4: Theoretical (lines) vs numerical (markers, 100000 trials) outage probability for VG system with different values of $p_{max,R}/n_0$. $\sigma_R^2 = p_A$, $\mu_A = \mu_B = \gamma_{thB} = n_0 = 1$, $l = 32$ taps, $n = 256$ subcarriers, and vary $p_A = p_B$. The delay profile exponent, δ, was set to 0.

In the former, increasing $\bar{\gamma}_{AR} = \bar{\gamma}_{BR}$[4] will cause a negligible growth in the distortion power, so the outage probability will decrease. However, in the latter, by increasing $\bar{\gamma}_{AR} = \bar{\gamma}_{BR}$ we push the *average* input power into the SEL sufficiently close to $p_{max,R}$. This causes a significant increase in distortion and thus, also, the outage probability. Consequently, we find that the minimum of the outage probability curves occur at the point where the network goes from being distortion limited to noise limited. We will investigate distortion limited networks in section 4.2.

It was also mentioned in section 3.2.2 that for the Bussgang parameters to be uniquely determined by the average input power to the SEL at the relay, σ_R^2, a sufficient number of channel taps was required in the incoming

[4]Since g_{FGk} is fixed for FG and ρ is proportional to $\bar{\gamma}_{AR} = \bar{\gamma}_{BR}$ for the VG case, this corresponds directly to an increase in the *average* input power to the SEL.

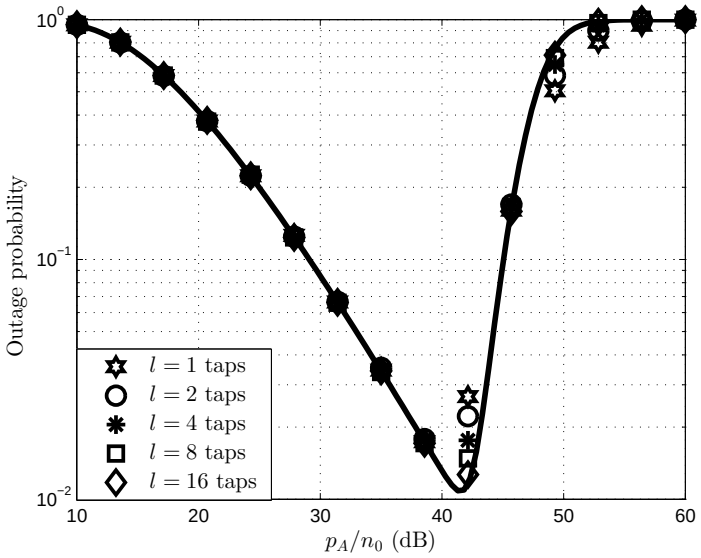

Figure 3.5: Theoretical (lines) vs numerical (50000 trials) (markers) outage probability as function of p_A/n_0 for an FG and VG network. We set $\sigma_R^2 = p_A = p_B$, $\mu_A = \mu_B = \gamma_{thB} = n_0 = 1$, $n = 128$ subcarriers, $p_{max,R}/n_0 = 50$dB, $p_{max,A} = p_{max,B} = \infty$, and δ (delay profile exponent) set to 0.

channels for FG. Specifically, we stated that 16 or more channel taps would be sufficient. We demonstrate this in Fig. 3.5, which shows outage probability as a function of p_A/n_0 for FG when different channel tap numbers are used in the Monte Carlo simulations. From this figure, we can clearly see that as l approaches 16, the theoretical and numerical results coincide very accurately. We also see that when the system is in a noise limited region (i.e., when the curves have a negative gradient), the theoretical model accurately predicts the numerical behavior even when l is small. This is expected because in this region there will be negligible discrepancies between the theoretical and numerical Bussgang coefficients (i.e., $\zeta_R \approx 1$ and $\eta_R \approx 0$ for both numerical and theoretical scenarios). Thus, the discrepancy will have a negligible effect on the resulting outage probability.

3.3.4 Extending Results to Distortion at the Sources

The outage expressions in (3.26) and (3.29) are obtained for the network when no distortion occurs at the source nodes. It is important to note that Bussgang's theorem can be legitimately applied at the source nodes too, and that when doing so this does not affect the applicability of Bussgang's theorem at the relay. This is because the central limit theorem can still be applied in the usual way and implies that the OFDM waveform at the relay will still be well approximated by a complex Gaussian distribution. Furthermore, the distortion produced by the nonlinear amplifier at the source is itself Gaussian. In what follows, we will extend these results to the scenario in which distortion also occurs at the source nodes.

When distortion also occurs at nodes A and B, node B receives extra self interference in the form of its own distortion, as well as distortion from A. Consequently, $\gamma_{Bk}^{(\alpha)}$ (3.21) becomes

$$\underline{\gamma}_{Bk}^{(\alpha)} = \frac{\zeta_A^2\gamma_A^2\zeta_R^2 g_{\alpha k}^2 |h_{Ak}|^2 |h_{Bk}|^2}{\zeta_R^2 g_{\alpha k}^2 |h_{Ak}|^2 |h_{Bk}|^2 \eta_A + |h_{Bk}|^2(\zeta_R^2 g_{\alpha k}^2 n_0 + \eta_R) + |h_{Bk}|^4 g_{\alpha k}^2 \underline{w} + n_0}, \quad (3.31)$$

where

$$\underline{w} = \zeta_B^2\sigma_B^2\left(1-\zeta_R\right)^2 + \eta_B\zeta_R^2. \quad (3.32)$$

By performing basic algebraic manipulations, it is easy to show that

$$\underline{\gamma}_{Bk}^{(\alpha)} < \gamma_{thB} \quad \text{if and only if} \quad \gamma_{Bk}^{(\alpha)}\Big|_{w=\underline{w}} < \frac{p_A\gamma_{thB}}{\sigma_A^2\zeta_A^2 - \gamma_{thB}\eta_A}. \quad (3.33)$$

Consequently, performing the substitutions $w \to \underline{w}$ and $\gamma_{thB} \to \frac{p_A\gamma_{thB}}{\sigma_A^2\zeta_A^2 - \gamma_{thB}\eta_A}$ in the previous outage probability expressions, we can calculate the outage probability of the network when distortion also occurs at the sources.

3.4 Gain Optimization and Interference Removal Assessment

This section describes how we should optimally select

$$\rho := \sigma_R^2/n_0, , \tag{3.34}$$

the *average* normalized input power to the SEL at the relay. For our optimization strategy the optimal value for ρ is independent of whether FG or VG is being considered. Our optimization is done for a network that performs perfect self-interference removal and experiences no distortion at the sources. We then show that when imperfect self-interference removal is executed, the degradation in the network's performance will be negligible.

3.4.1 Gain Optimization

3.4.1.1 One-way Optimization

When perfect self-interference removal is performed, we define the average SNDR at B for FG and VG systems to be

$$\bar{\gamma}_{Bk}^{(\alpha)} := \frac{\mathbb{E}\left[\zeta_R^2 g_{\alpha k}^2 \left|h_A h_B\right|^2 p_A\right]}{\mathbb{E}\left[\left|h_B\right|^2 \left(\zeta_R^2 g_{\alpha k}^2 n_0 + \eta_R\right) + n_0\right]}, \tag{3.35}$$

where $g_{\alpha k}$ is given by (3.8) or (3.9) dependent upon whether FG or VG is being considered, and the expectation is taken with respect to the channel coefficients. The following Lemma formalizes the optimal ρ that maximizes (3.35).

Lemma 1 *The optimal ρ that maximizes* (3.35) *is independent of whether FG or VG is being considered. As $p_{max,R}/n_0$ grows large, the optimal ρ is given to leading order by*

$$\rho_{opt,B} \sim p_{max,R} \Big/ \left(n_0 W \left(\frac{p_{max,R}\mu_B}{2n_0} \right) \right), \tag{3.36}$$

where $W(\cdot)$ is the Lambert-W function (i.e., $x = W(y) \Leftrightarrow y = xe^x$), [2].

Proof For both FG and VG, by calculating $\mathrm{d}\bar{\gamma}_{Bk}^{(\alpha)}/\mathrm{d}\rho = 0$, and after significant algebraic manipulation, we obtain $\rho_{opt,B} = \arg_\rho \left\{ \mathrm{erfc}\left(x(\rho)\right) = \frac{ux(\rho)}{p_{max,R}} \right\}$, where $u = \frac{2n_0}{\mu_B\sqrt{\pi}}$ and $x(\rho) = p_{max,R}/\rho n_0$. To leading order, we have $\rho_{opt,B} \sim \arg_\rho \left\{ \frac{e^{-x(\rho)^2}}{\sqrt{\pi}x(\rho)} = \frac{ux(\rho)}{p_{max,R}} \right\}$. The stated result follows immediately. ■

3.4.1.2 Bidirectional Optimization

To optimize the bi-directional performance, we choose

$$\rho_{opt,bi} = \arg_\rho \max \left\{ \min\{\bar{\gamma}_{Bk}^{(\alpha)}, \bar{\gamma}_{Ak}^{(\alpha)}\} \right\}, \tag{3.37}$$

where $\bar{\gamma}_{Ak}^{(\alpha)}$ is the average SNDR at node A, given by

$$\bar{\gamma}_{Ak}^{(\alpha)} := \frac{\mathbb{E}\left[\zeta_R^2 g_{\alpha k}^2 \left|h_A h_B\right|^2 p_B\right]}{\mathbb{E}\left[\left|h_A\right|^2 \left(\zeta_R^2 g_{\alpha k}^2 n_0 + \eta_R\right) + n_0\right]}. \tag{3.38}$$

Lemma 2 formalizes the solution to (3.37).

Lemma 2 *The bi-directional performance is optimized when* (3.37) *is sat-*

isfied. The solution to (3.37) *is given by*

$$\rho_{opt,bi} = \begin{cases} \rho_{opt,B}, & \bar{\gamma}_{Bk}^{(\alpha)}\left(\rho_{opt,B}\right) \leq \bar{\gamma}_{Ak}^{(\alpha)}\left(\rho_{opt,B}\right) \\ \rho_{opt,A}, & \bar{\gamma}_{Ak}^{(\alpha)}\left(\rho_{opt,A}\right) \leq \bar{\gamma}_{Bk}^{(\alpha)}\left(\rho_{opt,A}\right) \\ \rho^{\star}, & \text{otherwise} \end{cases}$$

where $\rho^{\star} = \arg_{\rho}\left\{\bar{\gamma}_{Ak}^{(\alpha)} = \bar{\gamma}_{Bk}^{(\alpha)}\right\}$, $\rho_{opt,B}$ *is given asymptotically by* (3.36), *and* $\rho_{opt,A}$ *is given (similar to* (3.36)*) asymptotically by*

$$\rho_{opt,A} \quad \sim \quad p_{max} \Big/ \left(n_0 W\left(\frac{p_{max,R}\mu_A}{2n_0}\right)\right). \tag{3.39}$$

Moreover, we have $\min_i\{\rho_{opt,i}\} \leq \rho_{opt,bi} \leq \max_i\{\rho_{opt,i}\}$.

Proof This is seen by noting that $\bar{\gamma}_{Ak}^{(\alpha)}$ and $\bar{\gamma}_{Bk}^{(\alpha)}$ have single global maxima as functions of ρ. ■

Figs. 3.6 and 3.7 show plots of the numerically calculated total outage probability [92]

$$P_{o,AB}^{(\alpha)} := \mathbb{P}\left[\gamma_{Ak}^{(\alpha)} < \gamma_{th,A} \cup \gamma_{Bk}^{(\alpha)} < \gamma_{thB}\right] \tag{3.40}$$

as a function of $p_{max,R}/n_0$ for FG and VG systems, respectively. These figures also show plots when rudimentary FG and VG gains are applied at the relay. These are given, respectively, by

$$g_{FGr} = \sqrt{\frac{p_{max,R} r}{p_A\mu_A + p_B\mu_B + n_0}} \tag{3.41}$$

or

$$g_{VGr} = \sqrt{\frac{p_{max,R} r}{p_A \left|h_{Ak}\right|^2 + p_B \left|h_{Bk}\right|^2 + n_0}}, \tag{3.42}$$

where r defines the fraction of the total available transmit power that the relay utilizes. In Figs. 3.6 and 3.7, the rudimentary curves approach the $\rho_{opt,bi}$ curve; then deviate away. This is because, during the approach, they underestimate the optimal gain; and during the deviation, they overestimate this gain. The point at which the curves end approaching and begin to deviate are points of optimal performance. These points touch the $\rho_{opt,bi}$ curve, suggesting that the $\rho_{opt,bi}$ gains achieve near optimal outage probability - they were designed to maximize the ratio of the average signal to average noise and distortion power. As an extra point of discussion, by inspecting very closely we can see from these figures that increasing the network's asymmetry (going from $\mu_A = \mu_B$ to $0.1\mu_A = \mu_B$) allows the gain with $r = 0.15$ to outperform that with $r = 0.1$ over a very slightly larger range of $p_{max,R}/n_0$. This suggests that the negative effects of distortion (which are more prevalent for larger r) are outweighed by the requirement for the relay to ensure that a signal is received at the distant destination in the asymmetric setting. Indeed, this reasoning turns out to be true, and we will discuss it in more detail in section 3.5.3 and Fig. 3.13 when we consider optimal power allocation strategies.

3.4.2 Interference Removal Assessment

We now show that the average self-interference term, normalized by n_0 and evaluated at $\rho_{opt,bi}$, is negligible for realistic networks; i.e., those for

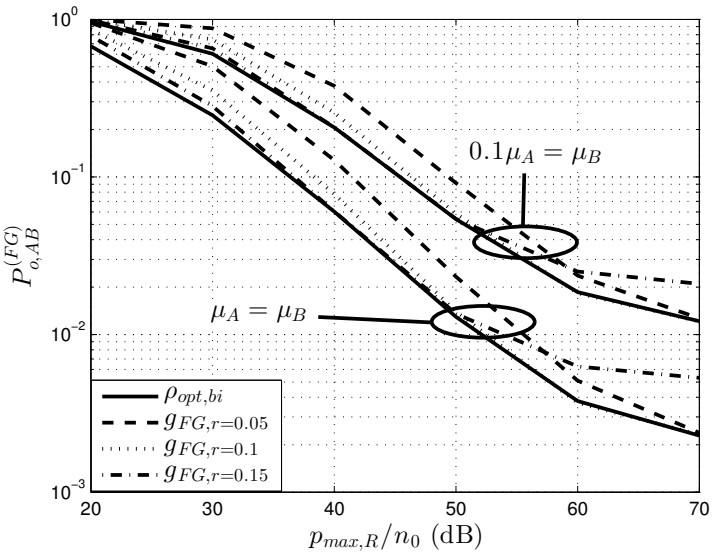

Figure 3.6: Monte Carlo based (50000 trials) FG total outage probability, (3.40), when gains from Lemma 2 and (3.41) are applied at the relay. $\mu_A = 1$, $\gamma_{th,A} = \gamma_{thB} = 10$, $n_0 = 1$, $\bar{\gamma}_{AR} = \bar{\gamma}_{BR} = 40$ dB, the number of taps $l = 32$, profile decay exponent $\delta = 0.1$ and vary $p_{max,R}$.

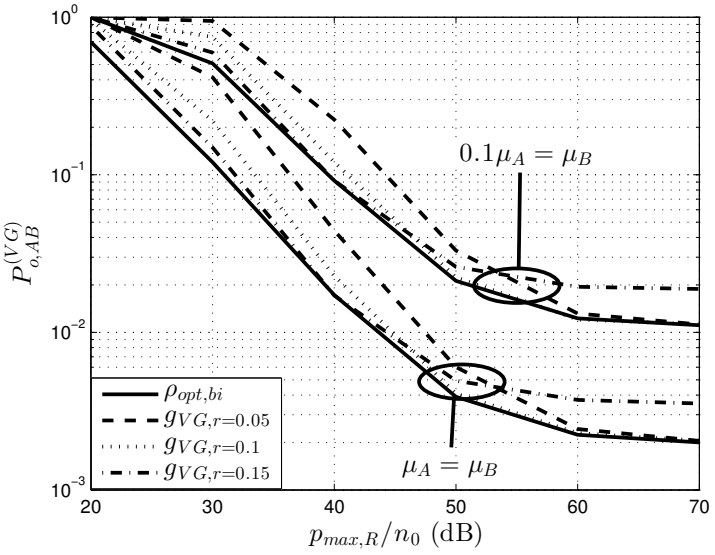

Figure 3.7: Monte Carlo based (50000 trials) VG total outage probability, (3.40), when gains from Lemma 2 and (3.42) are applied at relay. We fix $\mu_A = 1$, $\gamma_{thA} = \gamma_{thB} = 10$, $n_0 = 1$, $\bar{\gamma}_{AR} = \bar{\gamma}_{BR} = 40$ dB, $l = 32$ taps, profile decay exponent $\delta = 0.1$ and vary $p_{max,R}$.

which $p_{max,R} \gg n_0$. We do this by considering the FG self-interference and reason that the self-interference term for VG will be on the same order of magnitude. With g_{FGk} as in (3.8), the average normalized self-interference term at B is

$$w_{avg}(\rho) = \frac{\mathbb{E}\left[g_{FGk}^2 |h_{Bk}|^4 \, w\right]}{n_0} = \frac{2 g_{FGk}^2 \mu_B^2 p_B (\zeta_R - 1)^2}{n_0}. \tag{3.43}$$

The following lemma is used to upper bound (3.43).

Lemma 3 *Without loss of generality, assume* $\max\{\rho_{opt,A}, \rho_{opt,B}\} = \rho_{opt,B}$. *With* $b = \frac{p_{max,R}\mu_B}{2n_0}$, *as* $p_{max,R}/n_0$ *grows large so that* (3.36) *becomes asymptotically exact, we have*

$$w_{avg}(\rho_{opt,bi}) \;\; \leq \;\; w_{avg}(\rho_{opt,B}) \leq \frac{p_B \mu_B (2\log b)^2}{(p_A \mu_A b W(b))}. \tag{3.44}$$

Proof The first inequality follows from the monotonicity of $w_{avg}(\rho)$ with ρ. The second inequality follows by evaluating ζ_R at $\rho_{opt,B}$ and performing a first order expansion at $p_{max,R} \to \infty$, so we have

$$\zeta_R(\rho_{opt,B}) = 1 - e^{-W\left(\frac{p_{max,R}\mu_B}{2n_0}\right)} + \sqrt{\frac{\pi W\left(\frac{p_{max,R}\mu_B}{2n_0}\right)}{2}} \operatorname{erfc}\left(\sqrt{W\left(\frac{p_{max,R}\mu_B}{2n_0}\right)}\right),$$

which is given asymptotically by

$$\zeta_R(\rho_{opt,B}) \overset{p_{max,R}}{\sim} 1 - \frac{\log\left(\frac{p_{max,R}\mu_B}{2n_0}\right)}{\left(\frac{p_{max,R}\mu_B}{2n_0}\right) \log\left(\frac{p_{max,R}\mu_B}{2n_0}\right)^{\frac{1}{\log\left(\frac{p_{max,R}\mu_B}{2n_0}\right)}}} + e^{-W\left(\frac{p_{max,R}\mu_B}{2n_0}\right)} \left(\sqrt{\frac{1}{2}} - \frac{\sqrt{\pi}}{2\sqrt{2}\pi W\left(\frac{p_{max,R}\mu_B}{2n_0}\right)}\right),$$

and can be bounded according to

$$\zeta_R\left(\rho_{opt,B}\right) \;\geq\; 1 - \frac{\log\left(\frac{p_{max,R}\mu_B}{2n_0}\right)}{\left(\frac{p_{max,R}\mu_B}{2n_0}\right)}. \tag{3.45}$$

This gives $\left(\zeta_R\left(\rho_{opt,B}\right)-1\right)^2 \leq \left(\log b \Big/ b\right)^2$. The stated result follows by substituting this inequality into (3.43). ■

It is easy to see that the upper bound in (3.44) becomes negligible for realistic network setups (i.e., when $p_{max,R} \gg n_0$). Fig. 3.8 shows $w_{avg}\left(\rho_{opt,B}\right)$ and its upper bound, (3.44). For typical relaying scenarios (i.e., when $p_{max,R} \gg n_0$), $w_{avg}\left(\rho_{opt,B}\right)$ is orders of magnitude smaller than n_0. As an example, from this figure when $p_{max,R}/n_0 = 50$dB, the average interference term is at least 30dB smaller than the noise term. Consequently, when maximizing the average SNDR, the network's performance is degraded much more severely by noise than self-interference.

3.5 Power Allocation Strategies with Perfect Self-interference Removal

In this section, we provide a comprehensive understanding of how power should be allocated among the nodes of the network presented in section 3.2 when perfect interference removal has been performed and distortion occurs only at the relay. Note, in order for perfect self-interference removal to be performed as per (3.15), it is necessary that A and B have access to the distortion characteristics of the relay's amplifier as well as the relevant CSI.

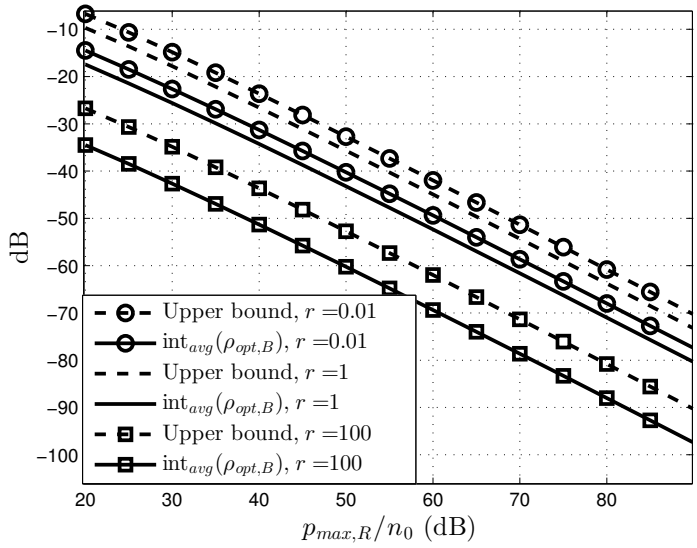

Figure 3.8: Plot of $w_{avg}(\rho_{opt,B})/n_0$, expressed in dB, (solid line) and its upper bound given by Lemma 3 as functions of $p_{max,R}/n_0$, for different $r := p_A\mu_A/p_B\mu_B$.

3.5.1 Power Allocation when Relay is not Considered in Power Budget

Our goal is to optimize the performance of our system by effectively allocating power among its nodes. To do this, we must first select a suitable performance metric. We might choose the total outage probability, which is defined to be

$$P_{o,AB}^{(\alpha)} = \mathbb{P}\left[\gamma_{Ak}^{(\alpha)} \leq \gamma_{th,A} \cup \gamma_{Bk}^{(\alpha)} \leq \gamma_{thB}\right], \tag{3.46}$$

where $\gamma_{\beta k}^{(\alpha)}$ and $\gamma_{th,i}$ are the instantaneous per-direction SNDRs and SNDR protection threshold at node $\beta \in \{A, B\}$, respectively. Alternatively, we might choose the average sum SER of the system. To the best of the authors' knowledge, no closed form solutions for these metrics exist. Con-

sequently, we focus on an alternative cost funtion. We reason that the overall performance of the system will be limited by the minimum of the directional performance. Furthermore, it is clear that there will be a (approximately[5]) monotonic relationship between SNDR and standard metrics such as outage probability or SER. Consequently, to optimize the performance of the system, we maximize the minimum of the directional average SNDRs. Mathemtically, our problem is:

$$\text{maximize } \min\left\{\bar{\gamma}_{Ak}^{(\alpha)}, \bar{\gamma}_{Bk}^{(\alpha)}\right\}, \quad \text{s.t.} \quad p_A + p_B \leq p \tag{3.47}$$

where

$$\bar{\gamma}_{Ak}^{(\alpha)} := \frac{p_B g_{FGk}^2 \zeta_R^2 \mu_A \mu_B}{\mu_A \left(g_{FGk}^2 \zeta_R^2 n_0 + \eta_R\right) + n_0} \tag{3.48}$$

$$\bar{\gamma}_{Bk}^{(\alpha)} := \frac{p_A g_{FGk}^2 \zeta_R^2 \mu_A \mu_B}{\mu_B \left(g_{FGk}^2 \zeta_R^2 n_0 + \eta_R\right) + n_0} \tag{3.49}$$

are the average directional SNDRs at nodes A and B, respectively, and we choose $g_{\alpha k}^2$ as in (3.8) to make the problem more tractable for VG. As we shall see later, this choice for $g_{\alpha k}^2$ works well when optimizing both FG and VG systems. This is not surprising for the FG system, but perhaps more so for the VG system. By inspecting the FG and VG gains defined in (3.8) and (3.9), we see that g_{FGk}^2 for the FG system is equivalent to g_{VGk}^2 for the VG system when the channel gains are evaluated at their means. This fact

[5]We say approximately because the end-to-end average SNDR of a relay link is a function of multiple parameters; e.g., source/relay transmit power, the average fading coefficient of the first/second hop, etc. Thus, it will be possible to find different parameterizations that give the same average end-to-end average SNDR, but acheive different values of another performance metric; e.g., outage probability or SER.

goes someway to explaining the generality of our method. We then use

$$p_i^\star \tag{3.50}$$

to denote the solutions of (3.47).

Because $\bar{\gamma}_{Ak}^{(\alpha)}$ and $\bar{\gamma}_{Bk}^{(\alpha)}$ are monotonically increasing with p_B and p_A, respectively, the solution to (3.47) occurs when

$$\bar{\gamma}_{Ak}^{(\alpha)} = \bar{\gamma}_{Bk}^{(\alpha)} \text{ and } p_A + p_B = p. \tag{3.51}$$

Since ζ_R and η_R are not functions of p_A or p_B, we can expand the left-hand equation of (3.51) (including the gain terms), substituting $p_B = p - p_A$, to obtain the quadratic equation

$$x p_A^2 + y p_A + z = 0, \tag{3.52}$$

where

$$x = (\mu_A - \mu_B)\left(\eta_R(\mu_A + \mu_B) + 2n_0\right) \tag{3.53}$$

$$\begin{aligned} y = & -p(\mu_A - \mu_B)(n_0 + \eta_R\mu_B) + n_0(2n_0 + \eta_R(\mu_A + \mu_B)) \\ & + p\mu_B(2n_0 + \eta_R(\mu_A + \mu_B)) + n_0\zeta_R^2(\mu_A + \mu_B)\gamma_R^2 \end{aligned} \tag{3.54}$$

$$z = -n_0 p(\eta_R\mu_B + n_0) - \mu_B p^2(\eta_R\mu_B + n_0) - \mu_B n_0 p\gamma_R^2\zeta_R^2 \tag{3.55}$$

and p_B is written as

$$p_B = p - p_A. \tag{3.56}$$

Clearly, the positive root of (3.52) is the one that should be chosen, which gives

$$p_A^\star = \frac{-y + \sqrt{y^2 - 4xz}}{2x}. \tag{3.57}$$

We now have a complete solution to the problem presented in (3.47). To obtain $p_B^\star$, we calculate $p - p_A^\star$.

Figs. 3.9 and 3.10 show plots of the total outage probability, (3.46), as a function of $p_{max,R}/n_0$ for an FG and VG system, respectively. In these figures, power is allocated between nodes A and B according to 1) our optimal scheme, and 2) a rudimentary scheme in which p_A is fixed to some constant fraction of the total available power p, where $p_B = p - p_A$. In this model, 16 channel taps are considered in the channel models used to generate these plots. It is clear from these figures that our optimal power allocation strategy provides the best performance because it lower bounds all the other rudimentary power allocation strategies. Interestingly, one of the rudimentary approaches also provides near optimal performance over the entire $p_{max,R}$ region for this particular setup (i.e., $p_A = 0.1p$). It is important to note, however, that the rudimentary power allocation schemes in these figures will not be robust to changes in the network's asymmetry (i.e., changes in μ_A/μ_B). Consequently, the rudimentary approaches that provide near optimal performance in these figures will perform sub-optimally if the network's asymmetry were to change. The behavior of the optimal power allocation scheme as a function of network asymmetry will be discussed in

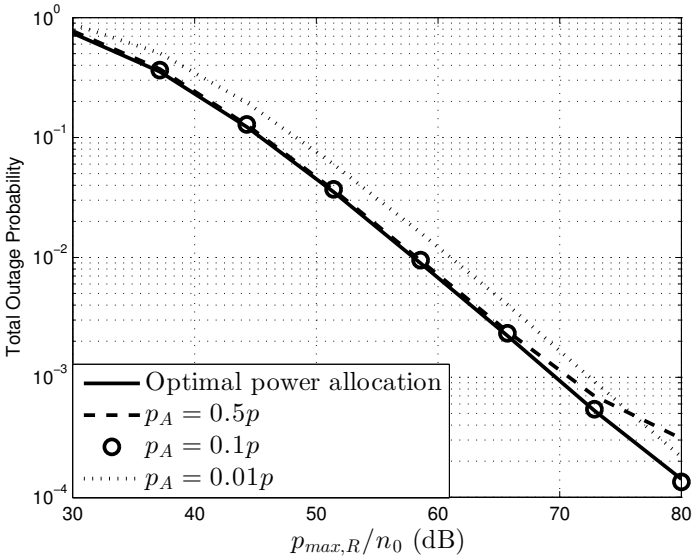

Figure 3.9: Monte Carlo based (100000 trials) FG total outage probability for two-way system with asymmetric channel, $\mu_B = 0.01\mu_A$, 16 channel taps, p the total power budget of nodes A and B is equal to $p_{max,R}$, and the profile decay exponent $\delta = 0.1$. For rudimentary gains, $\sigma_R^2 = 0.1p_{max,R}$.

detail in section 3.5.3.

3.5.2 Power Allocation when Relay is Considered in Power Budget

In this section, we take a more complete view of the power allocation problem considered in section 3.5.1. In particular, we assume that the relay's transmit power is part of the total power budget. This modified problem takes the following form:

$$\text{maximize } \min\left\{\bar{\gamma}_{Ak}^{(\alpha)}, \bar{\gamma}_{Bk}^{(\alpha)}\right\}, \text{ s.t. } p_A + p_B + p_R \leq p. \tag{3.58}$$

At present, (3.58) is neither convex nor log-convex. Strictly speaking, the objective function is neither concave nor log-concave. Consequently,

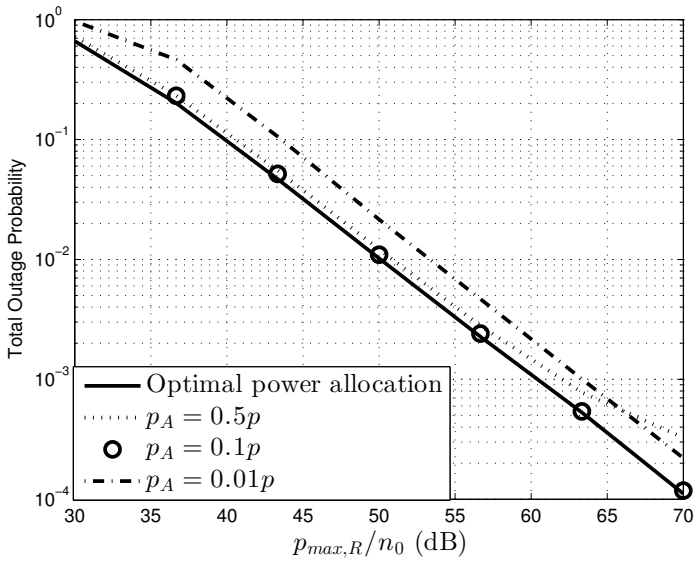

Figure 3.10: Monte Carlo based (100000 trials) VG total outage probability for two-way system with asymmetric channel, $\mu_B = 0.01\mu_A$, $p = p_{max}$, 16 taps, profile decay exponent $\delta = 0.1$. For rudimentary gains, $\sigma_R^2 = 0.1p_{max}$.

the fruitful theory of convex optimization cannot be employed to solve our problem in its current form. It turns out, however, that there exists a particular substitution that we can apply to convert our non-concave objective function into one that is log-concave. This is formalized in the following lemma.

Lemma 4 *By applying the substitution*

$$p_{i\log} = \log p_i,\ i \in \{A, B, R\} \tag{3.59}$$

the objective function in (3.58) *becomes log-concave as a function of* $p_{i\log}$ *for* $0 \leq p_R \leq p_{max}$ *and* $p_A, p_B \geq 0$.

Proof Since the $\min\{\cdot,\cdot\}$ operator preserves concavity, if

$$\frac{\mathrm{d}^2 \log \bar{\gamma}_{Ak}^{(\alpha)}}{\mathrm{d}\left(\log p_i\right)^2} := \frac{\mathrm{d}^2 \log \bar{\gamma}_{Ak}^{(\alpha)}}{\mathrm{d}p_{i\log}^2} \leq 0 \; \forall \; i \in \{A, B, R\}, \; p_{R\log} \leq \log p_{max,R}, \quad (3.60)$$

we will reach our result. Note,

$$p_i \frac{\mathrm{d}^2 \log \bar{\gamma}_{Ak}^{(\alpha)}}{\mathrm{d}p_i^2} + \frac{\mathrm{d} \log \bar{\gamma}_{Ak}^{(\alpha)}}{\mathrm{d}p_i} \leq 0 \quad (3.61)$$

implies (3.60). Demonstrating (3.61) for $i \in \{A, B\}$ is trivial. Letting $\bar{\gamma}_{A,k,nd}^{(\alpha)}$ denote the equivalent average SNDR expression when no distortion occurs (i.e., when $\eta_R = 0$ and $\zeta_R^2 = 1$) we can also trivially demonstrate

$$p_R \frac{\mathrm{d}^2 \log \bar{\gamma}_{A,k,nd}^{(\alpha)}}{\mathrm{d}p_R^2} + \frac{\mathrm{d} \log \bar{\gamma}_{A,k,nd}^{(\alpha)}}{\mathrm{d}p_R} \leq 0. \quad (3.62)$$

Furthermore, it is easy to see that

$$\frac{\mathrm{d} \log \bar{\gamma}_{A,k,nd}^{(\alpha)}}{\mathrm{d}p_R} \geq \frac{\mathrm{d} \log \bar{\gamma}_{Ak}^{(\alpha)}}{\mathrm{d}p_R} \text{ and } \frac{\mathrm{d}^2 \log \bar{\gamma}_{A,k,nd}^{(\alpha)}}{\mathrm{d}p_R^2} \geq \frac{\mathrm{d}^2 \log \bar{\gamma}_{Ak}^{(\alpha)}}{\mathrm{d}p_R^2},$$

for $p_R \leq p_{max}$, which immediately gives us our result. ■

Thus, by applying the substitution in (3.59) and noting that $\{(p_{A\log}, p_{B\log}, p_{R\log})\,; e^{p_{A\log}} + e^{p_{B\log}} + e^{\bar{p}_R} \leq p\}$ is convex, (3.58) becomes convex. To obtain $p_i^\star$ we invert (3.59).

Although (3.58) can be converted into a convex problem, we can take extra steps - similar to the quadratic based steps above - to simplify it further. To do this, let us begin by making some observations about (3.58).

Similar to before, the solutions $p_i^\star$, $i \in \{A, B, R\}$, satisfy

$$\bar{\gamma}_{Ak}^{(\alpha)} = \bar{\gamma}_{Bk}^{(\alpha)} \text{ and } p_A + p_B + p_R = p. \tag{3.63}$$

However, this time we have two equations with three unknowns. Thus, there will be more than one tri-variate solution to (3.63). Also, p_R is not selected by the designer explicitly. Instead, σ_R^2 is selected, which acts as an argument for the gains defined in (3.8) and (3.9). By rearranging (2.36), we obtain

$$\sigma_R^2 = \left(\frac{1 + \frac{p_R}{p_{max,R}} W\left(-\frac{p_{max,R}}{p_R} e^{-\frac{p_{max,R}}{p_R}} \right)}{p_R} \right)^{-1}, \tag{3.64}$$

where $W(\cdot)$ is the Lambert-W function.

We can use the equality constraint in the right hand side of (3.63) to remove p_A from $\bar{\gamma}_{Ak}^{(\alpha)} = \bar{\gamma}_{Bk}^{(\alpha)}$. After some algebraic manipulation, this gives

$$x p_B^2 + y p_B + z = 0,$$

where

$$x = (\mu_B - \mu_A)(n_0 + n_0 + \eta_R(\mu_A + \mu_B))$$

$$\begin{aligned} y = {} & n_0(n_0 - \mu_A(p - p_R)) + \eta_R \mu_A (n_0 - 2p_R\mu_A + 2p\mu_A) + \\ & n_0(n_0 + (p - p_R)(2\mu_A - \mu_B)) + n_0\eta_R\mu_B + \zeta^2 n_0 \sigma_R^2 (\mu_A + \mu_B) \end{aligned}$$

$$\begin{aligned} z &= (p_R - p)((n_0 - \mu_A (p_R - p))(n_0 + \mu_A \eta_R)) \\ &\quad + (p_R - p)\, \zeta^2 \mu_A n_0 \sigma_R^2. \end{aligned}$$

Note, σ_R^2 is a function of p_R (see (3.64)). We now have a functional relationship between p_B and p_R when (3.63) is satisfied. By substituting

$$p_A = p - p_B\,(p_R) - p_R, \tag{3.65}$$

where $p_B\,(p_R)$ is given by

$$p_B\,(p_R) = \frac{-b + \sqrt{b^2 - 4ac}}{2a}, \tag{3.66}$$

into $\bar{\gamma}_{Ak}^{(\alpha)}$, the number of variables being searched over falls from three to one. The problem in (3.58) then reduces to

$$\text{maximize } \bar{\gamma}_{Ak}^{(\alpha)}, \text{ s.t. } p_R \leq p_{max,R}, \text{ and (3.65), (3.66) are satisfied} \tag{3.67}$$

This problem is still log-concave as a function of $p_{R\log}$. Thus, a standard convex optimization tool can be used to find $p_{R\log}^{\star}$ (the optimal value of $p_{R\log}$). $p_R^{\star}$ is obtained by calculating $e^{p_{R\log}^{\star}}$, $p_B^{\star}$ can then be obtained from (3.66), so that $p_A^{\star}$ can be obtained from (3.65).

Figs. 3.11 and 3.12 show plots of the total outage probability as a function of $p_{max,R}/n_0$ for FG and VG systems with different power allocation schemes: optimal allocation and rudimentary allocation schemes where p_R and p_B are constant fractions of p_{max} and p_A, respectively. We see in Fig. 3.12 that the performance of the VG system when power is allocated according to $p_R = 0.15 p_{max,R},\ p_B = 0.1 p_A$ is *slightly* better than our proposed

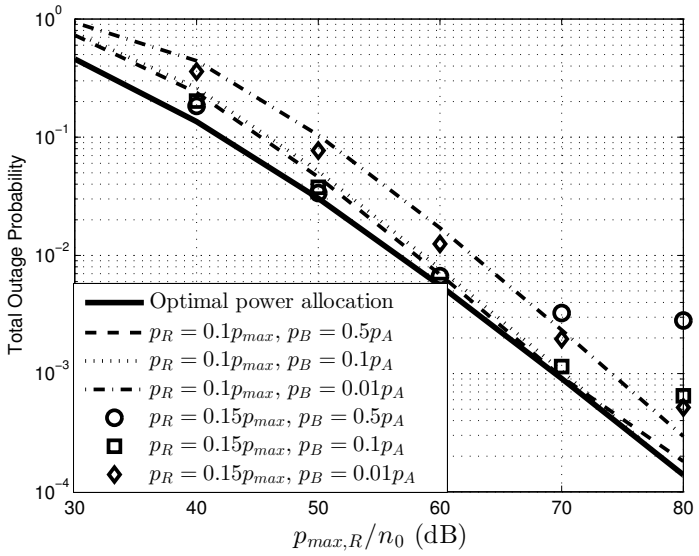

Figure 3.11: Monte Carlo based (100000 trials) FG total outage probability for two-way system with asymmetric channel, $\mu_B = 0.01\mu_A$, $p = 2p_{max,R}$ according to the constraint (3.58) and 16 channel taps, $\delta = 0.1$.

power allocation scheme at $p_{max,R}/n_0 \approx 60$dB. Note, however, that as before the rudimentary power allocation schemes are not robust to changes in the network's asymmetry. This is testament to the fact that our optimization is being performed with respect to the average SNDR of the system, while the results are presenting total outage probability (cf. (3.46)). Nevertheless, our methods are clearly effective.

3.5.3 Discussion and Further Results

In Fig. 3.13, we now provide insight into the behavior of our complete power allocation scheme, (3.67), as the network's asymmetry changes. This figure also contains plots of the distortion and maximum transmit power at the relay. For small μ_B/μ_A, we see that $p_B^\star$ is much larger than $p_A^\star$. If this were not the case, as μ_B/μ_A decreased, the power received from A would tend to

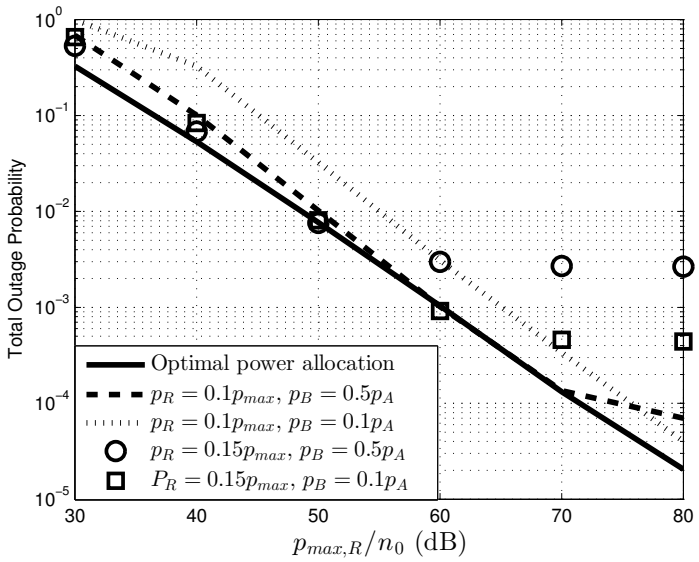

Figure 3.12: Monte Carlo based (100000 trials) VG total outage probability for two-way system with asymmetric channel, $\mu_B = 0.01\mu_A$, $p = 2p_{max,R}$ according to the constraint (3.58) and 16 channel taps, $\delta = 0.1$.

dominate that received from B. Because the relay is also subject to a power constraint, if such a scenario arose, it would be forced to allocate more of its own power budget to forward A's transmission, rather than B's. We can also see that as μ_B/μ_A decreases, the relay is pushed closer to its maximum transmit power threshold, which corresponds directly to an increase in the distortion power, η_R. Consequently, for largely asymmetric networks the negative effects of distortion are outweighed by the desire for the relay to ensure that signals are received at the destinations.

3.6 Summary

In this chapter, we derived theoretical results for the outage probability of two-way AF relay networks that have a nonlinear amplifier at the relay. We showed how these results can be extended trivially to the scenario in which

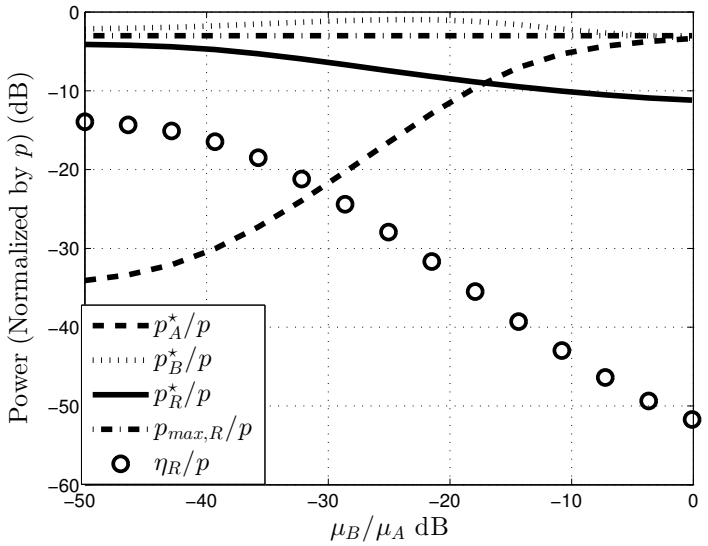

Figure 3.13: Power plots as functions of the average channel gain ratio when power is allocated according to (3.67) with $n_0 = 1$.

distortion also occurs at the sources. We then optimized the amplification factor of such systems. Following this, we considered the behavior of the network when perfect and imperfect self-interference removal are performed. It was shown that, in regions of interest, the optimal performance attained by the two approaches is essentially the same. Finally, we studied the problem of allocating power among the nodes of the network. We considered two allocation problems: 1) where the destination nodes are subject to a total power budget, and the relay is limited by its own independent power constraint; 2) where the relay's transmit power is included within the total power budget, whilst also being subject to an independent power constraint. A closed form solution is obtained for the former. For the latter, we have shown that the problem can be converted into one that is convex and thus solvable using convex optimization techniques. Results were then presented to demonstrate the efficacy of our approaches.

Chapter 4

One-way Networks: Distortion Limitation, Symbol Error Rate and Experimental Testing

This chapter is the second of our research chapters. In it, we continue our study of the system described in section 3.2. In partiular, we focus on the special case when the network becomes one-way; i.e., $p_B \to 0$. For this special case, we begin by studying the system when distortion power dominates noise power. The log-log decay of the outage probability with the source/relay transmit powers is shown to be (asymptotically) 0 for FG and 1 for VG if distortion occurs at the relay; if distortion occurs only at the source, this decay will be 1 for both. With $\epsilon_\beta = n_0/\eta_\beta$ (n_0 the noise power, η_β the non-linear distortion power at node $\beta \in \{S, R\}$, i.e., the source or relay), we then demonstrate the emergence of an ϵ-critical signal-to-noise plus distortion ratio (SNDR) threshold (a threshold that emerges when $\min\{\epsilon_\beta\}$ becomes small) for both forwarding protocols. We

show that crossing this threshold in distortion limited regions will cause a phase transition in the network's outage probability. Our results reveal that, for distortion limited networks, small reductions in the required end-to-end transmission rate can have significant reductions in the network's outage probability.

Following the distortion limited analysis, we calculate a closed form expression for the SER of the one-way FG system with general noise conditions. From this, we are able to calculate the optimal relay gain that should be applied to minimize the SER. Finally, we demonstrate the performance gain achieved through the application of the optimal relay gain through both numerical simulations and real-world experimentation using a USRP relay network testbed. The real-world experimentation, section 4.4, was set up and performed by David Halls, of Toshiba Research Laboratory, Bristol.

4.1 Introduction

As was discussed in the introduction of the previous chapter, understanding the effects of distortion in OFDM-based relaying systems is of great practical importance. The literature pertaining to the study of peak-power constrained OFDM-based relaying systems was discussed in section 3.1. Section 3.1 also included a table (Table 3.1) to provide a high level overview of previous pertinent literature and how the work contained in Chapters 3 and 4 relates to this larger body of work. The focus of Chapter 3 was to study peak-power constrained OFDM-based two-way relaying systems. To the best of the author's knowledge, such systems have never been studied in the general two-way relaying scenario prior to this work.

In this chapter, we focus on the one-way special case of the network studied in the previous chapter. While such networks have been studied in the literature prior to our work, to the best of the author's knowledge no attempts have been made to establish:

1. how extreme distortion levels affect the performance of such systems [11] (here we find that FG is more significantly affected than VG),

2. how theoretical gain optimization affects the performance of a real world test-bed [10] (here we find that it is very affective).

It is the goal of this chapter to fill in these research gaps.

4.2 Distortion Limited Networks

Consider the system model in section 3.2 when $p_B \to 0$. We begin by considering general noise and distortion conditions, with the aim of quantifying the effects that distortion limitations have on performance.

The per-subcarrier outage probability at B is defined to be

$$P_{oB}^{(\alpha)} := \mathbb{P}\left[\gamma_{Bk}^{(\alpha)} \leq \gamma_{th,B}\right], \tag{4.1}$$

where $\gamma_{Bk}^{(\alpha)}$ is the one-way SNR (from (3.21), letting $p_B \to 0$) and $\gamma_{th,B}$ is an SNDR protection threshold. For FG, the solution to (4.1) is given in [10, eq. (16)] when relay distortion occurs, and can be obtained as a special case of (3.26) when the destination power goes to zero. It is given by

$$P_{oB}^{(FG)} = 1 - 2e^{-\frac{u_1\gamma_{th,B}}{\bar{\gamma}_{AR}}}\sqrt{\frac{(u_1+\bar{\gamma}_{AR})\gamma_{th,B}}{\bar{\gamma}_{AR}\bar{\gamma}_{RB}}}K_1\left(2\sqrt{\frac{(u_1+\bar{\gamma}_{AR})\gamma_{th,B}}{\bar{\gamma}_{AR}\bar{\gamma}_{RB}}}\right). \tag{4.2}$$

For VG, the outage probability of the two-way network when distortion occurs at the relay is given by (3.29). Again, by considering the limit as the transmit power at the destination node goes to zero, (4.1) becomes

$$P_{oB}^{(VG)} = \begin{cases} 1 - 2e^{-q_6}\sqrt{q_5}K_1\left(2\sqrt{q_5}\right), & \zeta_R^2\sigma_R^2 > \gamma_{th,B}\eta_R \\ 1, & \zeta_R^2\sigma_R^2 \leq \gamma_{th,B}\eta_R \end{cases}, \tag{4.3}$$

when distortion occurs only at the relay; where $K_1(\cdot)$ is the first order modified Bessel function of the second kind,

$$q_5 := \frac{\gamma_{th,B}}{\bar{\gamma}_{AR}\bar{\gamma}_{RB,cr}}\left(1 + \frac{\bar{\gamma}_{RB}\gamma_{th,B}}{\bar{\gamma}_{RB,cr}}\right); \quad q_6 := \frac{\gamma_{th,B}}{\bar{\gamma}_{RB,cr}}\left(1 + \frac{\bar{\gamma}_{RB}}{\bar{\gamma}_{AR}}\right);$$

we define

$$\bar{\gamma}_{RB,cr} := \bar{\gamma}_{RB} - \frac{(1+\gamma_{th,B})\mu_B}{\epsilon_R} \tag{4.4}$$

to be the average *critical* second-hop SNR[1], and $\epsilon_R := n_0/\eta_R$. As discussed in section 3.3.4, the solution for the outage probability when distortion occurs only at the relay can be trivially extended to the scenario in which distortion is also introduced at the source by making the substitution $\gamma_{th,B} \to \gamma_{th,B}p_A/(\sigma_S^2\zeta_S^2 - \gamma_{th,B}\eta_S)$, where $\sigma_S^2\zeta_S^2 - \gamma_{th,B}\eta_S \leq 0$ implies outage will occur surely[2].

4.2.1 Distortion Limited Performance

Let us consider the behavior of $P_{oB}^{(\alpha)}$ when the distortion power dominates the noise power. To do this, we make the following assumptions:

[1] We use this term because $\bar{\gamma}_{RB,cr} \leq 0$ implies outage will occur almost surely.

[2] The distinction between an event occuring almost surely and surely is the same as the subtle distinction between it happening with a probability of 1 and always happening.

1. the source power is proportional to the relay power,

2. the power clipping ratios, $p_{max,\beta}/\sigma_\beta^2$, are fixed.

With these assumptions, ζ_β becomes fixed and we can write

$$p_R = \underline{p}_R p_A, \quad \sigma_\beta^2 = \underline{\sigma}_\beta^2 p_A \text{ and } \eta_\beta = \underline{\eta}_\beta p_A, \tag{4.5}$$

where $\underline{p}_R$, $\underline{\sigma}_R^2$, $\underline{\eta}_\beta \in \mathbb{R}^+$ are proportionality constants.

Because of our assumptions, analyzing the system when it is distortion limited (i.e., when $\max\{\eta_S, \eta_R\} \gg n_0$) is identical to analyzing the system in the high transmit power regime (see (4.5)). Consequently, if we are to study the distortion limited performance of the network, it is of interest to study the first order behavior of $P_{oB}^{(\alpha)}$ as $p_A \to \infty$. With $\underline{\sigma}_S^2\zeta_S^2 - \gamma_{th,B}\underline{\eta}_S > 0$, for FG (4.1) is given to first order by

$$P_{oB}^{(FG)} \sim \left(1 - e^{-\frac{\underline{\eta}_R \gamma_{th,B}}{\left(\underline{\sigma}_S^2\zeta_S^2 - \gamma_{th,B}\underline{\eta}_S\right)\underline{\sigma}_R^2\zeta_R^2}}\right) + \log\left(p_A\right)\left(\xi_{FG}p_A\right)^{-1}; \tag{4.6}$$

while for VG, from (4.3), it is given by

$$P_{oB}^{(VG)} \sim \left(\xi_{VG}p_A\right)^{-1}, \tag{4.7}$$

where ξ_α, $\alpha \in \{FG, VG\}$, is the coding gain, given by

$$\xi_{FG} = \frac{\underline{p}_R\underline{\sigma}_R^2\zeta_R^2\mu_B\left(n_0\gamma_{th,B}\left(\underline{\eta}_R + \underline{\sigma}_R^2\zeta_R^2\right)\right)^{-1}}{\exp\left(-\frac{\underline{\eta}_R\gamma_{th,B}}{\underline{\sigma}_R^2\zeta_R^2\left(\underline{\sigma}_S^2\zeta_S^2 - \gamma_{th,B}\underline{\eta}_S\right)}\right)}, \tag{4.8}$$

$$\xi_{VG} = \frac{\left(\underline{\sigma}_R^2\zeta_R^2 - \frac{\underline{\eta}_R\gamma_{th,B}}{\left(\underline{\sigma}_S^2\zeta_S^2 - \gamma_{th,B}\underline{\eta}_S\right)}\right)\mu_A\mu_B}{n_0\gamma_{th,B}\left(\mu_A + \underline{p}_R\mu_B\right)} \tag{4.9}$$

for FG and VG, respectively. Assuming $\sigma_S^2\zeta_S^2 - \gamma_{th,B}\eta_S > 0$, the limiting log-log decay[3] of $P_{oB}^{(\alpha)}$ with p_A is given by

$$d_{FG} := -\lim_{p_A\to\infty}\left(\frac{\log P_{oB}^{(FG)}}{\log p_A}\right) = \begin{cases} 0 & \underline{\eta}_R \neq 0 \\ 1 & \underline{\eta}_R = 0 \end{cases} \tag{4.10}$$

for FG; while for VG, it is independent of $\underline{\eta}_R$, and given by

$$d_{VG} := -\lim_{p_A\to\infty}\left(\frac{\log P_{oB}^{(VG)}}{\log p_A}\right) = 1. \tag{4.11}$$

We find that, for a fixed power clipping ratio, $p_{max,\beta}/\sigma_\beta^2$, and assuming $\sigma_\beta^2\zeta_\beta^2 - \gamma_{th,B}\eta_\beta > 0$, relay distortion only affects the asymptotic decay of the outage probability for FG, while distortion at the source has no affect on the decay for either forwarding strategy. Note, the coding gains are affected by the distortion. These observations contrast with known results for FG and VG relaying [71] where it was observed that, without nonlinear distortion at the relay, the performance differences between FG and VG are negligible at high transmit power. An illustration of (4.10) and (4.11) is shown in Fig. 4.1, showing that if relay distortion occurs, the outage probability will decay continually as a function of p_A at a negative (log-log) gradient of 1 for VG but will not for FG. Thus, this figure clearly illustrates the results in (4.10) and (4.11).

[3]We refrain from referring to (4.10) and (4.11) as diversity gains. This is because, strictly speaking, diversity defines the limiting log-log decay of the outage probability with the average SNR/SNDR. With the assumptions that have been made, distortion stops the SNDR from growing without bound with p_A.

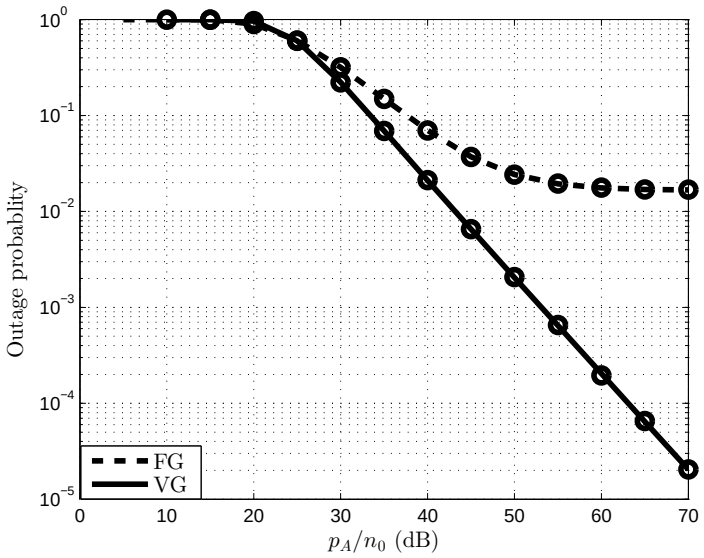

Figure 4.1: Figure illustrating diversity results in (4.10) and (4.11). Lines - theoretical results. Markers - Monte Carlo (1000000 trials). We set $\sigma_R^2 = p_A$, $p_{max,R} = 8p_A$, $p_{max,A} = \infty$, $\gamma_{th} = 20$ dB, $l = 32$ taps, $n = 128$ subcarriers.

4.2.2 The ϵ-critical Phase Transition

To explain the results that were seen above (e.g., why VG asymptotically outperforms FG with relay distortion, or why the first order expansion of the FG outage probability is lower bounded by the bracketed term of (4.6)), we will now define the ratio between the noise power and the distortion power at node β to be ϵ_β; i.e.,

$$\epsilon_\beta := \frac{n_0}{\eta_\beta},\ \beta \in \{S, R\}. \tag{4.12}$$

With (4.12), for FG we can write (3.21) as

$$\gamma_{Bk}^{(FG)} = \frac{\underline{\sigma}_S^2 \zeta_S^2 \underline{\sigma}_R^2 \zeta_R^2 |h_1|^2 \Big/ (\mu_A \max\{\eta_\beta\})}{a_{FG}^{(1)} + a_{FG}^{(2)} \epsilon_\star + a_{FG}^{(3)} {\epsilon_\star}^2} \tag{4.13}$$

where

$$\epsilon_\star = \min_\beta\{\epsilon_\beta\}, \tag{4.14}$$

$a_{FG}^{(1)} = \frac{\underline{\eta}_R}{\max\{\underline{\eta}_\beta\}} + \frac{\underline{\sigma}_R^2\zeta_R^2|h_1|^2\underline{\eta}_S}{\max\{\underline{\eta}_\beta\}\mu_A}$, $a_{FG}^{(2)} = \frac{1}{|h_{2k}|^2} + \frac{\underline{p}_R}{\mu_A}$, and $a_{FG}^{(3)} = \frac{\underline{\eta}_R}{\mu_A|h_{2k}|^2}$; and for VG (3.21) becomes

$$\gamma_{Bk}^{(VG)} = \frac{\underline{\sigma}_S^2\zeta_S^2\underline{\sigma}_R^2\zeta_R^2 \Big/ \max\{\eta_\beta\}}{a_{VG}^{(1)} + a_{VG}^{(2)}\epsilon_\star + a_{VG}^{(3)}\epsilon_\star^2}. \tag{4.15}$$

where $a_{VG}^{(1)} = \frac{\underline{\eta}_R}{\max\{\underline{\eta}_\beta\}} + \frac{\underline{\sigma}_R^2\zeta_R^2\underline{\eta}_S}{\max\{\underline{\eta}_\beta\}}$, $a_{VG}^{(2)} = \frac{1}{|h_{2k}|^2} + \frac{\underline{p}_R}{|h_{1k}|^2}$, and $a_{VG}^{(3)} = \frac{\underline{\eta}_R}{|h_{1k}|^2|h_{2k}|^2}$.

Our goal is to analyze the system as $\epsilon_\star \to 0$. This can be done by letting $n_0 \to 0$ or $\max\{\eta_\beta\} \to \infty$. With the same assumptions as before, both approaches will yield

$$\gamma_{Bk}^{(FG)} \sim \frac{\underline{\sigma}_S^2\zeta_S^2\underline{\sigma}_R^2\zeta_R^2|h_1|^2}{\left(\underline{\eta}_R + \frac{\underline{\sigma}_R^2\zeta_R^2\underline{\eta}_S|h_1|^2}{\mu_A}\right)\mu_A}, \qquad \gamma_{Bk}^{(VG)} \sim \frac{\underline{\sigma}_S^2\zeta_S^2\underline{\sigma}_R^2\zeta_R^2}{\underline{\eta}_R + \underline{\sigma}_R^2\zeta_R^2\underline{\eta}_S}. \tag{4.16}$$

From (4.16), we see that the zeroth order behavior of $\gamma_{Bk}^{(VG)}$ is necessarily non-random, while for $\gamma_{Bk}^{(FG)}$ it is non-random only if source distortion exists and the relay is distortion free. Crucially, neither of these terms contain the variable p_A, which is why the outage probability for FG is lower bounded (i.e., does not decay asymptotically) when relay distortion occurs, while for VG it always decays to 0. Furthermore, the lower bound on the FG outage probability, i.e., the bracketed term of (4.6), is simply the CDF of $\gamma_{Bk}^{(FG)}$'s zeroth order behavior.

4.2.2.1 The ϵ-critical Phase Transition

We will now show for FG and VG that an ϵ-critical phase transition (a phase transition arising for small $\epsilon_\star$) will occur. We will then calculate the outage probability drop that occurs during this phase transition.

For FG, consider the outage probability of $\gamma_{Bk}^{(FG)}$'s zeroth order approximation (see (4.16)), which can be manipulated into

$$\mathbb{P}\left[\frac{\underline{\sigma}_R^2\zeta_R^2|h_1|^2}{\mu_A\underline{\eta}_R}\left(\underline{\sigma}_S^2\zeta_S^2-\gamma_{th,B}\underline{\eta}_S\right)\leq\gamma_{th,B}\right]. \tag{4.17}$$

From (4.17), we see that if $\underline{\sigma}_S^2\zeta_S^2/\underline{\eta}_S \leq \gamma_{th,B}$ outage will occur surely as $p_A \to \infty$ (i.e., $\epsilon_\star \to 0$); otherwise, it will go to the bracketed term of (4.6). Consequently, we expect to observe a phase transition in the distortion limited region for the FG network at the critical $\gamma_{th,B}$ point

$$\gamma_{th,c}^{(FG)} = \underline{\sigma}_S^2\zeta_S^2/\underline{\eta}_S. \tag{4.18}$$

A similar event occurs for VG, but because the zeroth order behavior of $\gamma_{Bk}^{(VG)}$ is necessarily deterministic, the critical $\gamma_{th,B}$ point follows immediately from (4.16), and is given by

$$\gamma_{th,c}^{(VG)} = \underline{\sigma}_S^2\zeta_S^2\underline{\sigma}_R^2\zeta_R^2\Big/\left(\underline{\eta}_R+\underline{\sigma}_R^2\zeta_R^2\underline{\eta}_S\right). \tag{4.19}$$

We call (4.18) and (4.19) the ϵ-critical SNDR thresholds.

Figs. 4.2 and 4.3 show plots of the outage probability as a function of $\gamma_{th,B}$ for FG and VG, and the ϵ-critical values of $\gamma_{th,B}$ (vertical dashed lines), (4.18) and (4.19). From these figures, it is easy to see that as p_A grows (i.e.,

as $\epsilon_\star$ becomes small), crossing the ϵ-critical value of $\gamma_{th,B}$ causes a dramatic reduction (a phase transition) in the outage probability of the network. This clearly demonstrates that small increases in the desired rate can have dramatic consequences for the outage probability if the network is operating in a distortion limited scenario and γ_{th} is close to the ϵ-critical threshold ((4.18) or (4.19)). These figures also contain Monte Carlo generated plots (circular markers), and plots of the first order expansions (expanded about $\gamma_{th,B} = 0$) of the outage probability functions (straight diagonal dashed lines), which will be calculated below. The intersection of the first order expansions with the outage probability curves are denoted by the ordinate points. These points will be used below to establish the size of the outage probability drop that occurs as the ϵ-critical threshold is crossed.

As an extra note, interestingly these figures also illustrate the diversity gain results of (4.10) and (4.11). This is seen by noting that the vertical shift associated with the FG outage curves (Fig. 4.2) decreases as p_A grows. This vertical shift will eventually go to zero, indicating that $d_{FG} = 0$. Meanwhile, the vertical shift associated with the VG outage curves (Fig. 4.3) remains fixed as p_A increases. This indicates that $d_{VG} \neq 0$.

4.2.2.2 Outage Drop about the ϵ-critical SNDR Threshold

To establish the size of the outage probability drop about $\gamma_{th,c}^{(\alpha)}$, we begin by calculating the first order expansions of the outage expressions at $\gamma_{th,B} = 0$.

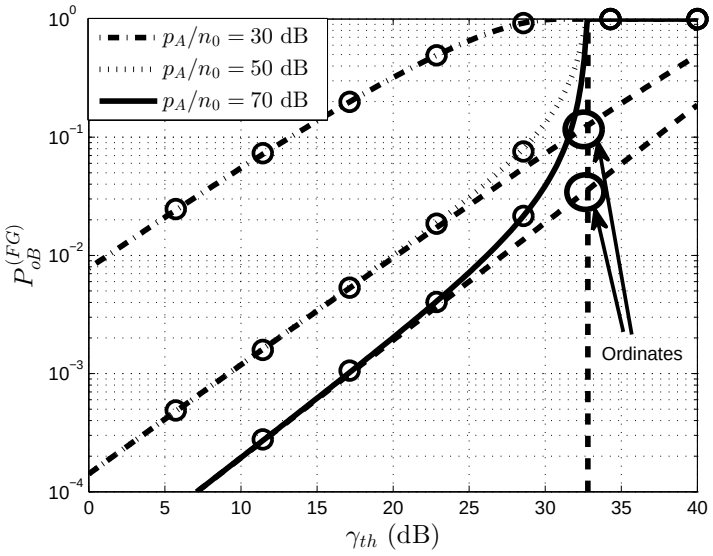

Figure 4.2: $P_{oB}^{(FG)}$ as function of $\gamma_{th,B}$. $\mu_A = \mu_B = n_0 = 1$, $p_{max,A}/\sigma_A^2 = 5$, $p_{max,R}/\sigma_R^2 = 8$. Lines - theoretical results. Markers - Monte Carlo (100000 trials) with $n = 512$ subcarriers, 40 channel taps, profile decay exponent $\delta = 0$. Vertical dashed line is $\gamma_{th,c}^{(FG)}$, (4.18). Straight diagonal dashed lines - (4.20). Ordinates given (asymptotically) by (4.22).

For FG, this is given by

$$P_{oB}^{(FG)} \sim z\gamma_{th,B}[\bar{\gamma}_{BR} + \bar{\gamma}_{AR}\mu_B/\epsilon_R + (1+\bar{\gamma}_{AR})\,(1-2\chi-\log\left[z\gamma_{th,B}\,(1+\bar{\gamma}_{AR})\right])], \quad (4.20)$$

where χ is the Euler-Mascheroni constant [93] and $z = 1\Big/\left(\frac{\sigma_S^2\zeta_S^2\mu_A}{n_0}\frac{\sigma_R^2\zeta_R^2\mu_B}{n_0}\right)$. For VG, it is given by

$$P_{oB}^{(VG)} \sim z\gamma_{th,B}\,(1 - 2\chi + \bar{\gamma}_{AR} + \bar{\gamma}_{BR} - \log\left(z\gamma_{th,B}\right)). \quad (4.21)$$

We now use (4.20) and (4.21) to understand the phase transitions observed in Figs. 4.2 and 4.3. This is done by evaluating them at the ϵ-critical SNDR threshold ((4.18) or (4.19)), which will give us the ordinates illus-

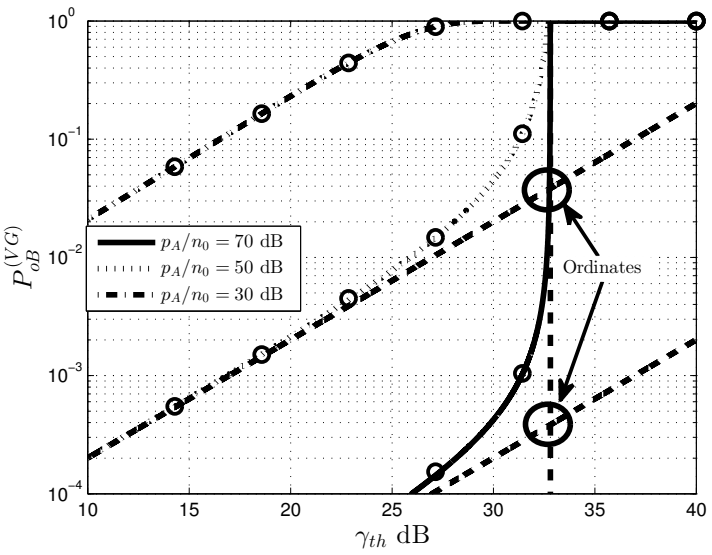

Figure 4.3: $P_{oB}^{(VG)}$ as function of $\gamma_{th,B}$. $\mu_A = \mu_B = n_0 = 1$, $p_{max,A}/\sigma_A^2 = \infty$, $p_{max,R}/\sigma_R^2 = 5$. Lines - theoretical results. Markers - Monte Carlo simulations (100000 trials) with $n = 512$ subcarriers, 40 channel taps, profile decay exponent $\delta = 0$. Vertical dashed line - $\gamma_{th,c}^{(VG)}$, (4.19). Straight diagonal dashed lines - (4.21). Ordinates given (asymptotically) by (4.23).

trated in these figures and indicate the outage probability drop that should be expected as the ϵ-critical threshold is crossed. For FG, with $\underline{\eta}_S \neq 0$, the ordinate is given to leading order about $\epsilon_\star = 0$ by

$$\mathrm{ord}_{FG} \sim \frac{\epsilon_\star \max\{\underline{\eta}_\beta\}}{\underline{\eta}_S \underline{\sigma}_R^2 \zeta_R^2 \mu_B} \left(\frac{\mu_B}{\epsilon_R} + \log\left(\frac{\underline{\eta}_S \underline{\sigma}_R^2 \zeta_R^2 \mu_B}{\epsilon_\star \max\{\underline{\eta}_\beta\}} \right) \right); \tag{4.22}$$

while for VG, it is given by

$$\mathrm{ord}_{VG} \sim \frac{\epsilon_\star^2 \max\{\underline{\eta}_\beta\}}{a_{VG} \mu_A \mu_B} \log\left(\frac{a_{VG} \mu_A \mu_B}{\epsilon_\star^2 \max\{\underline{\eta}_\beta\}} \right). \tag{4.23}$$

These ordinates indicate the size of the outage probability drop that will occur as the ϵ-critical threshold is crossed.

4.2.3 A Discussion of the ϵ-critical Phase Transition

In this subsection we will elucidate some observations made in sections 4.2.2.1 and 4.2.2.2. First, from (4.18) and (4.19), we find that

$$\gamma_{th,c}^{(FG)} - \gamma_{th,c}^{(VG)} = \underline{\sigma}_S^2 \zeta_S^2 \underline{\eta}_R \Big/ \left(\underline{\eta}_S \underline{\eta}_R + \underline{\sigma}_R^2 \zeta_R^2 \underline{\eta}_S \right). \tag{4.24}$$

Consequently, $\gamma_{th,c}^{(VG)} \leq \gamma_{th,c}^{(FG)}$, where equality is maintained when the relay is distortion free. It follows that if $\gamma_{th,c}^{(VG)} < \gamma_{th,B} < \gamma_{th,c}^{(FG)}$ FG will outperform VG in distortion limited regions. This is the only point at which distortion limited FG networks appear favorable over distortion limited VG networks. Moreover, if $\gamma_{th,B}$ belongs to this interval, by considering the FG outage probability lower bound (the bracketed term of (4.6)), FG will outperform VG at most by the factor

$$1 - \exp\left(-\underline{\eta}_R \gamma_{th,c}^{(VG)} \Big/ \left(\underline{\sigma}_S^2 \zeta_S^2 - \gamma_{th,B} \underline{\eta}_S \right) \underline{\sigma}_R^2 \zeta_R^2 \right).$$

Turning our attention to the outage probability drop that occurs about $\gamma_{th,c}^{(\alpha)}$, from (4.22) and (4.23) we find that the ordinate of the drop scales at best (i.e., when $\epsilon_R = \infty$) like $O\left(-\epsilon_S \log \epsilon_S\right)$ for FG, while it always scales like $O\left(-\epsilon_\star^2 \log \epsilon_\star^2\right)$ for VG. Consequently, much larger outage probability drops should be expected for the VG network. Furthermore, when $\epsilon_R \neq \infty$, (4.22) becomes $O(1)$; i.e., it becomes independent of $\epsilon_\star$. This makes sense from our observation that the outage probability for the FG network is lower bounded (i.e., its decay rate is asymptotically 0) when distortion occurs at the relay.

4.3 Fixed-gain Performance Analysis and Gain Optimization

In this section, we calculate the SER of the FG one-way relay network studied above when distortion occurs only at the relay for general noise conditions. We then discuss how our analysis can be used to minimize the SER of the link and apply our techniques to a real-world testbed.

4.3.1 Symbol Error Rate Calculation

The form of the average SER on a given subcarrier for many general modulation schemes is given by [94]

$$\bar{P}_s = \mathbb{E}\left[aQ\left(\sqrt{2b\gamma_{Bk}^{(FG)}}\right)\right] \tag{4.25}$$

where a and b are parameters that are specific to the constellation employed, $Q(\cdot)$ is the Gaussian Q-function, $\gamma_{Bk}^{(FG)}$ is the end-to-end SNDR on a given subcarrier, and the expectation is taken over the channel coefficients. For BPSK, we have $a = 1$ and $b = 1$; for QPSK, $a = 2$ and $b = 0.5$; and for q-ary pulse-amplitude modulation, $a = 2(q-1)/q$ and $b = 3/(q^2-1)$ [94]. By employing integration by parts and applying the chain rule, we can use (4.25) to express the SER for the one-way FG network at node B as the integral

$$\bar{P}_{sB}^{(FG)} = \frac{a}{2}\sqrt{\frac{b}{\pi}}\int_0^\infty \gamma_{th,B}^{-\frac{1}{2}} e^{-b\gamma_{th,B}} P_{oB}^{(FG)}(\gamma_{th,B})\,\mathrm{d}\gamma_{th,B}. \tag{4.26}$$

Using $P_{oB}^{(FG)}$ as in (4.2), we can evaluate the integral in (4.26), the solu-

tion to which is given by [95, eq. (2.16.6.3)]

$$\bar{P}_{sB}^{(FG)} = \frac{a}{2} - \frac{a}{4}\sqrt{\frac{b\bar{\gamma}_{AR}\pi}{u + b\bar{\gamma}_{AR}}}U\left(\frac{1}{2}, 0, \frac{u + \bar{\gamma}_{AR}}{(u + b\bar{\gamma}_{AR})\bar{\gamma}_{RB}}\right) \tag{4.27}$$

where u is given by (3.23) and $U(\cdot,\cdot,\cdot)$ is the confluent hypergeometric function of the second kind (Tricomi solution), [95].

We show a plot of (4.27) in Fig. 4.4 to demonstrate its accuracy when compared to Monte Carlo simulations. Three plots are shown for different values of $p_{max,R}/p_A$. The reason these plots have lower bounds is because the gain at the relay is kept fixed. Consequently, the power clipping ratio, $p_{max,R}/\sigma_R^2$ also tends towards a fixed value as p_A grows large. As we saw in the previous section, fixing the power clipping ratio will cause the network to become distortion limited in the high transmit power regime and the FG network will have a lower bounded outage probability (and a diversity order of zero, (4.10)) if distortion occurs at the relay. This explains why the SER is lower bounded.

4.3.2 Optimal Relay Gain

Fig. 4.5 shows a plot of the SER as a function of the relay's gain. From this, it can be seen that correctly selecting our relay gain is important if optimal SER performance is to be achieved. The optimal gain can be determined by solving $d\bar{P}_{sB}^{(FG)}/dg_{FGk} = 0$ for g_{FGk}. Note, however, that both u and $\bar{\gamma}_{RB}$ are functions of g_{FGk} in (4.27). This complicates the expression for the derivative, leading to an implicit transcendental function of g_{FGk}. In general, a root-finding algorithm must be employed to obtain this.

Fig. 4.6 shows the SER as a function of $p_{max,R}$ when optimal and sub-

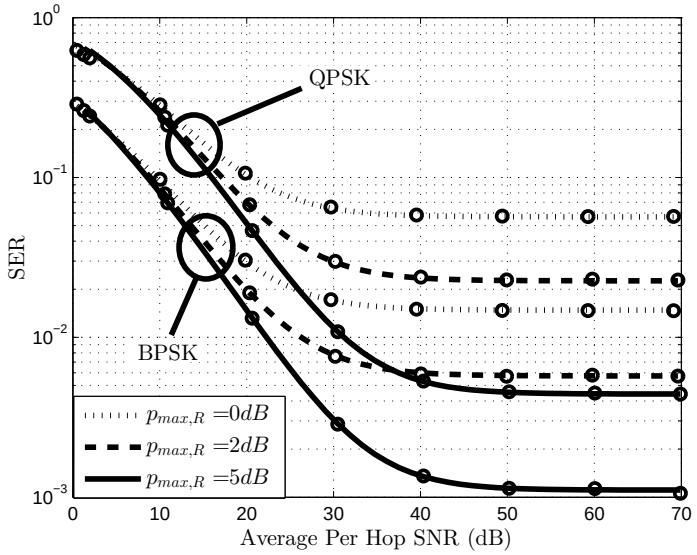

Figure 4.4: Theoretical (lines) and numerical (markers, 50000 trials) SER results for different $p_{max,R}$ (in dB relative to p_A) as function of average per-hop SNR, $(\bar{\gamma}_{AR} + \bar{\gamma}_{RB})/2$ for BPSK and QPSK modulation. Plot is generated by fixing g_{FGk}, μ_A, μ_B and n_0 to one and sweeping p_A across a range of values to obtain $(\bar{\gamma}_{AR} + \bar{\gamma}_{RB})/2$. $l = 32$ taps and $\delta = 0.1$ profile.

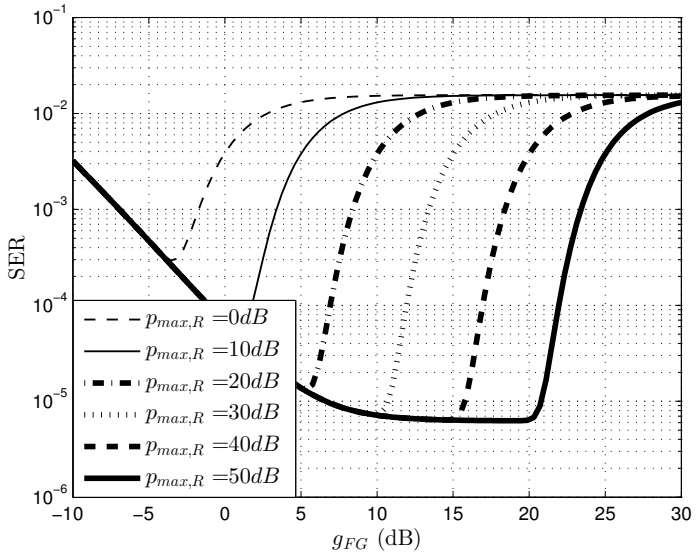

Figure 4.5: The SER (4.27) plotted as a function of g_{FGk} for different $p_{max,R}$ ($p_{max,R}$ is given in dB relative to the average received signal power at the relay). The plot is generated for QPSK with μ_A, μ_B and n_0 fixed to one and $p_A = 10^4$. $l = 32$ taps and $\delta = 0.1$ profile exponent.

optimal gains are applied at the relay. To obtain the numerical results corresponding to the optimal gains, the root of $d\bar{P}_{sB}^{(FG)}/dg_{FGk} = 0$ for g_{FGk} was found using the bisection method. To obtain the results related to suboptimal gain configurations, the gain definition

$$g_{FG,r} = \sqrt{\frac{p_{max,R}r}{p_A\mu_A + n_0}} \tag{4.28}$$

was employed [71, 96]. Note, r represents the fraction of the total available power that is input to the relay's SEL. The superior performance of the optimal gain strategy is evident for all values of $p_{max,R}$ that were tested. This example also illustrates the intuitive result that the system is less sensitive to the gain parameter when the clipping power is high since the outage probability becomes limited by the first hop.

4.4 Physical Universal Software Radio Peripheral Relay Testbed and Results

Given the complexities of the nonlinear system that was studied, it is important that our theoretical results be validated as much as possible through practical experimentation. In this section, we provide details of a physical relay testbed implementation that uses universal software radio peripherals[4] (USRP). We then present performance results for the testbed setup.

[4]The testbed was set up and run by David Halls of Toshiba Research Laboratory, Bristol.

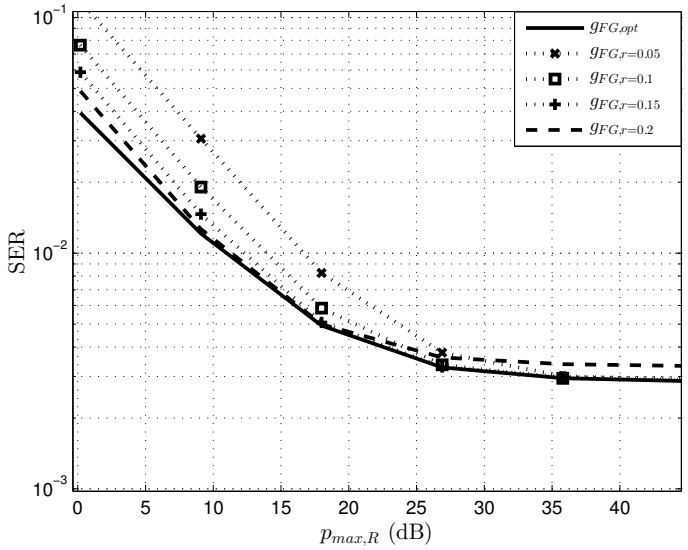

Figure 4.6: The SER plotted as a function of $p_{max,R}$ ($p_{max,R}$ is given in dB relative to the received noise power at the relay) for optimal SER gains (solid line) compared with gains obtained from (4.28) for different values of r (non-solid lines). The plot is generated for a QPSK system by fixing μ_A, μ_B and n_0 to one and setting $\bar{\gamma}_{AR} = 25$ dB. $l = 32$ taps and $\delta = 0.1$ profile.

4.4.1 Implementation

The USRPs connect to a host computer via a gigabit Ethernet link, which the host-based software uses to receive and transmit the baseband IQ stream. The host controls the USRP using USRP hardware driver (UHD) commands, including setting parameters such as amplifier gain. The USRP then performs the necessary baseband processing then up/down-conversion and transmission/reception. We used the Ettus Research N210 USRP, which consists of a motherboard and a radio frequency (RF) daughterboard (the XCVR2450); more details can be found in [97].

For this work, we used GNURadio [98] as the host-processing software. The software in these experiments used a heavily modified version of the "OFDM_tx" and "OFDM_rx" flow graph examples provided in GNURadio

Figure 4.7: USRP testbed topology. From the left: source, relay, destination.

at the source and destination, respectively. Bespoke code was created for the relay, which included a gain block and an SEL block. The SEL block allowed us to test the theory without running into other problems, e.g. exceeding the dynamic range of the DAC.

4.4.1.1 Topology and Frame Format

We used a 3-node, 2-hop topology, as shown in Fig. 4.7. The USRPs each had a single 3dBi omni-directional antenna (at 2.4 - 2.5 GHz and 4.9 - 5.85 GHz). The source and destination USRPs were connected to one laptop by a gigabit switch and the relay USRP was connected to a second laptop. All three USRPs were connected to an external synchronization signal as detailed in section 4.4.1.3. A metal obstruction was placed in between source and relay, and relay and destination, to ensure an NLoS channel. The configuration was such that equal average channel gains were achieved between source and relay, and relay and destination, respectively. Symbolically, this equates to the condition $\mu_A = \mu_B$.

In order to perform synchronization and channel estimation, preambles

consisting of two synchronization symbols and a header symbol were used. These were transmitted at the beginning of each packet. The preambles were followed by the payload symbols.

4.4.1.2 OFDM Parameters

We employed an OFDM solution with 64 subcarriers. There were 48 data subcarriers, with a DC carrier, 11 guard carriers, and 4 pilot carriers at frequency indices -21, -7, 7 and 21. We employed a CP of 1/4 (i.e., 16 samples) and a center frequency of $f_c = 2.4$ GHz with a 1 MHz bandwidth (i.e., 1 MS/s sampling rate). Each packet contained 16 OFDM symbols and no channel coding was implemented in the system.

4.4.1.3 Synchronization

Symbol Timing Synchronization OFDM symbol timing was achieved using the well-known Schmidl and Cox technique [99]. Any timing inaccuracy would result in a rotation in phase in the frequency domain. As long as the timing estimation error is less than the CP length, the received signal remains ISI free. Under this assumption, the phase rotations cannot be distinguished from the phase delay caused by the channel, therefore they can be compensated through channel estimation and equalization.

Frequency Synchronization The USRP devices take two reference signals in order to synchronize clocks and time: a 10 MHz reference to provide a single frequency reference across devices and a 1 pulse-per-second (PPS) signal to synchronize the sample time across devices. Using external synchronization the USRPs will be mutually frequency- and phase-locked. For

all experiments detailed herein, there was external synchronization between all USRPs, so there was negligible carrier frequency offset, which would otherwise be caused by the inaccuracy of the respective internal temperature-compensated crystal oscillators in each USRP.

4.4.2 Testbed Results

We collected SER results from the testbed using QPSK modulation for a range of $p_{max,R}/(p_A\mu_A)$ values, incrementing in 2.5 dB steps. For each value, we tested the corresponding optimal gain and the gain obtained from (4.28) with $r = 0.1$. A total of 131 packets were sent, which resulted in a total of 100,608 symbols per data point. Each set of experiments was run five times. The results can be seen in Fig. 4.8.

From this figure we see that the SER performance in the optimal gain case outperforms the case where gains are calculated sub-optimally with $r = 0.1$. Note, however, that although the relative performance of the two approaches detailed in Fig. 4.8 is in line with theoretical predictions (i.e., the curve plotted with $g_{FG,opt}$ performs best), the exact performance deviates from theory shown in Fig. 4.6. This disagreement follows from discrepancies between the theoretical and experimental models. For example, the experimental channel is not ergodic, i.e., it is relatively static and thus the experiments could not be used to obtain SER results averaged over all channel states. As a result, the channel more closely resembles an AWGN channel, and thus the attainable SER (with increasing $p_{max,R}$) is much lower than for a truly ergodic channel. This explains the lack of an error floor in Fig. 4.8. Other factors that contributed to the differences between the theoretical predictions and the experimental measurements in-

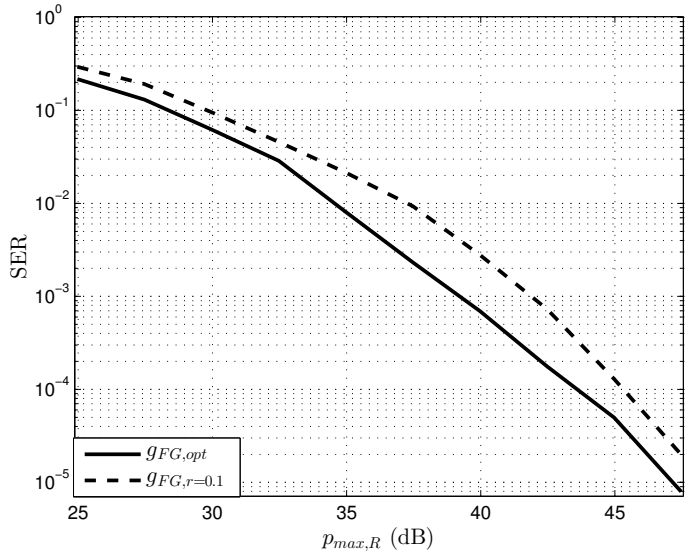

Figure 4.8: QPSK SER for testbed as function of $p_{max,R}$ (relative to n_0) for optimal SER gains (solid line) and gains obtained from (4.28) for $r = 0.1$ (dashed line). Plot is generated for an average first hop SNR of 25 dB.

clude the physical impairments (e.g., channel estimation errors, carrier frequency offset, etc) that are inherent to practical demonstrations.

Despite the aforementioned differences, optimal gain selection based on theoretical performance analysis will clearly lead to a practical performance improvement. Indeed, our experiments have gone some way to demonstrating that our theoretically motivated gain optimisation procedure is robust to changes in the fading characteristics of the environment in which a relay system operates.

4.5 Summary

This chapter is the last that provides an analysis of the system model presented in section 3.2. In it, we studied the one-way special case of this system. We began by considering the scenario in which the network op-

erates in a distortion limited region. It was shown that distortion at the source will not affect the asymptotic decay rate of the outage probability, while distortion at the relay will affect this, but only for FG amplification. We then revealed a critical operational SNDR threshold for both FG and VG, which we termed the ϵ-critical SNDR threshold. It was shown that crossing the threshold in distortion limited scenarios will cause a phase transition in the network's outage probability. Following this, we derived the theoretical SER of a one-way two-hop FG OFDM relay network operating with nonlinearities at the relay. This analysis was used to calculate the FG gain value that minimizes the SER given various dependent system parameters. We then tested this theory with simulations as well as through experiments conducted using a USRP relay testbed. Our findings demonstrate that the gains chosen using the theoretical framework do, indeed, result in performance improvements in practice relative to a standard benchmark. Additionally, the discrepancies between the theoretical and experimental models demonstrate the robustness of our approach.

Chapter 5

Multihop MIMO Networks: Capacity and Power Scaling Laws

In this chapter, we focus our study on an single-carrier (SC) frequency flat n-hop ($n > 2$) MIMO AF relay network. We present a novel framework that can be used to study the capacity and power scaling properties of this network when each node is equipped with d antennas. This is done by modeling it as a RDS and calculating its d Lyapunov exponents. Our analysis can be applied to systems with any per-hop channel fading distribution, although in this chapter we focus on Rayleigh fading. Our main results are twofold: 1) the total transmit power at the nth node will follow a deterministic trajectory through the network governed by the network's maximum Lyapunov exponent, 2) the capacity of the ith eigenchannel[1] at the nth node will follow a deterministic trajectory through the network governed by the network's ith Lyapunov exponent. Before concluding, we concentrate on some applications of our results. In particular, we show how the Lyapunov

[1]The parallel subchannels that emerge when spatial mutiplexing is performed are the eigenchannels. For more information on this, see (2.15) and the surrounding text.

exponents are intimately related to the rate at which the eigenchannel capacities diverge from each other, and how this relates to the amplification strategy and number of antennas at each relay. We also use them to determine the extra cost in power associated with each extra multiplexed data stream.

5.1 Introduction

Consider a MIMO link with m_S source antennas and m_D destination antennas. It is well known that, under some basic assumptions (i.e., independent channel fading between each antenna pair), the capacity will *almost surely* scale linearly with $\min\{m_S, m_D\}$, [43].

Now, consider an n-hop MIMO link, aided by $n-1$ relay nodes, where each relay node is equipped with d transmit and receive antennas. Furthermore, assume that signals received at the ith relay node propagate only as far as the $(i+1)$th node (Fig. 5.1). The end-to-end capacity, c_n, of such links has been studied in many works: see, e.g., [100–105] for AF studies, and [106–110] for DF studies. By considering the max-flow min-cut theorem [111], it is trivial to show that the capacity of linear multihop networks is achieved by employing DF relaying[2]. To see this, note that the end-to-end capacity of an n-hop DF network is given by the minimum of the per-hop

[2]It is important to acknowledge that the capacity of a two-hop relay channel *with* direct source-destination link is still unknown [112, 113]. In our work, if we considered the scenario in which signals from the ith node traveled further than the $i+1$th node then we would have a network that built upon this three node system. Consequently, if this were the case it is unknown which relaying strategy would achieve capacity.

capacities, e.g., when each hop is a SISO fading channel with Gaussian noise

$$c_n = \min_{i \in \{1,\ldots,n\}} \{\log(1+\gamma_i)\}, \tag{5.1}$$

where γ_i is the instantaneous SNR of the ith hop. Eq. (5.1) coincides exactly with the upper bound on the achievable capacity that is obtained when we apply the max-flow min-cut theorem. However, when larger numbers of nodes are deployed, DF-based protocols may result in prohibitive latency/complexity because of the decoding process that takes place at each relay. AF protocols become interesting at this point since they can be employed to yield low complexity and/or low latency solutions. Under certain scenarios, they also have the potential to offer greater diversity when compared to DF schemes [65].

The analysis of DF networks in the general multihop setting is made easier by the fact that a local view can often be taken – i.e., the transmission is "reset" at each relay node, and thus sequential hops can, to a certain extent, be treated independently. This is not the case for AF networks, which must be observed *globally* in the general case since the end-to-end transmission is affected by a composition of mappings, one for each hop. Consequently, although AF relay networks may exhibit potential in multihop applications, relatively little is known about how these systems scale.

A number of results exist pertaining to AF relay networks that scale in size. For a linear n-hop network, it was shown in [100, 101] that $\lim_{n\to\infty} \lim_{m_D\to\infty} (c_n/m_D)/n$ exists *almost surely* and is strictly positive, provided m/m_D scales at least linearly with n (i.e., $m/m_D = \Omega(n)$), where c_n is the capacity at the nth node of the network. This work also considered the

aforementioned limit for other forwarding strategies; namely, DF, compress-and-forward, and quantize-and-forward. In [104], the asymptotic (in matrix dimension) eigenvalue distribution of the channel's covariance matrix for linear n-hop MIMO channels with noiseless relays was established. Using free probability theory and, again, under the premise that negligible noise was received at the relays, it was shown in [102] that when linear precoding was applied at each relay, c_n would converge *almost surely* to a limit as m grows large. The singular vectors of the optimal precoding matrices for such a network when noise is negligible at the relays was also established in [102]. When noise was present at the relays, ergodic capacity and average bit error rate results were established in [103] for multihop AF MIMO networks when arbitrary signaling occurs at the source node and, again, m grows without bound. Meanwhile, in [105], c_n was assessed for general n-hop AF networks in terms of the limiting (in m) eigenvalue distribution of products of random matrices when noise is *not* negligible at the relay nodes. Related work on the diversity-multiplexing tradeoff, [62], for various MIMO multihop relaying strategies can be found in [106, 114–116].

Other attempts to determine the behavior of AF networks as they scale (not necessarily in the number of hops) can be found in [56, 61, 117]. In more detail, [61] considers a network of n source-destination nodes communicating through a set of k relays in a two-hop fashion. It is shown that, provided k grows fast enough with n, in the large n limit the network will 'crystallize' into a set of nonfading source-destination links with strictly positive capacity. In [117] a single-antenna source-destination pair aided by layered relays is studied. It is shown that such networks will approach the cut-set bound as the received power at each relay increases. An m antenna

source-destination pair assisted by k single-antenna two-hop relays is studied in [56], where it is shown that for fixed m, the capacity of the network will obey $c = m/2 \log k + O(1)$ as $k \to \infty$.

To the best of the authors' knowledge, all attempts to study the statistical behavior of the end-to-end capacity for n-hop ($n > 2$) AF MIMO networks have leveraged a viewpoint in which the number of antennas at each node grows large[3]. To achieve this, results from random matrix theory [5] have commonly been employed; e.g., [119–121], which describe the asymptotic/limiting spectral properties of large random matrices. The limitations of such approaches are that statistical spectrum behavior is established only at a macroscopic scale[4]. In this chapter, we establish statistical laws for each of the spectra individually. Crucially, this allows us to determine capacity scaling laws for each of the subchannels of a network when the number of antennas at each node is *finite*. This is done by employing the formalism of RDS[5], [6]. Such systems have also been used to study econometrics [123], biological systems [124, 125], chemical reactions [125], and the propagation of particles through fluidic media [126]. For relevant information on RDSs, the reader may refer to section 5.4.

Going into more detail, the Lyapunov exponents [6] of RDSs are known to characterize the exponential growth/decay rates of the spectrum of finite dimensional random matrix products [6, 127, 128]. In this chapter, we use

[3]Note, for $n = 2$ hops, results have been obtained for finite antenna systems (see, e.g., [118]).

[4]The term macroscopic scale is commonly used in random matrix theory to describe macroscopic/'global' observables such as the empirical eigenvalue distribution (see [122] for more details).

[5]The RDS formalism can be applied to any relay system that can be described as a product of random matrices. This encompasses all AF strategies. Because of the 'resetting' nature of digital relaying protocols (e.g., DF), it is unclear whether the RDS formalism can be employed to study the scaling properties of such networks.

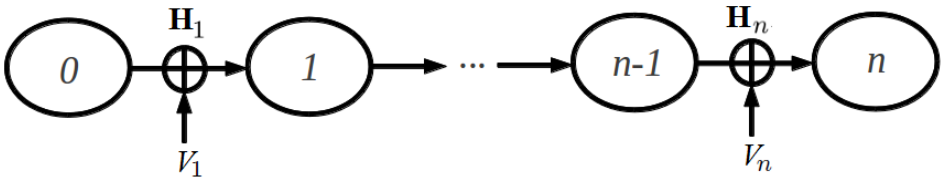

Figure 5.1: An illustration of a linear relay network. The ith hop's channel is described by the channel matrix $\mathbf{H}_i$. The noise received at the jth node is described by the vector V_j. Nodes 0 and n are the source and destination, respectively.

these Lyapunov exponents to study the spectral properties of the n-hop AF MIMO network[6]. The main result of this chapter is that the Lyapunov exponents of the network, which are obtained by studying the network as an RDS, can be used to evaluate the exponential growth/decay of the nth node transmit power and nth node end-to-end eigenchannel capacity when each of the nodes in the network has a finite number of antennas.

Section 5.2 introduces the system model. Section 5.3 clarifies the key results obtained in this chapter. Section 5.4 introduces the mathematical preliminaries and new RDS results that will be utilized throughout this chapter. In section 5.5 we calculate the Lyapunov exponents, and show that they can be used to characterize the network's transmit power and end-to-end eigenchannel capacity. Section 5.6 establishes applications of the results that are obtained in section 5.5. Section 5.7 provides numerical illustrations of the theory that has been developed. Finally, section 5.8 concludes the chapter.

[6]Note, Lyapunov exponents were used in [129, 130], where sum-capacity scaling laws were established for the non-ergodic Wyner cellular model as the number of cells grew large. In more detail, the upper Lyapunov exponent is used in [129, 130] by considering the Thouless formula, which relates the determinant of a large random matrix to a product of fixed size matrices.

5.2 System Model

Let us present the signaling model studied in this chapter. Consider an n-hop AF relay network, as depicted in Fig. 5.1. We assume that each node has $m \geq 1$ transmit and receive antennas. Independent frequency-flat Rayleigh fading [131] is assumed to take place between each node pair. Thus, the channel for the ith hop can be described by a $m \times m$ random matrix, $\mathbf{H}_i$, whose elements are circularly symmetric complex Gaussian [131] with total variance μ_i; i.e., for $h_{ab,i} \sim \mathcal{CN}(0, \mu_i)$, we have

$$\mathbf{H}_i = \begin{bmatrix} h_{11,i} & h_{12,i} & \cdots & h_{1m,i} \\ h_{21,i} & h_{22,i} & \cdots & h_{2m,i} \\ \vdots & & \ddots & \vdots \\ h_{m1,i} & h_{m2,i} & \cdots & h_{mm,i} \end{bmatrix}. \tag{5.2}$$

At each node (apart from the zeroth node; i.e., the source) we assume noise is introduced into the system. We use $V_j \in \mathbb{C}^m$ to denote the vector of noise terms introduced at the jth relay. The elements of V_j correspond to the noise samples received at each antenna of node j and are independent complex Gaussian random variables with total variance n_0.

An information vector

$$X_0 = [x_{0,1}, \ldots, x_{0,m}]^T \tag{5.3}$$

is constructed at the source (node 0). We assume each element of X_0 has a mean of zero and average power given by $\mathbb{E}[|x_{0,i}|^2] = p_0/m$. The ith element of X_0 is then transmitted from the ith antenna of node 0.

We assume the jth relay node receives the transmission only from the $(j-1)$th node in one time slot. This relay then applies a scalar gain, g_j, to the received signal on each of its antennas and transmits in the next time slot. Thus, the relays operate in a half-duplex manner. The gain for the jth relay is either a FG parameter, depending only upon the average statistics of the channel matrix of the previous hop, given by

$$g_{FG,j} = \sqrt{\frac{p_j}{p_{j-1} m \mu_j + m n_0}}; \tag{5.4}$$

or a VG parameter given by [132, eq. (7)]

$$g_{VG,j} = \sqrt{\frac{p_j}{\frac{p_{j-1}}{m} \|\mathbf{H}_j\|_F^2 + m n_0}}. \tag{5.5}$$

The term p_j is selected by the relay, and represents the average transmit power at node j. Also, we assume that $\lim_{n\to\infty}(1/n)\log(p_n/p_0) < \infty$. This assumption implies that the average transmit power does not grow at a super-exponential rate. Similar assumptions have also been made in [101]. It is important to note that we are implicitly assuming the relays have access to statistical CSI in the form of μ_i for FG and $\|\mathbf{H}_j\|_F^2$ for VG. The precise mechanism by which these are obtained is beyond the scope of this work. Needless to say, using tools such as received signal strength indicators, it is possible for these to be gleaned from a channel output without having to perform decoding operations at each relay.

The information bearing content of the signal (herein referred to as the

information component) at the nth node is given by

$$\mathcal{I}_n^{(\alpha)} = g_{\alpha,n}\mathbf{H}_n\mathcal{I}_{n-1}^{(\alpha)} \tag{5.6}$$

$$= \prod_{j=1}^{n} g_{\alpha,j}\mathbf{H}_j X_0, \tag{5.7}$$

where $\alpha \in \{FG, VG\}$ dependent upon whether FG or VG is being implemented. Similarly, the total transmitted signal at the nth node is given by

$$X_n^{(\alpha)} = g_{\alpha,n}\left(\mathbf{H}_n X_{n-1}^{(\alpha)} + V_n\right) = \mathcal{I}_n^{(\alpha)} + \underbrace{g_{\alpha,n}\sum_{i=1}^{n}\prod_{j=i+1}^{n} g_{\alpha,j-1}\mathbf{H}_j V_i}_{\mathcal{N}_n^{(\alpha)}}, \tag{5.8}$$

where $\prod_{j=n+1}^{n} g_{\alpha,j-1}\mathbf{H}_j V_n := V_n$ and $\mathcal{N}_n^{(\alpha)}$ denotes the accumulated noise at node n. Owing to our choice of gain, and by the definition of the source transmit vector (5.3), for all $i \in \mathbb{N} \cup \{0\}$ the ith node is subject to the following average power constraint:

$$\mathbb{E}\left[X_i^{(\alpha)\dagger} X_i^{(\alpha)}\right] \leq p_i. \tag{5.9}$$

Note, the channel input, (5.8), can be re-expressed as the first m entries of the following matrix product:

$$\begin{bmatrix} X_n^{(\alpha)} \\ \sqrt{n_0} \end{bmatrix} = \prod_{j=1}^{n} \mathbf{Q}_j^{(\alpha)} \begin{bmatrix} X_0 \\ \sqrt{n_0} \end{bmatrix}, \tag{5.10}$$

where

$$\mathbf{Q}_j^{(\alpha)} := \begin{bmatrix} g_{\alpha,j}\mathbf{H}_j & g_{\alpha,j}Z_j \\ \mathbf{0^T} & 1 \end{bmatrix} \tag{5.11}$$

and $Z_i = V_i/\sqrt{n_0}$. This matrix formulation will help us to establish power scaling laws for the network.

Finally, we give a definition for the capacity of the network described above.

Definition 1 *The information capacity of the n-hop network with amplification strategy α and average power constraint p_i for the ith node is*

$$c_n^{(\alpha)} = \max_{P_{X_0}(X)} I\left(X_0; X_n^{(\alpha)}/g_{\alpha,n}\right), \tag{5.12}$$

where P_{X_0} denotes the probability density function of the source vector, X_0, and $I\left(X_0; X_n^{(\alpha)}/g_{\alpha,n}\right)$ denotes the mutual information between X_0 and $X_n^{(\alpha)}/g_{\alpha,n}$.

Fact 1 *From [101], the end-to-end channel capacity of the network,* (5.12)*, is given by*

$$c_n^{(\alpha)} = \log\det\left(\mathbf{I}_m + \mathbf{R}_{\mathcal{I},n}^{(\alpha)}\mathbf{R}_{\mathcal{N},n}^{(\alpha)-1}\right) = \sum_{i=1}^{m} c_{n,i}^{(\alpha)} \text{ (nats/channel use)}, \tag{5.13}$$

where

$$\mathbf{R}_{\mathcal{I},n}^{(\alpha)} = \left(p_0\prod_{i=1}^{n} g_{\alpha,i}^2\right)\mathbf{H}_n\cdots\mathbf{H}_1\mathbf{H}_1^\dagger\cdots\mathbf{H}_n^\dagger, \tag{5.14}$$

$$\mathbf{R}_{\mathcal{N},n}^{(\alpha)} = n_0\left(\mathbf{I}_m + \sum_{l=2}^{n}\prod_{i=l}^{n} g_{\alpha,i}^2\mathbf{H}_n\cdots\mathbf{H}_l\mathbf{H}_l^\dagger\cdots\mathbf{H}_n^\dagger\right) \tag{5.15}$$

are covariance matrices; and $c_{n,i}^{(\alpha)} = \log\left(1 + \mathcal{E}_i\left(\mathbf{R}_{\mathcal{I},n}^{(\alpha)}\mathbf{R}_{\mathcal{N},n}^{(\alpha)-1}\right)\right)$ is the capac-

ity of the ith eigenchannel at the nth node.

5.3 Key Results

One of the key insights that we provide in this chapter is that n-hop AF MIMO systems can be studied from the viewpoint of RDS. To the best of our knowledge, this is the first time such an approach has been taken in the literature. This viewpoint then leads us to obtain the following results:

- In Lemma 6 and Theorem 2, we show that the $m \times m$ antenna MIMO AF network has associated with it an ordered set $\{\lambda^{(\alpha)}_{\mathbf{H},1}, \cdots, \lambda^{(\alpha)}_{\mathbf{H},m}\}$ of Lyapunov exponents satisfying

$$\lambda^{(\alpha)}_{\mathbf{H},1} > \cdots > \lambda^{(\alpha)}_{\mathbf{H},m},$$

  where the $\alpha \in \{FG, VG\}$ term in the subscript denotes the amplification strategy that is being implemented. From this ordered set, two other sets of exponents are established. The first of these sets is constructed from elements of the form $\lambda^{(\alpha)}_{\mathbf{Q},i} = \max\{\lambda^{(\alpha)}_{\mathbf{H},i}, 0\}$, and is associated with the instantaneous total transmit signal at the nth node. The second of these sets is constructed from elements of the form $\lambda^{(\alpha)}_{\gamma,i} = \min\{2\lambda^{(\alpha)}_{\mathbf{H},i}, 0\}$, and is associated with the end-to-end SNR of the network's m eigenchannels.

- In Lemma 6, we show that the instantaneous transmit power, $\|X^{(\alpha)}_n\|^2$, at the nth node obeys the relationship

$$\|X^{(\alpha)}_n\|^2 = \Theta_{\mathbb{P}}\left(e^{2n\lambda^{(\alpha)}_{\mathbf{Q},1}}\right), \tag{5.16}$$

where, $f(n) = \Theta_{\mathbb{P}}(g(n))$ implies that $f(n)$ is equal to $g(n)$, to first order in the exponent [39, eq. (3.26)]. This is defined more rigorously in the notation section at the beginning of the thesis.

- In Theorem 2, we show that the SNR and capacity of the ith eigenchannel at the nth node, $\mathcal{E}_i\left(\mathbf{R}_{\mathcal{I},n}^{(\alpha)}\mathbf{R}_{\mathcal{N},n}^{(\alpha)-1}\right)$ and $c_{i,n}^{(\alpha)}$, satisfy the relations

$$\mathcal{E}_i\left(\mathbf{R}_{\mathcal{I},n}^{(\alpha)}\mathbf{R}_{\mathcal{N},n}^{(\alpha)-1}\right) = \Theta_{\mathbb{P}}\left(e^{n\lambda_{\gamma,i}^{(\alpha)}}\right) \text{ and } c_{i,n}^{(\alpha)} = \Theta_{\mathbb{P}}\left(e^{n\lambda_{\gamma,i}^{(\alpha)}}\right), \qquad (5.17)$$

  where $\mathbf{R}_{\mathcal{I},n}^{(\alpha)}$ and $\mathbf{R}_{\mathcal{N},n}^{(\alpha)}$ are given in (5.14) and (5.15), respectively.

On top of our main results, we also establish the following notable secondary results:

- In Lemma 6, we show that to ensure the instantaneous transmit power *almost surely* displays no exponential growth, and that the end-to-end capacity of the dominant eigenchannel *almost surely* displays no exponential decay (i.e., from (5.16) and (5.17), $\lambda_{\mathbf{H},1}^{(\alpha)} = 0$), the *average* transmit power *must* grow exponentially with n. Furthermore, this rate of average power growth can be reduced by:

  1. implementing VG instead of FG,
  2. increasing the number of antennas at each node.

- In (5.54), we show that the exponential rate at which the capacities of the ith and jth ($i < j$) eigenchannels diverge away from each other is given by $n\left(\lambda_{\gamma,i}^{(\alpha)} - \lambda_{\gamma,j}^{(\alpha)}\right)$. When the ith and jth eigenchannel capacities are either both decaying or both not decaying, this divergence rate is shown to be independent of whether FG or VG relaying is being performed. Furthermore, from Lemma 9 and Corollary 1, with

$i = 1$, to ensure that this rate is asymptotically bounded away from infinity (so that multiplexing j streams is asymptotically viable) we must either:

1. ensure that $\lambda^{(\alpha)}_{\mathbf{H},j} \geq 0$,
2. ensure that the number of antennas at each node grows like $m = \Omega(n)$. This result complements those presented in [100, 101].

- In Remark 3, we assign a transmit power cost to the nth node for each extra data stream that is multiplexed over the network. In particular, if i data streams are being multiplexed, then, to multiplex one extra stream, we must increase the nth relay's instantaneous transmit power by a factor of $\exp(n/(m-i))$.

On the way to proving the above mentioned results, we also obtain the following RDS results, which we believe are of independent interest.

- For $i \in \mathbb{N}$, let $\mathbf{A}_i \in \mathbb{C}^{m\times m}$ and $R_i \in \mathbb{C}^m$ be random matrices and vectors, respectively, with $\mathbb{E}\log^+ \|\mathbf{A}_1\| < \infty$, $\mathbb{E}\log^+ \|R_1\| < \infty$, and $R_i \overset{a.s.}{\neq} 0$. Suppose that there exists $\alpha_j, \beta_j \in \mathbb{R}$ such that $\mathbf{A}_1$ is equal in distribution to $\alpha_j \mathbf{A}_j$ and R_1 is equal in distribution to $\beta_j R_j$. In Lemma 5, we show that the Lyapunov exponents of an affine RDS taking the form

$$X_n = \mathbf{A}_n X_{n-1} + R_n, \tag{5.18}$$

are strictly positive, and, consequently, are identical to those of

$$\begin{bmatrix} X_n \\ 1 \end{bmatrix} = \begin{bmatrix} \mathbf{A}_n & R_n \\ \mathbf{0^T} & 1 \end{bmatrix} \cdots \begin{bmatrix} \mathbf{A}_1 & R_1 \\ \mathbf{0^T} & 1 \end{bmatrix} \begin{bmatrix} X_0 \\ 1 \end{bmatrix}. \tag{5.19}$$

- In Theorem 1, we show that the Lyapunov exponents of (5.19) are given by the non-negative Lyapunov exponents of

$$\pi_n(\mathbf{A}) := \mathbf{A}_n \cdots \mathbf{A}_1. \tag{5.20}$$

Less formally, our RDS results provide us with a framework for determining *all* of the Lyapunov exponents of m dimensional affine RDSs, which will be crucial to our information theoretic analysis.

5.4 Random Dynamical Systems

In this section, we introduce the RDS results that will be relied upon heavily throughout this chapter. The first subsection is devoted to presenting preexisting RDS theory, while the second subsection presents a new result which will be used to calculate the Lyapunov exponents of affine systems.

5.4.1 Preliminary Random Dynamical Systems Results

The study of dynamical systems is concerned with tracking the trajectory of a position (particle/state/point) through a state space. In the discrete case, this position is calculated through the repeated action of a deterministic map. Informally, an RDS occurs when this map is non-deterministic and drawn from a sample space according to some fixed probability distribution. Such systems are are often used to study econometrics [123], biological systems [124, 125], chemical reactions [125], and the propagation of particles through fluidic media [126]. The formal and rather intricate definition of an RDS can be found in [6].

In this chapter, we consider an RDS to be the action of a product of $m \times m$ ($m \in \mathbb{N}$) complex random matrices on an appropriately dimensioned vector (the initial state $X_0 \in \mathbb{C}^m$). The state of the RDS at time n ($X_n \in \mathbb{C}^m$) can then be written as either

$$X_n = \mathbf{A}_n \cdots \mathbf{A}_1 X_0, \tag{5.21}$$

or

$$X_n = \mathbf{A}_1 \cdots \mathbf{A}_n X_0 \tag{5.22}$$

where, in general, we assume that $\mathbf{A}_1, \ldots, \mathbf{A}_n$ are independent and identically distributed (i.i.d.) up to an arbitrary positive scaling factor. Mathematically, this means that $\exists\ a_j > 0$ such that $\mathbf{A}_1 \stackrel{d}{=} a_j \mathbf{A}_j$ for all j. Eqs. (5.21) and (5.22) are referred to as forward and backward RDSs, respectively, and take their names from the forward [6, Def'n. 1.1.1] and backward [6, Rem. 1.1.10] cocycle properties that their random mappings satisfy. It is interesting and important to note that, unlike (5.21), (5.22) is somewhat unnatural, in the sense that it is anticausal; however, all of the RDS properties that are to be described for (5.21) will apply to (5.22) as well, [6].

Suppose we wish to study the asymptotic behavior of

$$\|\pi_n(\mathbf{A})\| \tag{5.23}$$

as $n \to \infty$. A traditional approach is to exponentiate the logarithm of the norm; i.e., write (5.23) as

$$\|\pi_n(\mathbf{A})\| = e^{n \frac{1}{n} \log \|\pi_n(\mathbf{A})\|} \tag{5.24}$$

and investigate the behavior of the exponent, specifically, $\frac{1}{n}\log\|\pi_n(\mathbf{A})\|$ as n grows large. In this manner, the exponential growth/decay rate of the system can be observed. If $\{\mathbf{A}_j\}$ was a set of scalars (i.e., $m = 1$), the law of large numbers could be employed to evaluate the limiting behavior of $\frac{1}{n}\log\|\pi_n(\mathbf{A})\|$; however, this is not the case for general m.

The question of whether $\frac{1}{n}\log\|\pi_n(\mathbf{A})\|$ tends to a limit does not have a clear answer in most cases. Under the condition that $\mathbb{E}[\log^+\|\mathbf{A}_1\|] < \infty$ and $\lim_{n\to\infty} 1/n\sum_{i=1}^{n}\log^+|g_i| < \infty$, however, the theorem of Furstenberg and Kesten [6] guarantees that the limit exists. We then obtain the *Lyapunov index*:

Definition 2 *The Lyapunov index is given by*

$$\iota(\mathbf{A}) := \limsup_{n\to\infty}\frac{1}{n}\log\|\pi_n(\mathbf{A})\|\,. \tag{5.25}$$

The Lyapunov index can be used to describe the exponential growth rate of $\|\pi_n(\mathbf{A})\|$. By evaluating the Lyapunov index at a specific initial position within the state space, we then obtain the *Lyapunov exponent*:

Definition 3 *The Lyapunov exponent is given by*

$$\lambda(\mathbf{A}, X) := \limsup_{n\to\infty}\frac{1}{n}\log\|\pi_n(\mathbf{A})X\|\,. \tag{5.26}$$

The Lyapunov exponent can be used to describe the exponential growth rate of the norm of a trajectory through its state space, where the initial state of the trajectory is given by X.

Remark 1 *In the definitions of the Lyapunov index and exponent (*(5.25) *and* (5.26)*, respectively), if the system is linear then the* lim sup *can be*

replaced with a limit, [6].

Fact 2 *From [6, pp.* $114-115$*, Theorem 3.3.3], assuming* $\mathbb{E}[\log^+ \|\mathbf{A}_1\|] < \infty$ *and* $-\infty < \lim_{n\to\infty} 1/n \sum_{i=1}^{n} \log^+ |g_i| < \infty$ *(where* $\mathbf{A}_1 \stackrel{d}{=} g_i \mathbf{A}_i$*), the Lyapunov exponent has the following properties [6]:*

1. $\lambda(\mathbf{A}, X) \in \mathbb{R} \cup \{-\infty\}\ \forall\ X \in \mathbb{C}^m$*, where* $\lambda(\mathbf{A}, \mathbf{0}) := -\infty$*;*

2. *The number,* p*, of distinct values,* λ_i*, that* $\lambda(\mathbf{A}, X)$ *can take on for* $X \in \mathbb{C}^m \backslash \{\mathbf{0}\}$ *is at most* m*, and we have* $-\infty \leq \lambda_p < \cdots < \lambda_1 < \infty$*.*

3. *The sets*

$$\mathcal{V}_i := \{X : \lambda(\mathbf{A}, X) \leq \lambda_i\} \tag{5.27}$$

are linear subspaces, form a filtration

$$\{0\} =: \mathcal{V}_{p+1} \subset \mathcal{V}_p \subset \cdots \subset \mathcal{V}_1 = \mathbb{C}^m \tag{5.28}$$

(where all inclusions are proper), and

$$\lambda_i = \lambda(\mathbf{A}, X) \Leftrightarrow X \in \mathcal{V}_i \setminus \mathcal{V}_{i+1},\ i = 1, \ldots, p. \tag{5.29}$$

The integer $m(i) := \dim \mathcal{V}_i - \dim \mathcal{V}_{i-1}$ *is the multiplicity of* λ_i*.*

4. *The limiting behavior for the ordered singular values of the matrix product* $\pi_n(\mathbf{A})$ *satisfies*

$$\frac{1}{2n} \log \mathcal{E}_i \left\{\pi_n(\mathbf{A}) \pi_n(\mathbf{A})^\dagger\right\} \to \lambda_i. \tag{5.30}$$

Consequently, the random variable $\mathcal{E}_i\left\{\pi_n(\mathbf{A})\pi_n(\mathbf{A})^\dagger\right\}$ *satisfies*

$$\mathcal{E}_i\left\{\pi_n(\mathbf{A})\pi_n(\mathbf{A})^\dagger\right\} = \Theta_{\mathbb{P}}\left(e^{2n\lambda_i}\right). \tag{5.31}$$

In what follows, we will often drop the functional notation $\lambda(\mathbf{A}, X)$ and simply write $\lambda_{\mathbf{A},i}$ to refer to the ith ordered Lyapunov exponent of the system corresponding to $\pi_n(\mathbf{A})$. When it is clear, we may also omit the subscript $\mathbf{A}$ as we did in Fact 2.

5.4.2 On the Lyapunov Exponents of Affine Random Dynamical Systems

Throughout this chapter, we will often be concerned with the Lyapunov exponents of affine systems of the form

$$X_n = \mathbf{A}_n X_{n-1} + R_n, \tag{5.32}$$

where $\mathbf{A}_n \in \mathbb{C}^{m\times m}$ is a random matrix and $R_n \in \mathbb{C}^m$ is a random vector with $R_n \overset{a.s.}{\neq} 0$ that satisfies $R_n \overset{d}{=} -R_n$. The following theorem will be used in the calculation of these exponents.

Theorem 1 *For* $i \in \mathbb{N}$*, consider the product of random matrices* $\pi_n(\mathbf{M})$*, where*

$$\mathbf{M}_i = \begin{bmatrix} \mathbf{A}_i & R_i \\ \mathbf{0^T} & a_i \end{bmatrix} \in \mathbb{C}^{(m+1)\times(m+1)} \tag{5.33}$$

$\mathbb{E}\log^+\|\mathbf{A}_i\| < \infty$*,* $\mathbb{E}\log^+\|R_i\| < \infty$*, and* $\mathbb{E}\log^+|a_i| < \infty$*. Under the assumption that* $\pi_n(\mathbf{A})$ *has* m *distinct Lyapunov exponents,* $\forall\ i\ \exists\ X_0 \in \mathbb{C}^m$

such that

$$\lambda\left(\mathbf{M}, \left[X_0^T \;\; 1\right]^T\right) = \max\left\{\lambda_{\mathbf{A},i}, \lambda_{a,1}\right\}. \tag{5.34}$$

Proof See Appendix B.1. ■

5.4.2.1 Applications and Implications of Theorem 1

We will now show that Theorem 1 can be used to calculate the Lyapunov exponents of (5.32). To do this, the affine structure of (5.32) will be captured by converting it into a linear (non-affine) $(m+1)\times(m+1)$ system of the following form:

$$\begin{bmatrix} X_n \\ 1 \end{bmatrix} = \begin{bmatrix} \mathbf{A}_n & R_n \\ \mathbf{0^T} & 1 \end{bmatrix} \cdots \begin{bmatrix} \mathbf{A}_1 & R_1 \\ \mathbf{0^T} & 1 \end{bmatrix} \begin{bmatrix} X_0 \\ 1 \end{bmatrix}. \tag{5.35}$$

One may naively assume that the Lyapunov exponents of (5.32) are trivially identical to those of (5.35). However, for this to be true, we must have $\lim_{n\to\infty} \frac{1}{n} \log \|X_n\| \geq 0$, because, clearly,

$$\lim_{n\to\infty} \frac{1}{n} \log \left\| [X_n \;\; 1]^T \right\| \geq 0. \tag{5.36}$$

We now provide the following lemma, which tells us that the Lyapunov exponents of (5.32) are indeed strictly non-negative, and that, consequently, the Lyapunov exponents of (5.32) and (5.35) are identical.

Lemma 5 *For X_n given by* (5.32)*, we have*

$$\lim_{n\to\infty} \frac{1}{n} \log ||X_n|| \geq 0.$$

Consequently, the Lyapunov exponents of the affine system, (5.32)*, and those of the linear-to-affine converted system,* (5.35)*, are identical.*

Proof See Appendix B.2. ■

From Fact 3 (below), it can be seen that the Lyapunov exponents of (5.35) (and consequently (5.32)) must belong to $\{\max\{\lambda_{\mathbf{A},i}, 0\} : i = 1, \ldots, m\}$.

Fact 3 *[133, Theorem 5], consider the product of random matrices* $\pi_n(\mathbf{M})$*, where*

$$\mathbf{M}_i = \begin{bmatrix} \mathbf{A}_i & R_i \\ \mathbf{0^T} & a_i \end{bmatrix} \in \mathbb{C}^{(m+1)\times(m+1)}, \tag{5.37}$$

$\mathbb{E}\log^+\|\mathbf{A}_i\| < \infty$*,* $\mathbb{E}\log^+\|R_i\| < \infty$*, and* $\mathbb{E}\log^+|a_i| < \infty$*. Then the Lyapunov exponents of* $\pi_n(\mathbf{M})$ *are given by* $\{\lambda_{\mathbf{A},i} : i = 1, \ldots, n\} \cup \lambda_{a,1}$*. Furthermore, the Lyapunov exponents of* $\pi_n(\mathbf{M})$ *are independent of the statistics of* R_i*.*

Notice that Fact 3 tells us nothing about how initial states of the form $\begin{bmatrix} X_0^T & 1 \end{bmatrix}^T$ (c.f. (5.35)), will affect the Lyapunov analysis. Consequently, we require a theorem that deals with such initial states. This provides the rationale behind Theorem 1. Theorem 1 also plays a pivotal role in the proof of Theorem 2.

5.5 Capacity and Power Scaling

In this section, we will use the network's Lyapunov exponents to establish the scaling behavior of the end-to-end capacity and nth node transmit power. The following theorem relates the Lyapunov exponents to the network's end-to-end capacity.

Theorem 2 *Let $\lambda_{\mathbf{H},i}^{(\alpha)}$ be the Lyapunov exponent of $\mathcal{I}_n^{(\alpha)}$ (which is defined in (5.6)) and $c_n^{(\alpha)} = \sum_{i=1}^m c_{n,i}^{(\alpha)}$ (nats/channel use) be the capacity of the n-hop AF network with amplification strategy $\alpha \in \{FG, VG\}$ (see Definition 1 and Fact 1), where $c_{n,i}^{(\alpha)}$ is the capacity of the ith eigenchannel at the nth node. Then the following statements hold.*

A. $\lim_{n\to\infty} \frac{1}{n} \log \mathcal{E}_i \left(\mathbf{R}_{\mathcal{I},n}^{(\alpha)} \mathbf{R}_{\mathcal{N},n}^{(\alpha)-1} \right) \stackrel{a.s.}{=} \min\{0, 2\lambda_{\mathbf{H},i}^{(\alpha)}\} =: \lambda_{\gamma,i}^{(\alpha)}$. *Hence, the SNR of the ith eigenchannel obeys*

$$\mathcal{E}_i \left(\mathbf{R}_{\mathcal{I},n}^{(\alpha)} \mathbf{R}_{\mathcal{N},n}^{(\alpha)-1} \right) = \Theta_{\mathbb{P}} \left(e^{n\lambda_{\gamma,i}^{(\alpha)}} \right). \tag{5.38}$$

B. $\lim_{n\to\infty} \frac{1}{n} \log c_{n,i}^{(\alpha)} \stackrel{a.s.}{=} \min\{0, 2\lambda_{\mathbf{H},i}^{(\alpha)}\} =: \lambda_{\gamma,i}^{(\alpha)}$. *Thus, the capacity of the ith eigenchannel obeys*

$$c_{n,i}^{(\alpha)} = \Theta_{\mathbb{P}} \left(e^{n\lambda_{\gamma,i}^{(\alpha)}} \right). \tag{5.39}$$

Proof See Appendix B.3. ■

The next lemma will evaluate the Lyapunov exponent $\lambda_{\mathbf{H},i}^{(\alpha)}$, and establish how it relates to the Lyapunov exponents of $X_n^{(\alpha)}$ and the average transmit power at the nth node. This lemma will in turn allow us to establish a trade off between capacity decay and power growth across the network. It will also have implications on gain design.

Lemma 6 *With $\mathcal{I}_n^{(\alpha)}$ given by (5.6), $X_n^{(\alpha)}$ given by (5.8), and the average transmit power at the nth node given by p_n, the following statements hold.*

A. *The ith Lyapunov exponent of $\mathcal{I}_n^{(\alpha)}$ is given by*

$$\lambda_{\mathbf{H},i}^{(\alpha)} = \frac{1}{2} \left(L \left({g_\alpha}^2 \mu \right) + \psi(m - i + 1) \right), \; i = 1, \cdots, m; \tag{5.40}$$

where $\psi(\cdot)$ is the digamma function [2, eq. (6.3.1)] and

$$L(g_\alpha^2 \mu) := \lim_{n\to\infty} \frac{1}{n} \sum_{i=1}^{n} \log(g_{\alpha,i}^2 \mu_i). \tag{5.41}$$

The ith Lyapunov exponent of $X_n^{(\alpha)}$ is given by

$$\lambda_{\mathbf{Q},i}^{(\alpha)} \;:=\; \lambda\left(\mathbf{Q}, \left[X_0^T \ \sqrt{n_0}\right]\right) = \max\left\{0, \lambda_{\mathbf{H},i}^{(\alpha)}\right\}. \tag{5.42}$$

Hence, the information power and total transmit power obey

$$\left\|\mathcal{I}_n^{(\alpha)}\right\|^2 \;=\; \Theta_{\mathbb{P}}\left(e^{2n\lambda_{\mathbf{H},1}^{(\alpha)}}\right), \tag{5.43}$$

$$\left\|X_n^{(\alpha)}\right\|^2 \;=\; \Theta_{\mathbb{P}}\left(e^{2n\lambda_{\mathbf{Q},1}^{(\alpha)}}\right). \tag{5.44}$$

B. *For FG, we have*

$$\lim_{n\to\infty} \frac{1}{n} \log \frac{p_n}{p_0} \geq \max\left\{2\lambda_{\mathbf{H},1}^{(FG)} + \log m - \psi(m),\ 0\right\}; \tag{5.45}$$

for VG, we have

$$\lim_{n\to\infty} \frac{1}{n} \log \frac{p_n}{p_0} \geq \max\left\{2\lambda_{\mathbf{H},1}^{(VG)} + \psi(m^2) - \psi(m) - \log m,\ 0\right\}; \tag{5.46}$$

where equality is maintained only when $n_0 = 0$.

Proof See Appendix B.4. ■

5.5.1 A Brief Discussion of Theorem 2 and Lemma 6

From the first statement of Lemma 6, by ensuring $\lambda_{\mathbf{H},m}^{(\alpha)} < \cdots < \lambda_{\mathbf{H},1}^{(\alpha)} = 0$, we can avoid exponential growth in the instantaneous transmit power.

However, in this setup Theorem 2 tells us that all but the first eigenchannel will display an exponentially decaying capacity. Conversely, by ensuring $\lambda_{\mathbf{H},1}^{(\alpha)} > \cdots > \lambda_{\mathbf{H},q}^{(\alpha)} \geq 0 > \lambda_{\mathbf{H},q+1}^{(\alpha)} > \cdots > \lambda_{\mathbf{H},m}^{(\alpha)}$, we can stop the end-to-end capacity of the upper q eigenchannels from *almost surely* decaying exponentially. However, in this scenario, we must allow for exponential growth in the instantaneous power across the network. Thus, there is a clear tradeoff to be had between multiplexing multiple data streams across the network, and growth in the instantaneous transmit power at the nth node.

Focusing on the second statement of Lemma 6, it can be seen that the terms $\log m - \psi(m)$ and $\psi(m^2) - \psi(m) + \log m$ in (5.45) and (5.46), respectively, are strictly non-negative. Thus, this statement tells us that, asymptotically, the *average* transmit power must grow at a greater exponential rate than the instantaneous power. Crucially, we find that exponential growth in p_n can be allowed for whilst avoiding (with high probability) exponential instantaneous power growth at the relays. Said in a different way, as the network scales in size, the density function of the transmit power at the nth node becomes increasingly heavy tailed. Whilst most of the distribution's mass will be concentrated at the point governed by the Lyapunov exponent (cf. (5.44)), the distribution's heavy tail will push the average up exponentially. Combining this observation with Theorem 2, it can be seen that ensuring the first eigenchannel displays a non exponentially decaying capacity implies that the average transmit power will grow exponentially.

It can also be seen that, because $\log m - \psi(m) \geq \psi(m^2) - \psi(m) - \log m$, the lower bound on the exponential growth rate of the average transmit power for VG is strictly less than that for FG, which suggests that the VG

network can sustain an approximately constant instantaneous power trend with a reduced growth in the average transmit power. Furthermore, as the number of antennas grows large, both bounds in Lemma 6 converge towards the Lyapunpov exponents. Thus, ergodic behavior is induced as m grows large.

In summary, Theorem 2 and the first statement of Lemma 6 expose a fundamental trade off between capacity decay and instantaneous transmit power growth across the network. The second statement of Lemma 6 has important implications on gain design for scaled networks. In particular, it implies that the average transmit power at each node should grow exponentially with the network if an approximately constant instantaneous power trend is to be maintained. These implications contrast with the system model proposed in [100, 101], where the capacity was assessed under strictly linear scaling of p_n while the number of antennas at each node grew with the number of hops within the network. For the finite antenna system, we see that if linear scaling of p_n occurs, $\lim_{n\to\infty} \log(p_n/p_0)/n = 0$ and (from Lemma 6) $\lambda^{(\alpha)}_{\mathbf{H},1} < 0$. As has been seen in the Theorem 2, $\lambda^{(\alpha)}_{\mathbf{H},1} < 0$ will have serious implications on the network's end-to-end capacity. As an extra note, it can be seen that our result implicitly applies to a network whose length grows with the number of hops in the network (the extended regime); i.e., the distance between each node is fixed. For future work, it may be interesting to consider capacity and power scaling properties for networks when the end-to-end length of the network is fixed, and the distance between each of the nodes decreases with the number of hops (the dense regime), see [134]. However, this is beyond the scope of this chapter.

Finally, we would like to point out that it is unclear whether our RDS

and corresponding Lyapunov analysis can be applied to study other forwarding schemes (e.g., DF). For the AF scenario, the analysis relies on the ability to make a correspondence between the network and products of random matrices. Moving to other (non AF) forwarding scenarios, the relay network will be described by a composition of random nonlinear mappings. In general, when determining the Lyapunov exponents of a system, the multiplicative ergodic theorem [6] (MET) is referred to. This theorem is a linear result, and when one refers to the MET for a nonlinear system they are implicitly referring to the application of this theorem to the linearized version of the nonlinear system. Thus, we have two open questions about applying our approach to other forwarding schemes:

1. Does the linearization of a system describing forwarding such as DF make sense from a practical view point?

2. If the answer to 1) is yes, can analogous capacity and power results be obtained for such schemes?

5.6 Applications of Theorem 2 and Lemma 6

In this section, we will study some applications of Theorem 2 and Lemma 6. In particular, we will study the rates at which the eigenchannel capacities diverge away from each other, and how this relates to:

- the amplification strategy and number of antennas at each node,

- the growth in the instantaneous transmit power.

To discuss the above mentioned points, we will require the following preliminary definitions and lemmas.

5.6.1 Preliminary Definitions and Lemmas

Definition 4 *The (i,j)th normalized channel capacity, $i \leq j$, is defined to be*

$$\nu_{i,j,n}^{(\alpha)} := \frac{c_{i,n}^{(\alpha)}}{c_{j,n}^{(\alpha)}}. \tag{5.47}$$

Clearly, if $\nu_{1,j,n}^{(\alpha)} \approx 1$, the channel will be well suited for multiplexing j data streams, [42, 131], provided $c_{1,n}^{(\alpha)}$ is sufficiently large; otherwise, it will not.

Definition 5 *For both FG and VG, the (i,j)th* Lyapunov difference, *$i \leq j$, is defined to be*

$$\phi_{i,j}^{(\alpha)} := \lambda_{\gamma,i}^{(\alpha)} - \lambda_{\gamma,j}^{(\alpha)}. \tag{5.48}$$

The following two lemmas are used to bound $\phi_{i,j}^{(\alpha)}$, and will be employed in the ensuing analysis.

Lemma 7 *The (i,j)th Lyapunov difference is bounded as follows:*

$$0 \leq \phi_{i,j}^{(\alpha)} \leq 2\left(\lambda_{\mathbf{H},i}^{(\alpha)} - \lambda_{\mathbf{H},j}^{(\alpha)}\right) =: \bar{\phi}_{i,j}, \tag{5.49}$$

where lower equality is maintained if and only if $\lambda_{\mathbf{H},i}^{(\alpha)} > \lambda_{\mathbf{H},j}^{(\alpha)} \geq 0$, upper equality is maintained if and only if $\lambda_{\mathbf{H},j}^{(\alpha)} < \lambda_{\mathbf{H},i}^{(\alpha)} \leq 0$, and $\phi_{i,j}^{(\alpha)} = -2\lambda_{\mathbf{H},j}^{(\alpha)}$ otherwise. Furthermore, the upper bound is independent of whether FG or VG is being implemented.

Proof See Appendix B.5. ■

Finally, we will also exploit the following lemma later in this section.

Lemma 8 *For $i < j$, we have*

$$\bar{\phi}_{i,j} \quad = \quad \sum_{k=m-j+1}^{m-i} \frac{1}{k} = (\mathcal{H}_{m-i} - \mathcal{H}_{m-j}), \tag{5.50}$$

where $\mathcal{H}_i$ is the ith harmonic series defined to be

$$\mathcal{H}_i = \sum_{j=1}^{i} \frac{1}{j}. \tag{5.51}$$

Furthermore, by considering the first and last summands in (5.50)*, we can trivially construct the following bound:*

$$\frac{j-i+1}{m-i} \leq \bar{\phi}_{i,j} \leq \frac{j-i+1}{m-j+1}. \tag{5.52}$$

Proof This follows immediately from (5.40), Lemma 7, and applying the telescope property of the digamma function [2, eq. (6.3.5)]:

$$\psi(x+1) = \psi(x) + \frac{1}{x}. \tag{5.53}$$

■

5.6.2 Growth of $\nu_{i,j,n}^{(\alpha)}$ and $\|X_n\|^2$

We will now apply Theorem 2 and Lemma 6 to study $\nu_{i,j,n}^{(\alpha)}$ (Definition 4) and $\|X_n^{(\alpha)}\|^2$. Considering Theorem 2 first, from Definitions 4 and 5 we have

$$\lim_{n\to\infty} \frac{1}{n} \log \nu_{i,j,n}^{(\alpha)} = \phi_{i,j}^{(\alpha)} \iff \nu_{i,j,n}^{(\alpha)} = \Theta_{\mathbb{P}}\left(e^{n\phi_{i,j}^{(\alpha)}}\right). \tag{5.54}$$

We will now use (5.54) (in conjunction with Lemma 6) to study the following four problems:

1. The dependence of the growth in $\nu_{i,j,n}^{(\alpha)}$ on the amplification strategy.

2. The dependence of the growth in $\nu_{i,j,n}^{(\alpha)}$ on the number of antennas at each node

3. The behavior of the network when either $\phi_{1,i}^{(\alpha)} = 0$ or $\lambda_{\mathbf{H},1}^{(\alpha)} = 0$; i.e., when either $\nu_{i,j,n}^{(\alpha)}$ or $\|X_n^{(\alpha)}\|^2$ display no exponential growth, respectively.

4. The growth in $\nu_{i,i+1,n}^{(\alpha)}$ (i.e., rate at which adjacent eigenchannel capacities diverge away from each other), and the cost (in terms of instantaneous transmit power) associated with each extra multiplexed data stream.

5.6.2.1 Growth of $\nu_{i,j,n}$ and the Forwarding Strategy

Let us first establish how the amplification strategy affects the growth of $\nu_{i,j,n}^{(\alpha)}$. As an immediate consequence of Lemma 7, it can be seen that when $\lambda_{\mathbf{H},j}^{(\alpha)} < \lambda_{\mathbf{H},i}^{(\alpha)} \leq 0$ the exponential growth of $\nu_{i,j,n}^{(\alpha)}$ will be independent of the amplification strategy that has been implemented. The same holds true when $0 \leq \lambda_{\mathbf{H},j}^{(\alpha)} < \lambda_{\mathbf{H},i}^{(\alpha)}$, since we will have $\phi_{i,j,n}^{(\alpha)} = 0$. For $\lambda_{\mathbf{H},j}^{(\alpha)} < 0 < \lambda_{\mathbf{H},i}^{(\alpha)}$, we will have $\phi_{i,j,n}^{(\alpha)} = -2\lambda_{\mathbf{H},j}^{(\alpha)}$. Consequently, in this scenario $\nu_{i,j,n}^{(\alpha)}$ is given by

$$\nu_{i,j,n}^{(f)} = \Theta_{\mathbb{P}}\left(e^{-2\lambda_{f\mathbf{H},j}}\right) = \Omega_{\mathbb{P}}\left(e^{-\lim_{n\to\infty}\frac{1}{n}\log\frac{p_n}{p_0}+\log m-\psi(m-j+1)}\right), \qquad (5.55)$$

for FG, and

$$\nu_{i,j,n}^{(v)} = \Theta_{\mathbb{P}}\left(e^{-2\lambda_{v\mathbf{H},j}}\right) = \Omega_{\mathbb{P}}\left(e^{-\lim_{n\to\infty}\frac{1}{n}\log\frac{p_n}{p_0}-\log(m)+\psi\left(m^2\right)-\psi(m-j+1)}\right), \tag{5.56}$$

for VG, where the second equalities of (5.55) and (5.56) follow from Lemma 11. Notice that, because $\log m^2 > \psi\left(m^2\right)$,

$$e^{-\lim_{n\to\infty}\frac{1}{n}\log\frac{p_n}{p_0}+\log m-\psi(m-j+1)} \geq e^{-\lim_{n\to\infty}\frac{1}{n}\log\frac{p_n}{p_0}-\log(m)+\psi\left(m^2\right)-\psi(m-j+1)}. \tag{5.57}$$

5.6.2.2 Growth of $\nu_{i,j,n}$ and the Number of Antennas

We will now establish how the number of antennas at each node will affect the growth rate of $\nu_{i,j,n}^{(\alpha)}$. In particular, we will determine how $n\phi_{i,j}^{(\alpha)}$ (the term in the exponent of (5.54)) scales with n, and how the number of antennas relates to this. More specifically, in what follows (Lemma 9 and Corollary 1) we will determine conditions that give the following:

$$\lim_{n\to\infty}\left[n\phi_{i,j}^{(\alpha)}\right] = 0 \quad \Leftrightarrow \quad \phi_{i,j}^{(\alpha)} = o\left(1/n\right), \tag{5.58}$$

$$0 < \lim_{n\to\infty}\left[n\phi_{i,j}^{(\alpha)}\right] \leq K < \infty \quad \Leftrightarrow \quad \phi_{i,j}^{(\alpha)} = \Theta\left(1/n\right), \tag{5.59}$$

$$\lim_{n\to\infty}\left[n\phi_{i,j}^{(\alpha)}\right] = \infty \quad \Leftrightarrow \quad 1/\phi_{i,j}^{(\alpha)} = o\left(n\right). \tag{5.60}$$

Of course, if $\phi_{i,j}^{(\alpha)} = 0$ (i.e., $\lambda_{\mathbf{H},i}^{(\alpha)} > \lambda_{\mathbf{H},j}^{(\alpha)} \geq 0$) (5.58) is obtained trivially. We are therefore only interested in studying the behavior of $n\phi_{i,j}^{(\alpha)}$ when either $0 \geq \lambda_{\mathbf{H},i}^{(\alpha)} > \lambda_{\mathbf{H},j}^{(\alpha)}$ or $\lambda_{\mathbf{H},i}^{(\alpha)} > 0 > \lambda_{\mathbf{H},j}^{(\alpha)}$. We treat $0 \geq \lambda_{\mathbf{H},i}^{(\alpha)} > \lambda_{\mathbf{H},j}^{(\alpha)}$ in Lemma 9 and consider $\lambda_{\mathbf{H},i}^{(\alpha)} > 0 > \lambda_{\mathbf{H},j}^{(\alpha)}$ in its corollary.

Lemma 9 *When $0 \geq \lambda_{\mathbf{H},i}^{(\alpha)} > \lambda_{\mathbf{H},j}^{(\alpha)}$, for both FG and VG, to leading order*

about $m = \infty$ *(i.e.,* $i < j$ *fixed and* $m \to \infty$*)* $\phi_{i,j}^{(\alpha)}$ *is given by*

$$\phi_{i,j}^{(\alpha)} = \bar{\phi}_{i,j} = \frac{(j-i)}{m} + O\left(\frac{1}{m}\right)^2. \tag{5.61}$$

Consequently,

1. *the conditions that give* (5.58) *are* $1/m = o(1/n)$,

2. *the conditions that give* (5.59) *are* $1/m = \Theta(1/n)$

3. *the conditions that give* (5.60) *are* $m = o(n)$.

Proof Eq. (5.61) is obtained by performing a Taylor expansion of $\bar{\phi}_{i,j}$ about the point m and letting $m \to \infty$, with $i \leq j$ fixed. The following statements then follow immediately. ■

Corollary 1 *It is only possible to maintain* $\lambda_{\mathbf{H},i}^{(\alpha)} > 0 > \lambda_{\mathbf{H},j}^{(\alpha)}$ *when* $m = O(1)$. *From Lemma 9, when this occurs* $\lim_{n\to\infty} n\phi_{i,j}^{(\alpha)} = \infty$.

We will now discuss Lemma 9 and its corollary. These are seen to complement [101, Thrm. 4], where they were able to show that $\lim_{n\to\infty} \lim_{m_D\to\infty} (c_n/m_D)/n$ (where m_D is the number of destination antennas) will be strictly positive if and only if $m/m_D = \Theta(n^{1+\epsilon})$ for all $\epsilon \geq 0$ (note, the inequality for ϵ is not strict). In our work, if $m/j = \Theta(n^{1+\epsilon})$, for fixed j, $n\phi_{i,j}^{(\alpha)}$ will be bounded away from infinity $\forall\, i < j$ and consequently, from (5.54), $\nu_{i,j,n}^{(\alpha)}$ will *almost surely* display no exponential growth as n grows without bound[7]. Clearly, avoiding exponential growth of $\nu_{1,j,n}^{(\alpha)}$ is required if

[7]Note, for the work in [101] and our work, m_D and j can be thought of as the maximum number of data streams that can be multiplexed over the channel, respectively. This draws the connection between that work, where the scaling of the ratio m/m_D is assessed, and our work, where the scaling of m/j is assessed.

we are to multiplex over the j upper eigenchannels. Crucially, these results provide us with an alternative perspective to [101] on how the number of antennas (more precisely, the scaling of this number) at each node affects the end-to-end capacity of the network.

5.6.2.3 Network behavior when $\phi_{1,i}^{(\alpha)} = 0$ or $\lambda_{\mathbf{H},1}^{(\alpha)} = 0$

Suppose we wish to ensure that the $(1,i)$th normalized channel capacity displays no exponential growth; i.e., (from (5.54)) $\phi_{1,i}^{(\alpha)} = 0$. Furthermore, suppose this is achieved by ensuring that

$$\lambda_{\mathbf{H},1}^{(\alpha)} > \lambda_{\mathbf{H},i}^{(\alpha)} = 0. \tag{5.62}$$

Then (5.44) and Lemma 8 give us

$$\left\| X_n^{(\alpha)} \right\|^2 = \Theta_{\mathbb{P}} \left(e^{n(\mathcal{H}_{m-1} - \mathcal{H}_{m-i})} \right), \tag{5.63}$$

where the argument of $\Theta_{\mathbb{P}}(\cdot)$ in (5.63) is bound in the following way:

$$e^{\frac{ni}{m-1}} \leq e^{n(\mathcal{H}_{m-1} - \mathcal{H}_{m-i})} \leq e^{\frac{ni}{m-i+1}}. \tag{5.64}$$

Thus, ensuring $\phi_{1,i}^{(\alpha)} = 0$ implies that the transmit power must grow according to (5.63). This growth rate is strictly positive and bound according to (5.64). We can see that by increasing the number of antennas, m, for a fixed i, the rate at which the transmit power grows can be reduced. Conversely, by fixing m and increasing i (i.e., multiplexing more data streams), the rate at which the transmit power must grow will increase.

Suppose instead we wish to ensure that the transmit power displays no

exponential growth by setting $\lambda_{\mathbf{H},1}^{(\alpha)} = 0$. From (5.54) and Lemmas 7 and 8, this gives

$$\nu_{1,i,n}^{(\alpha)} = \Theta_{\mathbb{P}}\left(e^{n(\mathcal{H}_{m-1}-\mathcal{H}_{m-i})}\right). \tag{5.65}$$

Thus, all of the growth properties that applied to $\|X_n^{(\alpha)}\|^2$ when $\lambda_{\mathbf{H},i}^{(\alpha)} = 0$ apply to $\nu_{1,i,n}^{(\alpha)}$ when $\lambda_{\mathbf{H},1}^{(\alpha)} = 0$.

Remark 2 *Interestingly, from* (5.63) *and* (5.65)*, it can be seen that there is a duality between the exponential growth rate of* $\left\|X_n^{(\alpha)}\right\|^2$ *and* $\nu_{1,i,n}^{(\alpha)}$ *when either* $\lambda_{\mathbf{H},i}^{(\alpha)} = 0$ *or* $\lambda_{\mathbf{H},1}^{(\alpha)} = 0$*, respectively. This duality property will be exploited below.*

5.6.2.4 Adjacent Eigenchannel Capacity Divergence and Individual Data Stream Cost

For the final problem, let us consider the rate at which adjacent eigenchannel capacities diverge away from each other. Of course, we have already seen (Lemma 7 and (5.54)) that if $\lambda_{\mathbf{H},i}^{(\alpha)} > \lambda_{\mathbf{H},i+1}^{(\alpha)} \geq 0$ then $c_{i,n}$ and $c_{i+1,n}$ will not diverge away from each other. Thus, in what follows we consider the cases $0 \geq \lambda_{\mathbf{H},i}^{(\alpha)} > \lambda_{\mathbf{H},i+1}^{(\alpha)}$ and $\lambda_{\mathbf{H},i}^{(\alpha)} > 0 > \lambda_{\mathbf{H},i+1}^{(\alpha)}$.

When $0 \geq \lambda_{\mathbf{H},i}^{(\alpha)} > \lambda_{\mathbf{H},i+1}^{(\alpha)}$, by employing Lemma 8 we find that

$$\nu_{i,i+1,n}^{(\alpha)} = \Theta_{\mathbb{P}}\left(e^{\frac{n}{m-i}}\right). \tag{5.66}$$

Thus, the ith and $(i+1)$th channel capacities diverge away from each other at an exponential rate $1/(m-i)$. When $\lambda_{\mathbf{H},i}^{(\alpha)} \geq 0 > \lambda_{\mathbf{H},i+1}^{(\alpha)}$ we find that

$$\nu_{i,i+1,n}^{(\alpha)} = \Theta_{\mathbb{P}}\left(e^{-2n\lambda_{\mathbf{H},i+1}^{(\alpha)}}\right) = O_{\mathbb{P}}\left(e^{\frac{n}{m-i}}\right) \tag{5.67}$$

and the capacities diverge away from each other at an exponential rate $-2\lambda^{(\alpha)}_{\mathbf{H},i+1}$, which is upper bounded by the exponential rate of (5.66).

Remark 3 *By considering the discussion of duality in Remark 2, we can assign a cost (in terms of extra instantaneous power requirements) to each extra data stream that we attempt to multiplex. In particular, from* (5.66) *and because of the duality property, if we are multiplexing i data streams, then, to multiplex* 1 *more stream (whilst ensuring $\lambda^{(\alpha)}_{\mathbf{H},i+1} = 0$), we must increase the nth relay's instantaneous transmit power by (approximately) a factor of* $\exp(n/(m-i))$. *Furthermore, we find that the cost of each extra eigenchannel increases with i.*

5.7 Numerical Illustration

In this section, we will illustrate the theory that has been presented in the previous sections. It is important to mention firstly that the following Monte Carlo simulations were generated using the variable precision arithmetic (vpa) function within the Matlab symbolic toolbox, which allowed us to increase the accuracy of our calculations to (approximately) 100 decimal places. This is required because of the nature of our results: we are verifying as clearly as possible that the eigenchannel capacities follow exponential trends governed by their corresponding Lyapunov exponents. For large networks, this results in computational rounding within the simulations if vpa is not utilized. An immediate consequence of employing such high precision is that simulations are *very* computationally intensive. Crucially, this restricts us to demonstrating network trends when the number of antennas at each node are small (i.e., 3 or 4).

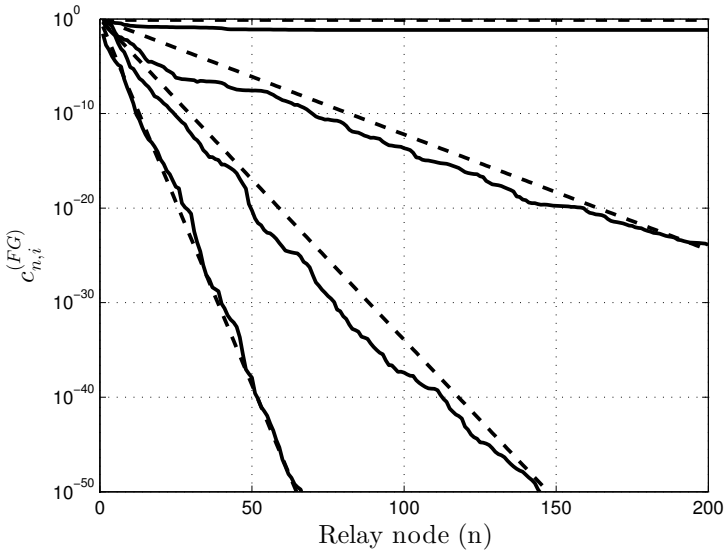

Figure 5.2: Figure demonstrating $c_{n,i}^{(FG)} = \Theta_{\mathbb{P}}\left(e^{n\lambda_{\gamma}^{(FG)}}\right)$ for a 4×4 FG MIMO system, see Theorem 2. Dashed lines represent $\exp\left(n\lambda_{\gamma,i}^{(FG)}\right)$; solid lines represent instantaneous realizations of $c_{n,i}^{(FG)}$, where, starting from the top, $i = 1, \cdots, 4$. For all $i = 1, \ldots, n$, we set $p_i = n_0 = \mu_i = 1$.

Figs. 5.2 and 5.3 illustrate the second statement of Theorem 2 for a 4×4 FG system. The first of these figures shows eigenchannel capacity as a function of network size, and clearly demonstrates that this will trend along a deterministic trajectory governed by the network's Lyapunov exponents. The second of these figures clearly shows convergence in the normalized logarithm of the eigenchannel capacity to the network's Lyapunov exponents. Figs. 5.4 and 5.5 illustrate analogous results to those above, but for a VG system. Interestingly, for all these figures we see that convergence to the stated trends occur quickly, sometimes in the order of 5 to 10 hops, which attests to the utility of our methods. Figs. 5.6 and 5.7 demonstrate (5.54) as a function of n for a 3×3 VG system. Similar plots occur for FG. As

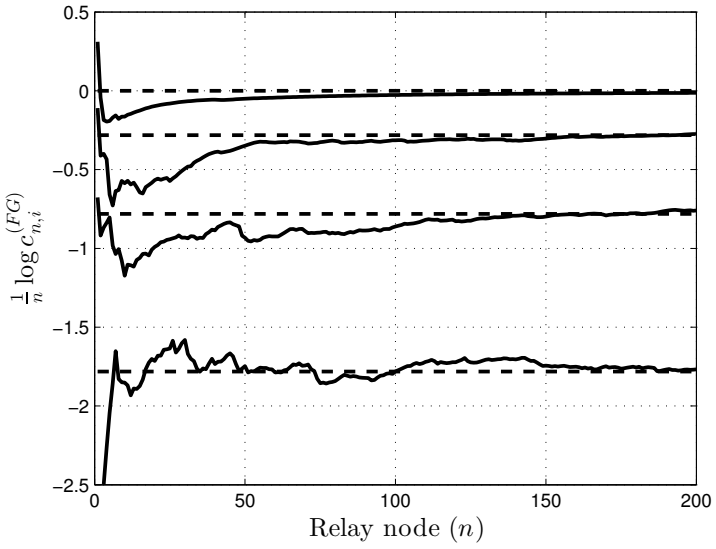

Figure 5.3: Figure demonstrating the second statement of Theorem 2 for a 4×4 FG MIMO system. Dashed lines represent the Lyapunov exponents $\lambda_{\gamma,i}^{(FG)}$, (2); solid lines represent instantaneous realizations of $\frac{1}{n}\log c_{n,i}^{(FG)}$, where, starting from the top, $i = 1, \cdots, 4$. For all $i = 1, \ldots, n$, we set $p_i = n_0 = \mu_i = 1$.

with above, convergence to the stated trends occurs quickly.

Because of the issues associated with computational complexity (mentioned at the beginning of this section), we were unable to employ Monte Carlo simulations to demonstrate (numerically) the relationship between antenna scaling with respect to number of hops, and the rate at which eigenchannel capacities diverge away from each other (see Lemma 9). We do, however, show Fig. 5.8, which plots $\bar{\phi}_{1,i}$ as a function of the number of antennas at each node. In this figure, when m is large the curves are seen to decay linearly on the log-log scale; i.e., they decay like $O(1/m)$ on a linear scale. This observation theoretically illustrates Lemma 9 (specifically, (5.61)), and consequently, that if super-linear antenna scaling occurs with respect to the number of hops within the network, the ith and jth eigen-

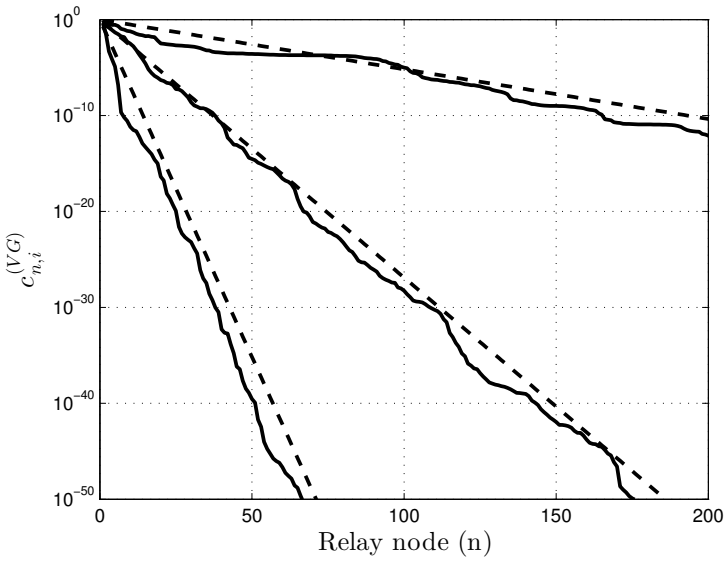

Figure 5.4: Figure demonstrating $c_{n,i}^{(VG)} = \Theta_{\mathbb{P}}\left(e^{n\lambda_{\gamma}^{(VG)}}\right)$ for a 3×3 VG MIMO system, see Theorem 2. Dashed lines represent $\exp\left(n\lambda_{\gamma,i}^{(VG)}\right)$; solid lines represent instantaneous realizations of $c_{n,i}^{(VG)}$, where, starting from the top, $i = 1, \cdots, 3$. For all $i = 1, \ldots, n$, we set $p_i = n_0 = \mu_i = 1$.

channel capacities will not exponentially diverge away from each other.

Finally, Fig. 5.9 shows an estimation of $\lambda_{\mathbf{H},i}^{(\alpha)}$ and its upper bound (B.44) for a VG network as a function of the transmit power at each node for a large network size, $n = 1000$. The choice of such a large n is only made to ensure that our results have converged significantly, where smaller values of n may exhibit less smooth plots. For this figure, we assume that the mean channel fading coefficient at the ith node is log-normally distributed. It is easy to see that the bound is very tight for large p_i/n_0.

5.8 Summary

In this chapter, we have employed the formalism of RDSs to study the scaling properties of the transmit power and end-to-end channel capacity of

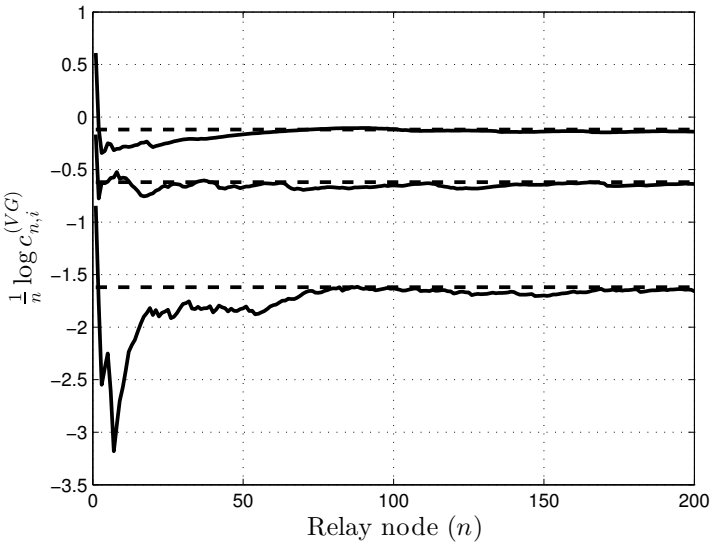

Figure 5.5: Figure demonstrating the second statement of Theorem 2 for a 3×3 VG MIMO system. Dashed lines represent the Lyapunov exponents $\lambda_{\gamma,i}^{(VG)}$, (2); solid lines represent instantaneous realizations of $\frac{1}{n}\log c_{n,i}^{(VG)}$, where, starting from the top, $i = 1, 2, 3$. For all $i = 1, \ldots, n$, we set $p_i = n_0 = \mu_i = 1$.

finite antenna MIMO AF relay networks. By employing the RDS formalism, we have been able to associate Lyapunov exponents (which are classically used to characterize the stability of RDSs) with the MIMO AF relay network. Our study has revealed that the exponential growth and/or decay of the transmit power and end-to-end channel capacity are completely characterized by the network's Lyapunov exponents. Furthermore, our methods can be applied to systems with arbitrary channel fading statistics, provided $\mathbb{E}\log^+ \|\mathbf{H}_i\| < \infty$, where $\mathbf{H}_i$ is the channel matrix for the ith hop; however, in this chapter we focus explicitly on the Rayleigh fading scenario. We then establish growth laws for the eigenchannel capacity divergence, how this relates to the amplification strategy and number of antennas at each node, and the cost (in terms of power) associated with multiplexing extra

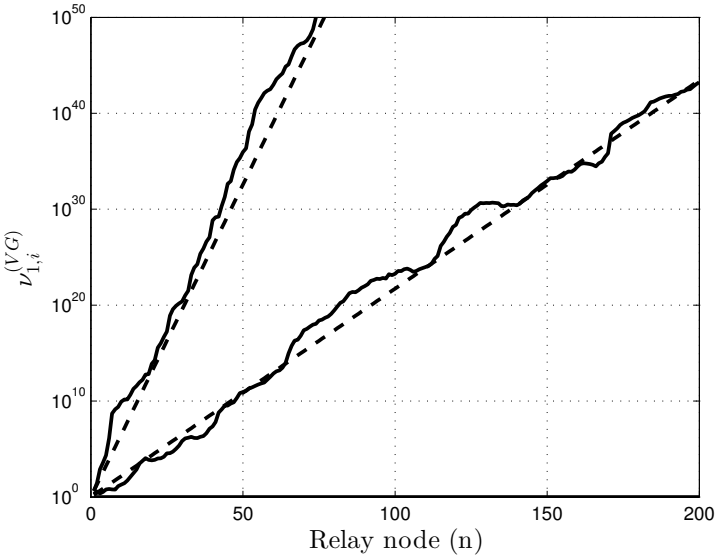

Figure 5.6: Figure demonstrating $\nu_{1,i,n}^{(VG)} := c_{n,1}^{(VG)}/c_{n,i}^{(VG)}$ given by $\nu_{1,i,n}^{(VG)} = \Theta_{\mathbb{P}}\left(e^{n\phi_{1,i}^{(VG)}}\right)$ for 3×3 VG system, see (5.54). Dashed lines represent $\exp\left(n\phi_{1,i}^{(VG)}\right)$; solid lines represent realizations of $\nu_{1,i,n}^{(VG)}$, where, from the top, $i = 1, \cdots, 3$. For all $i = 1, \ldots, n$, we set $p_i = n_0 = \mu_i = 1$.

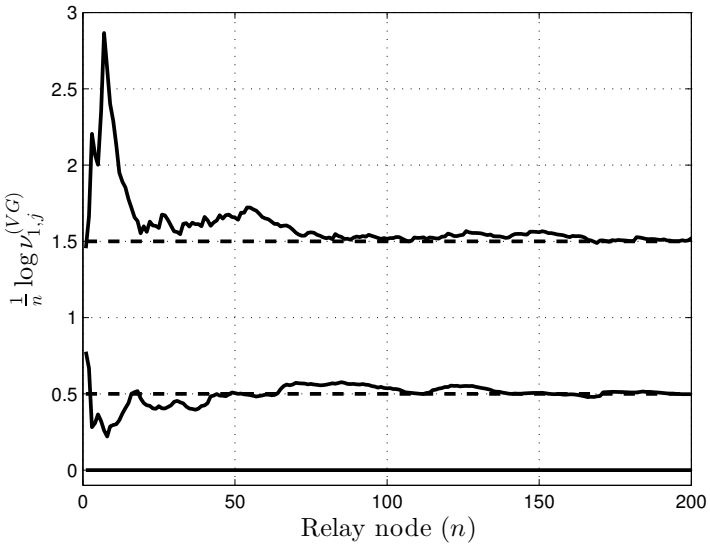

Figure 5.7: Figure demonstrating (5.54). Dashed lines represent the Lyapunov difference $\lambda_{\gamma,1}^{(VG)} - \lambda_{\gamma,i}^{(VG)}$, (5.48); solid lines represent instantaneous realizations of $\frac{1}{n}\log\nu_{1,i,n}^{(VG)}$, where, starting from the bottom, $i = 1, \ldots, 4$. For all $i = 1, \ldots, n$, we set $p_i = n_0 = \mu_i = 1$.

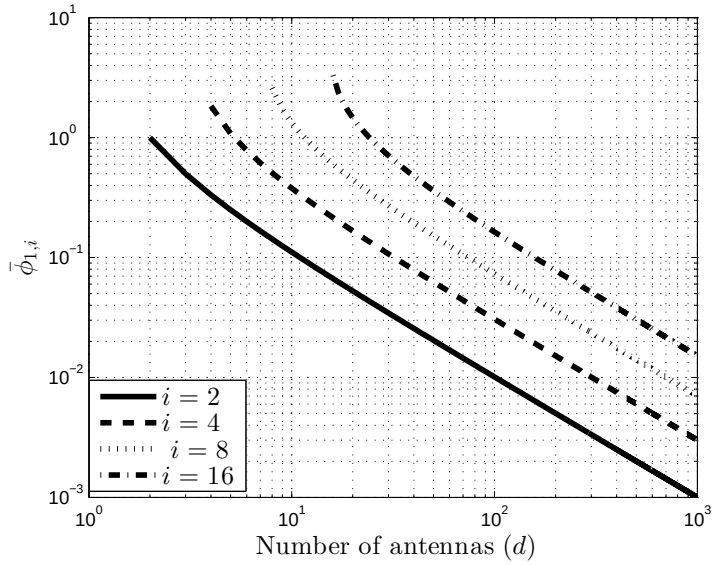

Figure 5.8: Figure demonstrating Lemma 9 for different values of i (the ith highest eigenchannel capacity) as a function of the number of antennas.

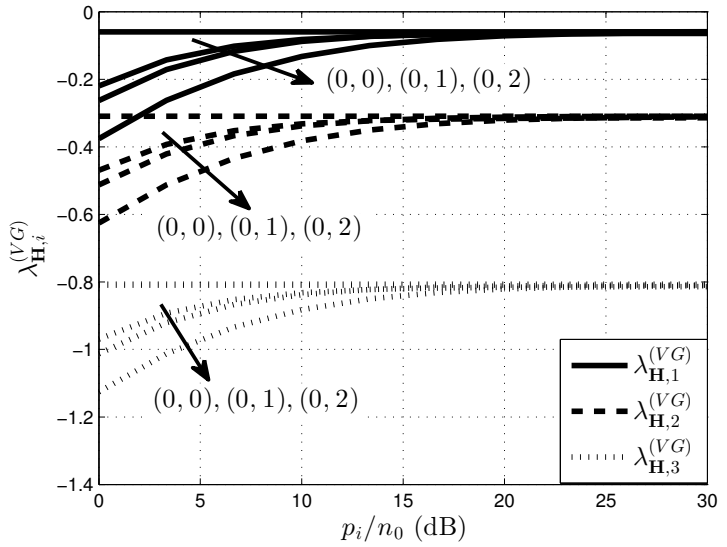

Figure 5.9: Figure showing numerically estimated $\lambda^{(VG)}_{\mathbf{H},i}$ (curved lines) for large network ($n = 1000$) and its upper bound (straight lines), (B.44), for a non-homogeneous VG 3×3 network. The average channel fading characteristics, μ_i, are assumed to be log-normally distributed with parameter pairs $(0,1),(0,2)$ and $(0,3)$; i.e., $\mu_i \sim \mathcal{LN}(a,b)$, $a = \mathbb{E}\log\mu_i$, $b = \mathbb{V}\log\mu_i$. The plot is taken as a function of the normalized transmit power at each node, with $p_i = p_{i-1}\ \forall\ i$.

data streams. Finally, we end the chapter with the following open question: Can our techniques be extended to study the capacity and power scaling properties of networks employing other (non AF) forwarding strategies?

Chapter 6

Multihop OFDM-based MIMO Networks: Peak-power Constraints

This chapter is our final research chapter. In it, we combine the techniques that were used to study the AF networks in Chapters 3, 4 and 5. In particular, we study the capacity and power scaling properties of peak-power constrained OFDM-based multihop AF networks, and how these relate to those of peak-power constrained frequency-flat SC AF networks. We conclude that, as the networks grow large, SC systems will always outperform OFDM-based systems at a subcarrier level. To demonstrate the above, we 1) study the capacity of SC AF networks; 2) apply Bussgang's theorem to calculate the distortion caused by power constraints within OFDM-based networks. Our result follows by noting that, from Bussgang's theorem, nonlinear distortion in OFDM-based networks (caused by the presence of peak power constraints) occurs when the ergodic transmit power gets close to

the peak-power thresholds; however, from the Lyapunov exponent analysis, this is not the case for frequency-flat SC systems. Finally, we show that employing VG relaying rather than FG relaying or increasing the number of antennas at each relay will improve the capacity scaling properties of the network. It is then shown that if the number of antennas at each node scales at a super-linear rate with the number of hops within the network, distortion growth can be circumvented in OFDM-based networks whilst avoiding exponential capacity decay.

The rest of this chapter is outlined as follows. Section 6.1 introduces the chapter, while section 6.2 outlines the system model. In section 6.3 we study the scalability of the OFDM AF relay network and present distortion mitigation strategies that can be employed to increase network scalability. Section 6.4 provides Monte Carlo simulations. Finally, section 6.5 concludes the chapter.

6.1 Introduction

As was discussed in the previous chapter, the study of capacity for multihop MIMO AF networks only has a very short history, beginning in 2002 [104]. This work and all other attempts [100–105] to study such networks always employed tools from random matrix theory [5]. These tools are limited in their scope because they rely on the assumption that the number of antennas at each relay grows asymptotically. The tools developed in the previous chapter allowed us to employ RDS theory [6] to study the capacity and power scaling properties of multihop AF networks, rather than exploiting results from random matrix theory. This allowed us to analyze these net-

works when each of the nodes was restricted to using a strictly finite number of antennas, and provided a much richer level of detail about how the capacity of the network behaves as the network grows. In particular, we were able to determine power scaling laws for the network and capacity scaling laws for each of the individual eigenchannels of the network. Our analysis applied specifically to SC systems, and a natural question to ask is, "what does this approach tell us about the capacity scaling properties on each subcarrier of an OFDM-based AF network?". A rudimentary response to this question might be, "Subcarriers behave like SC systems, so rules that apply to the SC system will also apply to the subcarriers of an OFDM-based system". While such reasoning may temporarily seem plausible, we must not forget about the particular effect that an accumulation of subcarriers has on the waveform's distribution at the transmitter of an OFDM-based system. Specifically, as was discussed in section 2.2.4, OFDM-based waveforms suffer from a large PAPR, and - as we shall see in this chapter - it is particularly important that we consider these effects when studying the capacity and power scaling properties of peak-power constrained OFDM-based AF networks.

The aim of this chapter is to perform a capacity and power scaling study of OFDM-based AF networks when power constraints are present at each relay. This is done by combining the tools developed in the previous chapter for studying the capacity and power scaling properties of SC AF networks with those used to study the effects of power constraints in OFDM-based systems. The main contributions of this chapter are:

1. We show that peak-power constraints quickly render OFDM-based multihop MIMO networks useless if each node has a fixed number

of antennas that it can use. This is because distortion will grow at an exponential rate if we set the network's upper Lyapunov exponent (5.40) to zero[1]. Note, this is *not* the case for peak-power constrained SC systems.

2. If the number of antennas at each node is allowed to scale linearly with the number of hops in the network, the effects of distortion can be circumvented.

6.2 System Model

We begin by describing the system in the *peak-power limit*[2]. Consider an n-node AF OFDM-based relay network whose topology is depicted in Fig. 5.1. We assume our system operates over m subcarriers. We further assume that each node has $m \geq 1$ transmit and receive antenna.

For the ith antenna, an information vector $[x_{0,1,i}, \ldots, x_{0,m,i}]^T$ is constructed at the source (node 0), the elements of which will be transmitted across each of the m subcarriers. We assume its elements to have a mean of zero and average power given by $\mathbb{E}[|x_{0,i,j}|^2] = \sigma_0^2/m$. After processing this vector with an inverse FFT, node zero inserts a CP of suitable length to allow the removal of inter-block interference. As in section 3.2, there are different ways in which CP insertion and removal can be performed in multi-hop relaying systems. For example, a single CP can be inserted at the source node with length as long as the entire memory of the n-hop channel,

[1]Remember, this is required if we are to ensure that the capacity of the upper eigenchannel of an SC system does not decay exponentially.

[2]The term peak-power limit is used to imply that the peak-power constraints at each node have been taken to ∞. We will use this term throughout the chapter.

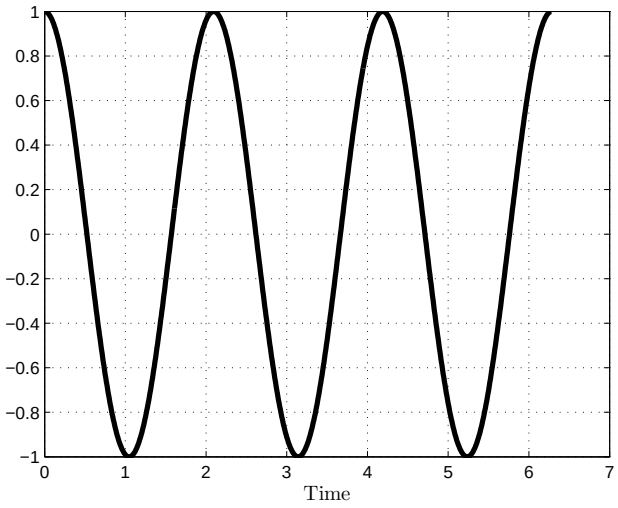

Figure 6.1: Plot showing the real part of a time-domain SC waveform.

or CP insertion and removal can be performed at each relaying node [88]. Whatever the case, we assume that the process has been performed in such a way that the system can be modeled at a subcarrier level, i.e., we model each subcarrier as an SC. To provide further insight to this reasoning, we present the following two figures (Figs. 6.1 and 6.2), which show time and frequency-domain plots of an SC waveform transmitted from any one of the m source antennas. By comparing these figures with those obtained for OFDM-based systems (see Figs. 2.6 and 2.7) we see that the time and frequency responses of an SC system are precisely those obtained for each of the subcarriers of an OFDM system: the time-domain waveform is a perfect sinusoid, while the frequency-domain waveform is a single sinc function. We now assume that node 0 transmits on the kth subcarrier an $m \times 1$ vector across its m antennas given by $X_{0,k} = [x_{0,k,1} \;\; x_{0,k,2} \;\; \ldots \;\; x_{0,k,m}]^T$.

Independent frequency flat channel fading is assumed to take place between each node pair on an individual subcarrier. The kth subcarrier chan-

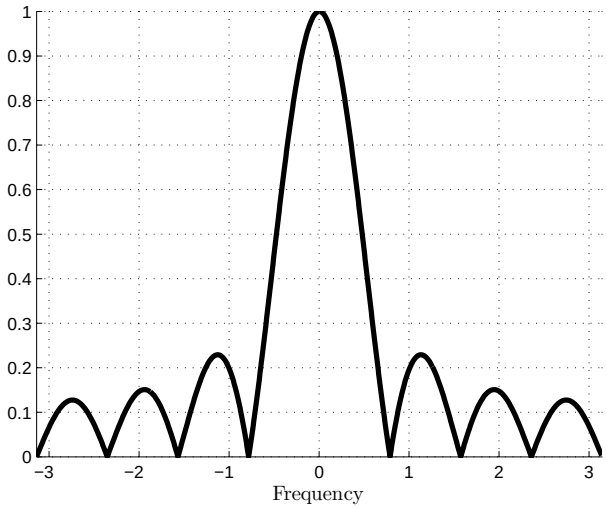

Figure 6.2: Plot showing (the absolute value of) the FFT of a time-domain SC waveform at baseband.

nel coefficients between node pairs $(0,1),\ldots,(n-2,n-1),(n-1,n)$ can be described by $m\times m$ complex random matrices, which are denoted respectively as $\mathbf{H}_{1,k},\ldots,\mathbf{H}_{n-1,k},\mathbf{H}_{n,k}$. The elements of these matrices are ZMCG with variance $\mu_j,\ j\in\{1,\ldots,n\}$. We therefore have

$$\mathbf{H}_{i,k}=\begin{bmatrix} h_{i,k,11} & h_{i,k,12} & \cdots & h_{i,k,1m} \\ h_{i,k,21} & h_{i,k,22} & \cdots & h_{i,k,2m} \\ \vdots & & \ddots & \vdots \\ h_{i,k,m1} & h_{i,k,m2} & \cdots & h_{i,k,mm} \end{bmatrix}. \tag{6.1}$$

At each node (apart from node 0) we assume noise is introduced into the system. We use $V_{j,k}\in\mathbb{C}^m$ to denote the vector of noise terms introduced at the jth relay on the kth subcarrier, where the elements of $V_{j,k}$ are ZMCG with total variance n_0. For brevity, apart from where necessary, we refrain from indexing subcarriers in what follows.

We assume the jth node applies the gain $g_{\alpha,j}$ to the received signal across all of its antenna. The subscript α signifies whether FG or VG is being implemented. For FG relaying, the gain is given by

$$g_{FGj} = \sqrt{\frac{\sigma_j^2}{\sigma_{j-1}^2 m\mu_j + mn_0}}; \tag{6.2}$$

while for VG relaying it is given by

$$g_{VGj} = \sqrt{\frac{\sigma_j^2}{\frac{\sigma_{j-1}^2}{m}\left\|\mathbf{H}_j\right\|_F^2 + mn_0}}. \tag{6.3}$$

The term σ_j^2 represents the average signal power on the kth subcarrier after amplification at the jth node. Thus, in the peak-power limit we can write the transmitted signal at the jth relay on any given subcarrier recursively as

$$X_j = g_{\alpha j}(\mathbf{H}_j X_{j-1} + V_j). \tag{6.4}$$

6.2.1 Power Constraints

In the peak-power constrained regime (i.e., not in the peak-power limit), we assume that at each node of the network the signal power is clipped. This is performed in a similar way as that in Chapters 3 and 4; i.e.,

1. the nth relay amplifies the received signal on the kth subcarrier by the amplification factor $g_{\alpha,n}$.

2. at each antenna, the nth relay then passes the *time-domain* OFDM

block through an SEL which clips the amplitude of the signal to

$$\sqrt{\frac{p_{max,n}}{m}}$$

so that the maximum transmit power at the nth relay is $p_{max,n}$.

Since the time-domain OFDM symbol is affected by the nonlinearity, we can apply Bussgang's extended theorem [7] (see section 2.2.4) to model the distortion introduced as a consequence of power clipping by each relay. By letting $r_{n,j,i}$ and $t_{n,j,i}$ be the input and output for the jth subcarrier on the ith antenna at the SEL of the nth node, Bussgang's theorem allows us to write the input-output relationship as [7–11]

$$t_{n,j,i} = \zeta_n r_{n,j,i} + d_{n,j,i}, \tag{6.5}$$

where

$$\zeta_n = 1 - e^{-\frac{p_{max,n}}{\sigma_n^2}} + \sqrt{\frac{p_{max,n}\pi}{4\sigma_n^2}}\text{erfc}\left(\sqrt{\frac{p_{max,n}}{\sigma_n^2}}\right), \tag{6.6}$$

$d_{n,j,i}$ is a distortion term, uncorrelated with $r_{n,j,i}$, which is well modeled by a ZMCG random variable with variance

$$\frac{\eta_n}{m} = \frac{p_n - \sigma_n^2\zeta_n^2}{m}, \tag{6.7}$$

and p_n, the total transmitted power at each relay, is given by

$$p_n := \mathbb{E}\|X_n\|^2 = \sigma_n^2\left(1 - e^{-\frac{p_{max,n}}{\sigma_n^2}}\right). \tag{6.8}$$

6.3 Scaling OFDM-based Amplify-and-forward Relay Networks

In Chapter 5, the capacity and power scaling properties of the peak-power unconstrained network are determined by studying it as an RDS. In particular, the Lyapunov exponents of the network are calculated and shown to characterize the exponential growth/decay rates of the transmit power and end-to-end capacity. Specifically, as a consequence of Theorem 2 and Lemma 6, in the peak-power limit we have

$$\|X_n\|^2 = \Theta_{\mathbb{P}}\left(e^{2n\lambda^{(\alpha)}_{Q,1}}\right) \tag{6.9}$$

$$c_{n,i} = \Theta_{\mathbb{P}}\left(e^{n\lambda^{(\alpha)}_{\gamma,i}}\right), \tag{6.10}$$

where

$$\lambda_{\mathbf{Q},1} = \max\{2\lambda^{(\alpha)}_{\mathbf{H},1}, 0\}, \tag{6.11}$$

$$\lambda_{\gamma,i} = \min\{2\lambda^{(\alpha)}_{\mathbf{H},i}, 0\} \tag{6.12}$$

and $\lambda^{(\alpha)}_{\mathbf{H},i}$ is the ith Lyapunov exponent of the network given by (5.40).

We now reach a crucial result within the chapter, which begins by making the following observations:

1. the nonlinearity begins to influence system performance when σ_n^2 gets close to $p_{max,n}$, an effect that can be observed through the Bussgang parameters ((6.6) and (6.7));

2. we have

$$\lim_{n\to\infty}\frac{1}{n}\log\frac{\sigma_n^2}{\sigma_0^2} \;\geq\; \lim_{n\to\infty}\frac{1}{n}\log\frac{p_n}{\sigma_0^2} \;\geq\; 2\lambda_{Q,1}^{(\alpha)} \;\geq\; 2\lambda_{\alpha\mathbf{H},1} \;\geq\; \lambda_{\gamma,1}^{(\alpha)}, \quad (6.13)$$

where the first inequality is strict in the peak-power constrained system, and the second/third inequalities follows from (5.45) and (5.46). The final inequality follows from (6.12).

Key Remark 1 *By combining points* 1*) and* 2*) above, we see that avoiding exponential growth*[3] *in* σ_n^2 *(i.e., setting* $\lim_{n\to\infty}\frac{1}{n}\log(\sigma_n^2/\sigma_0^2)=0$*) necessarily implies that the end-to-end capacity of the network in the peak-power limit will decay exponentially to zero (see* (6.10), (6.13)*). This in turn implies that the peak-power constrained end-to-end capacity will decay exponentially to zero. Conversely, avoiding capacity decay in the peak-power limit implies that* σ_n^2 *will grow exponentially, which implies that distortion will occur in the peak-power constrained OFDM-based system, (see* (6.7)*). It is important the reader understands that the this remark will not hold for SC (frequency-flat) systems. This is because, in such systems, exponential growth in* σ_n^2 *can be allowed for whilst ensuring, with probability approaching one, that the power of the instantaneous transmit signal does not grow exponentially (see* (6.9) *and* (6.13)*). Clearly then, in the limit of a large number of nodes, peak-power constrained OFDM-based networks do not scale as well as narrow-band SC peak-power constrained systems.*

[3] $\lim_{n\to\infty}\frac{1}{n}\log\sigma_n^2/\sigma_0^2\approx 0$ is required if distortion growth, which is expressed through the growth and decay in ζ_n and η_n, respectively, across the network is to be avoided in the peak-power constrained OFDM-based system.

6.3.1 Combating Issues of Distortion in OFDM-based Networks

Before assessing how the network's scalability can be improved, we provide the following definition, which is obtained by rearranging (6.13):

$$s_n^{(\alpha)} := \lim_{n\to\infty} \frac{1}{n} \log \frac{\sigma_n^2}{\sigma_0^2} - \lambda_{\gamma,1}^{(\alpha)} \in [0, \infty). \tag{6.14}$$

This parameter gives us a measure of the difference in the exponential divergence rates for the average (normalized) transmit power and the end-to-end SNR of the upper eigenchannel in the peak-power limit[4]. Said in a different way, the average (normalized) power at the nth node, normalized by the end-to-end channel capacity, will be given (from (6.10), (6.12))

$$\frac{\sigma_n^2/\sigma_0^2}{c_{n,i}} = \Theta\left(e^{ns_n^{(\alpha)}}\right). \tag{6.15}$$

The closer $s_n^{(\alpha)}$ is to zero, the more scalable the network will be. This is because, if its value is smaller, a reduced rate of distortion growth with respect to the channel capacity decay will occur in the peak-power constrained system. We will now discuss two different methods that can be employed to decrease $s_n^{(\alpha)}$.

6.3.1.1 Fixed-gain vs Variable-gain

Rather intuitively, one method that can be used to decrease $s_n^{(\alpha)}$ is to employ VG instead of FG. This can be seen from (5.45) and (5.46), which show that

[4]Note, it was shown in Theorem 2 that in the peak-power limit the exponential growth rates of the end-to-end SNR and capacity of the ith eigenchannel are given by the right-hand side of (6.12).

for FG

$$s_n^{(FG)} \geq \max\{2\lambda_{\mathbf{H},1}^{(FG)} - \lambda_{\gamma,1}^{(FG)} + \log m - \psi(m), -\lambda_{\gamma,1}^{(FG)}\}, \tag{6.16}$$

while for VG

$$s_n^{(VG)} \geq \max\{2\lambda_{\mathbf{H},1}^{(VG)} - \lambda_{\gamma,1}^{(VG)} + \psi(m^2) - \psi(m) - \log m, -\lambda_{\gamma,1}^{(VG)}\}. \tag{6.17}$$

Importantly, these inequalities become equalities as the noise power goes to zero, and in this scenario

$$\begin{aligned} s_n^{(f)} - s_n^{(v)} &= \max\{2\lambda_{\mathbf{H},1}^{(FG)} - \lambda_{\gamma,1}^{(FG)} + \log m - \psi(m), -\lambda_{\gamma,1}^{(FG)}\} \\ &\quad - \max\{2\lambda_{\mathbf{H},1}^{(VG)} - \lambda_{\gamma,1}^{(VG)} + \psi(m^2) - \psi(m) - \log m, -\lambda_{\gamma,1}^{(VG)}\} \geq 0. \end{aligned} \tag{6.18}$$

When $\lim_{n\to\infty} 1/n \log \sigma_n^2/\sigma_0^2$ is fixed, this quantity represents the greater exponential rate at which the end-to-end capacity will decay for an FG system compared to a VG system. When $\lambda_\gamma^{(FG)} = \lambda_\gamma^{(VG)}$, it represents the greater average power growth that will occur for FG when each network has the same exponential rate of capacity decay. Crucially, employing such a technique will marginally improve network scalability; but ultimately, both forwarding strategies have the same issue: if exponential capacity decay is to be avoided in the peak-power limit, the rate of average power growth (which is responsible for distortion) will necessarily be positive.

6.3.1.2 Increasing the Number of Antennas at Each Node

Another method that can be taken to reduce $s_n^{(\alpha)}$ is to increase the number of antennas at each relay. This can be seen from (6.16) and (6.17) where,

for both FG and VG, we have

$$s_n^{(\alpha)} = \frac{1}{2m} + O\left(\frac{1}{m}\right)^2. \tag{6.19}$$

An immediate consequence of (6.19) is that if the inverse of the number of antennas at each relay is given by

$$\frac{1}{m} = o\left(\frac{1}{n}\right), \tag{6.20}$$

$e^{ns_n^{(\alpha)}}$ will go to one for both forwarding strategies. From (6.15), this implies that the network will be able to support no exponential average power growth[5] across the network and no exponential capacity decay in the peak-power limit.

6.4 Numerical Results and Discussion

We now present Monte Carlo simulation results for the outage probability of an n-hop AF network. In this chapter, the outage probability at the nth node, $P_{o,n}^{(\alpha)}$, is defined to be the probability that the end-to-end instantaneous SNDR of the upper eigenchannel on any carrier, $\gamma_n^{(\alpha)}$ drops below a threshold value, γ_{th}; i.e.,

$$P_{o,n}^{(\alpha)} = \mathbb{P}\left[\gamma_n^{(\alpha)} \leq \gamma_{th}\right]. \tag{6.21}$$

Our first goal is to demonstrate that SC systems will outperform OFDM-based systems at a subcarrier level when the network grows large. To do

[5]This would be desirable in a peak-power limited OFDM-based AF network.

this, we consider a worst-case/best-case scenario for the SC/OFDM comparison, respectively. In particular, for the SC system we assume that the system fails completely (i.e., outage necessarily occurs) if any of the node's power constraints are exceeded; while for the OFDM-based system, we assume that each node possesses an SEL[6]. Clearly, from footnote 6 these two scenarios correspond to the worst/best situations for the respective systems. Figs. 6.3 and 6.4 show this comparison for an FG and VG network. From these figures, it is clear that, even for the worst case scenario, SC will *eventually* outperform OFDM. Also, this performance advantage will be more pronounced for more realistic SC distortion models. Furthermore, we can also see that increasing the number of antennas at each node allows the OFDM system to outperform the SC system for larger network sizes.

In Fig. 6.5, we plot the outage probability of an FG network with different levels of antenna scaling at each of the nodes and different levels of power growth across that network. Note, the jagged plots occur because the antenna scaling function has a non-continuous derivative. From this figure, we see that the networks with sublinear and linear antenna scaling hit a wall at around 6 or 7 nodes in length. At this point, the average transmit power has grown to the point that the negative effects of distortion begin to dominate the positive effects of average power growth across the network (which are expressed through the reduced rate of capacity decay in the peak-power limit). Meanwhile, the outage probability of the network with superlinear antenna scaling continues to decay with the network size. This is because the greater rate of antenna scaling allows for a reduced rate of

[6]The SEL is known to model the entire transmitter-side nonlinearity when ideal predistortion is implemented, [53].

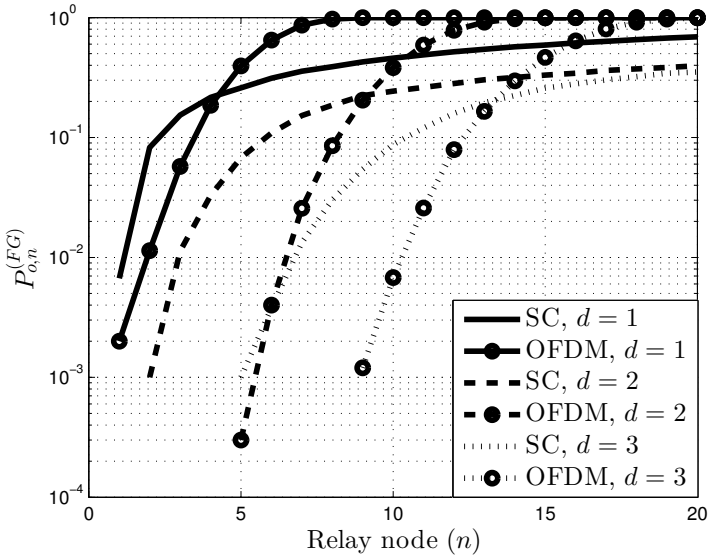

Figure 6.3: Figure comparing SC system to OFDM system for different number of antennas at each node for FG systems. Noise power is set to unity, $\lambda_{f\mathbf{H},1} = 0$, $\gamma_{th} = 1$, $p_0 = 100$, $p_{max,n} = 1000$ for all n.

average power growth to support the Lyapunov scaling properties of the capacity (see (6.10), (6.13), (6.14) and (6.19)).

6.5 Summary

This chapter is the last of our research chapters. In it, we have shown that peak-power constrained OFDM-based AF networks are inherently less scalable than their SC narrowband counterparts. This is because the distortion in OFDM-based networks is determined by the ergodic properties of the system, while the end-to-end capacity is determined by its Lyapunov properties. More specifically, to ensure a non-decaying end-to-end capacity, the average power should grow exponentially. However, for OFDM-based systems, such growth will quickly introduce nonlinear distortion and degrade the performance of the network. This is not the case for SC systems. Fi-

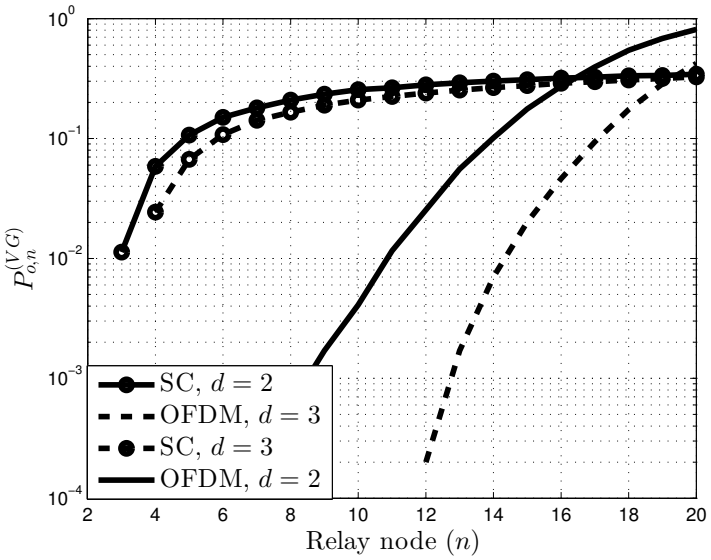

Figure 6.4: Figure comparing SC system to OFDM system for different number of antennas at each node for VG systems. Noise power is set to unity, $\lambda_{f\mathbf{H},1} = 0$, $\gamma_{th} = 1$, $p_0 = 100$, $p_{max,n} = 1000$ for all n.

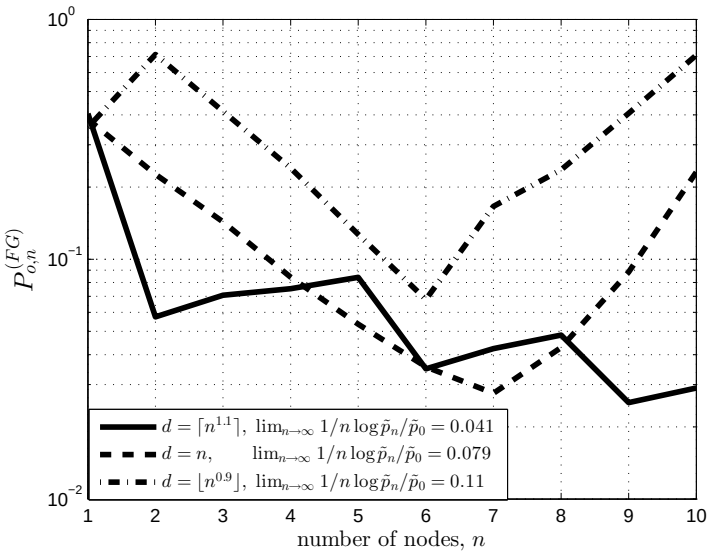

Figure 6.5: Figure showing (6.21) as a function of the network size for an FG network with different antenna and power growth configurations. Noise power is set to unity, $\sigma_0^2 = 3, p_{max,n} = 100$ for all n, and $\gamma_{th} = 1$.

nally, mitigation strategies are proposed, and it is shown that 1) compared to FG networks, VG networks can support a reduced rate of average power growth with respect to the end-to-end capacity decay; 2) having the number of antennas at each node scale at a superlinear rate with respect to the number of hops within the network causes the exponential rate of average power growth with respect to the capacity decay to go to zero.

Chapter 7

Conclusions and Future Work

Throughout this thesis, we have employed pre-existing and developed novel tools that can be used to study the performance of power and antenna constrained AF networks. The first of these tools is Bussgang's theorem, which provides a theoretical characterization of the distortion introduced by peak-power constraints. The second of these tools, codeveloped by the author of this thesis, provides a unique perspective on how the capacity and power behave across multihop AF networks when each of the network's nodes is constrained to using an arbitrary finite number of antennas. Our tool is derived from a particular branch of mathematics, RDS theory. Specifically, we demonstrated that key observable studied in RDS theory (Lyapunov exponents) can also be used to study the capacity and power scaling properties of AF networks. The intuition behind this is that channel capacity and power are related to the spectral properties of particular products of random matrices, while Lyapunov exponents describe the spectral growth properties of finite dimensional random matrix products[1]. It is through these separate

[1]This is a consequence of the Furstenberg-Keston theorem and Multiplicative Ergodic theorem.

relationships that we were able to form a correspondence between Lyapunov exponents, and capacity and power scaling across multihop networks.

The key conclusions that we were able to draw through the deployment of these tools were:

1. Two-hop power constrained OFDM-based AF networks can be analyzed successfully using the tools developed by Bussgang. Furthermore, such analysis can be used to successfully optimize the performance of these networks. Finally, theoretical optimization criteria proves successful when optimizing a real world test bed setup.

2. The framework that was codeveloped by the author (Chapter 5) provides new insight to the way capacity and power behave across SC multihop AF networks. With this framework, we were able to determine that when these networks have their antenna number constrained, the capacity on all but the first eigenchannel will decay exponentially to zero if peak power constraints are imposed on the network. Furthermore, relaxing the constraints on the number of antennas at each node will reduce the exponential rates at which the lower eigenchannels decay.

3. Finally, when considering power constrained OFDM multihop AF networks, the end-to-end capacity will necessarily decay to zero at an exponential rate if the antenna number is also constrained. Moreover, this exponential decay can be circumvented if we allow the number of antennas to scale at least linearly with the number of hops in the network.

Future Work

Throughout this thesis, we have dropped some hints to open questions that could motivate future work. We formalize these points - along with some others - in the following:

- A natural extension to the work contained in Chapters 3 and 4 is to study more complex network topologies. As an example, the standard 'butterfly' topology, see Fig. 2.9.

- In Chapter 5, it was noted that the capacity scaling properties of the network were implicitly studied when the multihop network's length grew linearly with the number of hops within the network. Future work may consider the scaling behavior for fixed length networks, as the node density grows large.

- In Chapter 5, we also noted that it was unclear whether the techniques that we have developed to study the capacity scaling properties of the AF network could be extended to other forwarding strategies; e.g., DF, CF. Future work may attempt to find such extensions.

- The capacity scaling results presented in Chapter 5 show that the capacity along each eigenchannel will follow a deterministic trajectory. It would be interesting to establish 1) how the capacity is distributed around this trajectory, and 2) does this distribution converge in probability to a stable distribution as the number of hops grows large?

- Much of the previous literature pertaining to the capacity of multihop AF networks considers behavior as the number of antennas at each

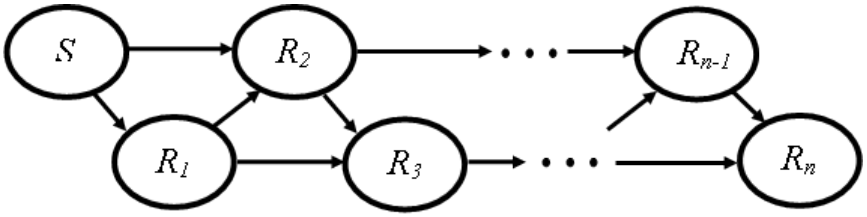

Figure 7.1: Depiction of a cooperative multihop network topology.

node grows large. The key contribution in Chapter 5 was to present methods for determining capacity scaling properties when each relay has a finite number of antennas, while the number of hops grows large. Future work may attempt to establish quantitative trade-offs between these two techniques, which may help engineers better utilize the methods within practical implementation.

- Finally, the work in Chapter 5 could be used to study the capacity and power scaling properties of other multihop topologies. Fig. 7.1 shows an example of a particular topology that may be of interest, a brief study of which can be found in [135].

Appendix A

Chapter 3 Proofs

The proofs for the outage probability of the FG and VG networks will utilize the identity [136, Sec 8.432 eq. (6)]

$$\int_{x=0}^{\infty} e^{-\frac{1}{x}-ax} dx = \frac{2}{\sqrt{a}} K_1\left(2\sqrt{a}\right), \ \mathbb{R}\{a\} > 0. \tag{A.1}$$

Let us begin with the proof for the FG system.

A.1 Outage Probability for FG System

The outage probability for he FG system is given by

$$P_{oB}^{(FG)} = P\left[\gamma_B^{(FG)} = \frac{\gamma_{AR}\gamma_{RB}}{\left(1+\gamma_{RB}\right)u + q\gamma_{RB}^2 + \bar{\gamma}_R} < \gamma_{th,B}\right]$$

which, expressed as an integral, is

$$
\begin{aligned}
P_{oB}^{(FG)} &= \int_{\gamma_{RB}=0}^{\infty} \int_{\gamma_{AR}=0}^{\frac{\gamma_{th,B}\left((1+\gamma_{RB})u+q\gamma_{RB}^2+\bar{\gamma}_R\right)}{\gamma_{RB}}} \frac{e^{-\frac{\gamma_{AR}}{\bar{\gamma}_{AR}}-\frac{\gamma_{RB}}{\bar{\gamma}_{RB}}}}{\bar{\gamma}_{AR}\bar{\gamma}_{RB}} d\gamma_{AR}d\gamma_{RB} \\
&= 1-\int_{\gamma_{RB}=0}^{\infty} \frac{e^{-\frac{\gamma_{th,B}}{\bar{\gamma}_{AR}}\left(\frac{(1+\gamma_{RB})u+q\gamma_{RB}^2+\bar{\gamma}_R}{\gamma_{RB}}\right)-\frac{\gamma_{RB}}{\bar{\gamma}_{RB}}}}{\bar{\gamma}_{RB}} d\gamma_{RB} \\
&= 1-e^{-\frac{\gamma_{th,B}u}{\bar{\gamma}_{AR}}} \int_{\gamma_{RB}=0}^{\infty} \frac{1}{\bar{\gamma}_{RB}} e^{-\frac{1}{\gamma_{RB}}\left(\frac{\gamma_{th,B}(u+\bar{\gamma}_R)}{\bar{\gamma}_{AR}}\right)-\gamma_{RB}\left(\frac{q\gamma_{th,B}\bar{\gamma}_{RB}+\bar{\gamma}_{AR}}{\bar{\gamma}_{RB}\bar{\gamma}_{AR}}\right)} d\gamma_{RB} \\
&= 1-2\sqrt{\frac{\gamma_{th,B}\left(u+\bar{\gamma}_R\right)}{\bar{\gamma}_{RB}\left(q\bar{\gamma}_{RB}\gamma_{th,B}+\bar{\gamma}_{AR}\right)}} e^{-\frac{\gamma_{th,B}u}{\bar{\gamma}_{AR}}} \int_{\gamma_{RB}=0}^{\infty} \frac{1}{2} \times \\
&\quad \sqrt{\frac{q\bar{\gamma}_{RB}\gamma_{th,B}+\bar{\gamma}_{AR}}{\gamma_{th,B}\left(u+\bar{\gamma}_R\right)}} e^{-\frac{1}{\gamma_{RB}}\left(\frac{\gamma_{th,B}(u+\bar{\gamma}_R)}{\bar{\gamma}_{AR}}\right)-\gamma_{RB}\left(\frac{q\gamma_{th,B}\bar{\gamma}_{RB}+\bar{\gamma}_{AR}}{\bar{\gamma}_{RB}\bar{\gamma}_{AR}}\right)} d\gamma_{RB}.
\end{aligned}
$$

By letting $\frac{1}{\gamma_{RB}} = \frac{1}{x}\left(\frac{\bar{\gamma}_{AR}}{\gamma_{th,B}(u+\bar{\gamma}_R)}\right)$ and setting $d = \frac{\left(q\gamma_{th,B}\bar{\gamma}_{RB}+\bar{\gamma}_{AR}\right)\gamma_{th,B}(u+\bar{\gamma}_R)}{\bar{\gamma}_{RB}\bar{\gamma}_{AR}^2}$ we obtain

$$
\begin{aligned}
P_o &= 1-2\sqrt{\frac{\gamma_{th,B}\left(u+\bar{\gamma}_R\right)}{\bar{\gamma}_{RB}\left(q\bar{\gamma}_{RB}\gamma_{th,B}+\bar{\gamma}_{AR}\right)}} e^{-\frac{\gamma_{th,B}u}{\bar{\gamma}_{AR}}} \int_{x=0}^{\infty} \frac{1}{2}\sqrt{d}e^{-\frac{1}{x}-dx}dx \\
&= 1-2\sqrt{\frac{\gamma_{th,B}\left(u+\bar{\gamma}_R\right)}{\bar{\gamma}_{RB}\left(q\bar{\gamma}_{RB}\gamma_{th,B}+\bar{\gamma}_{AR}\right)}} e^{-\frac{\gamma_{th,B}u}{\bar{\gamma}_{AR}}} K_1\left(2\sqrt{d}\right)
\end{aligned}
$$

where the last line follows from the integral representation of the Bessel function given in (A.1).

A.2 Outage Probability for VG System

We will now prove the outage probability expression for the VG network. It can be shown that the outage probability at node B is equivalent to

$$P_{oB}^{(VG)} = \mathbb{P}\left[\frac{\gamma_{AR}\left(f\gamma_{BR} - d\gamma_{th,B}\right)}{a\gamma_{BR}^2 + b\gamma_{BR} + d} \leq \gamma_{th,B}\right],$$

where $a = \left(\zeta_R - 1\right)^2 \rho + \bar{\eta}_R$, $b = (p_R + p_B)/n_0$, $d = p_B/n_0$, $\bar{\eta}_R = \eta_R/n_0$ and $f = \zeta_R^2\rho - \gamma_{thB}\bar{\eta}_R$. Since $a, b, d > 0$, if $(f\gamma_{BR} - d\gamma_{th,B}) < 0$ outage will occur with certainty. This makes sense since

$$f\gamma_{BR} < d\gamma_{th,B} \implies \gamma_B < \frac{\zeta^2\rho\left|h_B\right|^2}{\left|h_B\right|^2\bar{\eta}_R + 1} < \gamma_{th,B}.$$

Now, we have two scenarios:

1. If $f \leq 0 \implies f\gamma_{BR} - d\gamma_{th,B} < 0$ for all γ_{BR}. The outage probability of the system is then given by $P_{oB}^{(VG)} = 1$.

2. If $f > 0 \implies f\gamma_{BR} - d\gamma_{th,B} < 0$ for $\gamma_{BR} < d\gamma_{th,B}/f$. From the law of total probability, the outage probability is then given by

$$\begin{aligned} P_{oB}^{(VG)} = \; & \mathbb{P}\left[\gamma_{BR} < \frac{c\gamma_{th,B}}{f}\right] + \\ & \mathbb{P}\left[\gamma_{AR} \leq \frac{\gamma_{th,B}(a\gamma_{BR}^2 + b\gamma_{BR} + d)}{f\gamma_{BR} - d\gamma_{th,B}} \cap \gamma_{BR} > \frac{d\gamma_{th,B}}{f}\right] \end{aligned}$$

$$
\begin{aligned}
&= \int_0^{\frac{d\gamma_{th,B}}{f}} \frac{e^{-\frac{x}{\bar{\gamma}_{BR}}}}{\bar{\gamma}_{BR}} \mathrm{d}x + \\
&\quad \int_{\frac{d\gamma_{th,B}}{f}}^{\infty} \frac{e^{-\frac{x}{\bar{\gamma}_{BR}}}}{\bar{\gamma}_{BR}} \left(1 - e^{-\frac{\gamma_{th,B}(ax^2+bx+d)}{\bar{\gamma}_{AR}(fx-d\gamma_{thB})}}\right) \mathrm{d}x \\
&= 1 - \int_0^{\infty} \frac{e^{-\frac{g}{y}-hy-k}}{f\bar{\gamma}_{BR}} \mathrm{d}y \qquad \text{(A.2)}
\end{aligned}
$$

where

$$
\begin{aligned}
g &= \frac{\gamma_{thB}a}{f^2\bar{\gamma}_{AR}} + \frac{1}{f\bar{\gamma}_{BR}}, \qquad \text{(A.3)} \\
h &= \frac{1}{\bar{\gamma}_{AR}} \left(d\gamma_{thB} + \frac{bd\gamma_{thB}^2}{f} + \frac{ad^2\gamma_{thB}^3}{f^2}\right), \qquad \text{(A.4)} \\
k &= \frac{d\gamma_{thB}}{f\bar{\gamma}_{BR}} + \frac{1}{\bar{\gamma}_{AR}} \left(\frac{b\gamma_{thB}}{f} + \frac{2ad\gamma_{thB}^2}{f^2}\right). \qquad \text{(A.5)}
\end{aligned}
$$

and the substitution $y = fx - d\gamma_{th,B}$ has been used to obtain the final line. From (A.1), (1) and (A.2), the result follows immediately.

Appendix B

Chapter 5 Proofs

B.1 Proof of Theorem 1

Firstly, let

$$\prod_{i=1}^{n} \mathbf{M}_i \begin{bmatrix} X_0^T & 1 \end{bmatrix}^T := \begin{bmatrix} X_n^T & 1 \end{bmatrix}^T, \tag{B.1}$$

it is easy to see from Definition 3 that $\lambda\left(\mathbf{M}, \begin{bmatrix} X_0^T & 1 \end{bmatrix}^T\right) \geq \lambda_{a,1}$. Thus, from Fact 3

$$\lambda\left(\mathbf{M}, \begin{bmatrix} X_0^T & 1 \end{bmatrix}^T\right) \in \{\lambda_{\mathbf{A},i} \geq \lambda_{a,1}\} \cup \lambda_{a,1} =: \mathcal{L}. \tag{B.2}$$

The proof of the theorem now follows from Claim 1 (mentioned below).

Claim 1 *With* $\mathcal{Y} := \{[y_1 \ \cdots \ y_d \ 1]^T : y_i \in \mathbb{C}\}$, *the mapping*

$$\lambda(\mathbf{M}, \cdot) : \mathcal{Y} \to \mathcal{L} \tag{B.3}$$

is surjective.

Proof of Claim 1: If $\lambda_{\mathbf{A},1} < \lambda_{a,1}$ then $\mathcal{L} = \{\lambda_{a,1}\}$, $\lambda(\mathbf{M}, Y) = \lambda_{a,1}$ $\forall\, Y \in \mathcal{Y}$ and the surjectivity of (B.3) is satisfied. Thus, w.l.o.g., we assume

that $\exists\, k \leq d$ such that

$$\lambda_{\mathbf{A},1} > \cdots > \lambda_{\mathbf{A},k} \geq \lambda_{a,1} > \lambda_{\mathbf{A},k+1} > \cdots > \lambda_{\mathbf{A},d}. \tag{B.4}$$

In what follows, we consider the scenario in which $\lambda_{\mathbf{A},k} > \lambda_{a,1} > \lambda_{\mathbf{A},k+1}$. The proof can easily be extended to the case when $\lambda_{\mathbf{A},k} = \lambda_{a,1}$.

Consider the filtration,

$$\{0\} =: \mathcal{V}_{p+1} \subset \mathcal{V}_p \subset \cdots \subset \mathcal{V}_1 = \mathbb{C}^{d+1} \tag{B.5}$$

where $Y \in \mathcal{V}_i \setminus \mathcal{V}_{i+1} \Leftrightarrow \lambda(\mathbf{M}, Y) = \lambda_i$ (the existence of such a filtration is guaranteed by Fact 2.3). The proof of Claim 1 then follows immediately from Claim 2 (mentioned below).

Claim 2 *Let $\mathcal{V}_i$ be as in* (B.5) *and $\mathcal{Y}$ be as in Claim 1. Then $(\mathcal{V}_i \setminus \mathcal{V}_{i+1}) \cap \mathcal{Y} \neq \emptyset$ for all $i = 1, \ldots, k+1$, where $\lambda_{\mathbf{A},k} > \lambda_{a,1} > \lambda_{\mathbf{A},k+1}$.*

Proof of Claim 2: Claim 2 follows immediately from Claim 3 (mentioned below).

Claim 3 *Let $\mathcal{V}_i$ be as in* (B.5), *$\mathcal{Y}$ be as in Claim 1, and suppose that $\lambda_{\mathbf{A},k} > \lambda_{a,1} > \lambda_{\mathbf{A},k+1}$. Then:*
1) for all $i \leq k$, $(\mathcal{V}_i \setminus \mathcal{V}_{i+1}) \cap \mathcal{Y} = \emptyset$ implies $(\mathcal{V}_l \setminus \mathcal{V}_{l+1}) \cap \mathcal{Y} = \emptyset$ for all $l < i$,
2) $(\mathcal{V}_1 \setminus \mathcal{V}_2) \cap \mathcal{Y} \neq \emptyset$.

Proof of Claim 3: We will begin by proving the first part of the claim. To do this, we first note the following: all the Lyapunov exponents have multiplicity 1 (i.e., they are distinct); consequently, from Fact 3, $\dim \mathcal{V}_j - \dim \mathcal{V}_{j+1} = 1\ \forall\ j$ and

$$\dim \mathcal{V}_j = d + 2 - j. \tag{B.6}$$

Clearly,

$$(\mathcal{V}_i \setminus \mathcal{V}_{i+1}) \cap \mathcal{Y} = \emptyset \Leftrightarrow \mathcal{V}_i \cap \mathcal{Y} = \emptyset \text{ or } \mathcal{Y} \subseteq \mathcal{V}_{i+1} \subset \cdots \subset \mathcal{V}_1. \tag{B.7}$$

However, if $\mathcal{V}_i \cap \mathcal{Y} = \emptyset$ is satisfied, it can be seen that because $\mathcal{V}_i$ is a vector space all vectors in $\mathcal{V}_i$ must have their $(d+1)$th element equal to zero. Thus,

$$\begin{aligned}
&\mathcal{V}_i \cap \mathcal{Y} = \emptyset \\
&\Rightarrow \mathcal{V}_i = \left\{X = [y_1 \ \cdots \ y_d \ 0]^T : \ \lambda(\mathbf{M}, X) \leq \lambda_{\mathbf{A},i}\right\} \\
&\Rightarrow \dim \mathcal{V}_i = \dim \left\{X' = [y_1 \ \cdots \ y_d]^T : \ \lambda(\mathbf{A}, X') \leq \lambda_{\mathbf{A},i}\right\} \\
&\qquad\qquad = d + 1 - i.
\end{aligned} \tag{B.8}$$

But from (B.6), $\dim \mathcal{V}_i = d + 2 - i$, so $\mathcal{V}_i \cap \mathcal{Y} = \emptyset$ gives us a contradiction so (B.7) becomes

$$(\mathcal{V}_i \setminus \mathcal{V}_{i+1}) \cap \mathcal{Y} = \emptyset \quad \Leftrightarrow \quad \mathcal{Y} \subseteq \mathcal{V}_{i+1} \subset \cdots \subset \mathcal{V}_1, \tag{B.9}$$

and

$$(\mathcal{V}_j \setminus \mathcal{V}_{j+1}) \cap \mathcal{Y} = \emptyset, \ \forall \ j \leq i. \tag{B.10}$$

This proves the first part of the Claim.

We will now prove the second part of the claim. From (B.9) we have $(\mathcal{V}_1 \setminus \mathcal{V}_2) \cap \mathcal{Y} = \emptyset \Leftrightarrow \mathcal{V}_2 \supseteq \mathcal{Y}$. But $\mathcal{Y}$ contains a d dimensional subspace $\mathcal{A} := \{[y_1 \ \cdots \ y_d \ 0]^T : y_i \in \mathbb{C}\}$, and $\mathcal{V}_2$ is also d dimensional, so

$$\mathcal{V}_2 \supseteq \mathcal{Y} \supseteq \mathcal{A} \Rightarrow \mathcal{A} = \mathcal{V}_2 \Rightarrow \mathcal{A} = \mathcal{Y}. \tag{B.11}$$

But $\mathcal{A} \subset \mathcal{Y}$, so from (B.11) $\mathcal{V}_2 \supseteq \mathcal{Y}$ gives us a contradiction. Thus $\mathcal{V}_2 \not\supseteq \mathcal{Y}$, which (from (B.9)) gives

$$(\mathcal{V}_1 \setminus \mathcal{V}_2) \cap \mathcal{Y} \neq \emptyset. \tag{B.12}$$

This completes the proof.

B.2 Proof of Lemma 5

We have

$$\begin{aligned}
\lim_{n\to\infty} \frac{1}{n} \log ||X_n|| &= \lim_{n\to\infty} \frac{1}{n} \log ||\mathbf{A}_n X_{n-1} - R_n + 2R_n|| \\
&\leq \max \left\{ \lim_{n\to\infty} \frac{1}{n} \log ||\mathbf{A}_n X_{n-1} - R_n||, \lim_{n\to\infty} \frac{1}{n} \log ||2R_n|| \right\} \\
&\overset{a.s.}{=} \max \left\{ \lim_{n\to\infty} \frac{1}{n} \log ||X_n||, 0 \right\}, \qquad \text{(B.13)}
\end{aligned}$$

where the second line follows from Lemma 10 (below) and the last line follows from the symmetry of R_n. If

$$\lim_{n\to\infty} \frac{1}{n} \log ||X_n|| \geq 0,$$

our result is reached trivially; if

$$\lim_{n\to\infty} \frac{1}{n} \log ||X_n|| = \lambda < 0,$$

from Lemma 10 (below), the line above (B.13) holds with equality, which

gives $\lambda = 0$. This contradicts our assumption that $\lambda < 0$. Therefore,

$$\lim_{n\to\infty} \frac{1}{n} \log ||X_n|| \geq 0.$$

This completes the proof.

Lemma 10 *For* $\alpha_n, \beta_n \in \mathbb{C}^d$,

$$\lim_{n\to\infty} \frac{1}{n} \log ||\alpha_n + \beta_n|| \leq \max \left\{ \lim_{n\to\infty} \frac{1}{n} \log ||\alpha_n|| \, , \, \lim_{n\to\infty} \frac{1}{n} \log ||\beta_n|| \right\}, \quad \text{(B.14)}$$

where equality holds when

$$\lim_{n\to\infty} \frac{1}{n} \log ||\alpha_n|| \neq \lim_{n\to\infty} \frac{1}{n} \log ||\beta_n||. \quad \text{(B.15)}$$

Proof For $\alpha_n, \beta_n \in \mathbb{C}^d$,

$$\lim_{n\to\infty} \frac{1}{n} \log ||\alpha_n + \beta_n|| \leq \max \left\{ \lim_{n\to\infty} \frac{1}{n} \log ||\alpha_n|| \, , \, \lim_{n\to\infty} \frac{1}{n} \log ||\beta_n|| \right\} \quad \text{(B.16)}$$

since $||\alpha_n + \beta_n|| \leq 2 \max\{||\alpha_n||, ||\beta_n||\}$. To show that (B.16) holds with equality when

$$\lim_{n\to\infty} \frac{1}{n} \log ||\alpha_n|| \neq \lim_{n\to\infty} \frac{1}{n} \log ||\beta_n||, \quad \text{(B.17)}$$

w.l.o.g., we assume that $\lim_{n\to\infty} \frac{1}{n} \log ||\alpha_n|| < \lim_{n\to\infty} \frac{1}{n} \log ||\beta_n||$. Eq. (B.16)

then gives us

$$\lim_{n\to\infty}\frac{1}{n}\log||\alpha_n+\beta_n|| \leq \lim_{n\to\infty}\frac{1}{n}\log||\beta_n|| \tag{B.18}$$

$$= \lim_{n\to\infty}\frac{1}{n}\log||\alpha_n+\beta_n-\alpha_n||$$

$$\leq \max\left\{\lim_{n\to\infty}\frac{1}{n}\log||\alpha_n+\beta_n||, \lim_{n\to\infty}\frac{1}{n}\log||\alpha_n||\right\} \tag{B.19}$$

It follows that if $\lim_{n\to\infty}(1/n)\log||\alpha_n+\beta_n|| < \lim_{n\to\infty}\frac{1}{n}\log||\alpha_n||$ then (from (B.18) and (B.19)) $\lim_{n\to\infty}(1/n)\log||\beta_n|| \leq \lim_{n\to\infty}(1/n)\log||\alpha_n||$ which contradicts our assumption. Consequently, $\lim_{n\to\infty}(1/n)\log||\beta_n||$ is sandwiched either side by $\lim_{n\to\infty}(1/n)\log||\alpha_n+\beta_n||$ and so must be equal to it. ■

B.3 Proof of Theorem 2

Theorem 2 contains two statements. We prove these separately in the following two subsections.

B.3.1 First Statement

We prove the first statement in two parts. Each of these parts will involve manipulating the inverse of $\left(\mathbf{R}^{(\alpha)}_{\mathcal{I},n}\mathbf{R}^{(\alpha)-1}_{\mathcal{N},n}\right)$, which is given by

$$\left(\mathbf{R}^{(\alpha)}_{\mathcal{I},n}\mathbf{R}^{(\alpha)-1}_{\mathcal{N},n}\right)^{-1} = \mathbf{R}_{\mathcal{N},n}\mathbf{R}^{(\alpha)-1}_{\mathcal{I},n}$$

$$= \left(\mathbf{R}^{(\alpha)-1}_{\mathcal{I},n} + \sum_{l=2}^{n}\mathbf{H}_n\cdots\mathbf{H}_l\mathbf{R}^{(\alpha)-1}_{\mathcal{I},l-1}\mathbf{H}_l^{-1}\cdots\mathbf{H}_n^{-1}\right), \tag{B.20}$$

where, without loss of generality, we have assumed that $n_0 = 1$. The first part constructs an upper bound on the limit in question. The second part constructs a lower bound on the same limit, which is identical to the lower bound. This proves the first part of the theorem.

B.3.1.1 Upper Bound

Our aim is to show that

$$\lim_{n\to\infty} \frac{1}{n} \log \mathcal{E}_i \left(\mathbf{R}_{\mathcal{I},n}^{(\alpha)} \mathbf{R}_{\mathcal{N},n}^{(\alpha)-1} \right) \overset{a.s.}{\leq} \min\{0, 2\lambda_{\alpha\mathbf{H},i}\}. \tag{B.21}$$

By noting that

$$\mathcal{E}_i \left(\mathbf{R}_{\mathcal{I},1}^{(\alpha)-1} \right) \overset{a.s.}{\neq} 0,$$

and does not depend on n, we obtain

$$\lim_{n\to\infty} \frac{1}{n} \log \mathcal{E}_i \left(\mathbf{R}_{\mathcal{I},1}^{(\alpha)-1} \right) \overset{a.s.}{=} 0. \tag{B.22}$$

Also, from the definition of $\mathbf{R}_{\mathcal{I},n}^{(\alpha)}$ and property 4 of Fact 2, it is clear that

$$\lim_{n\to\infty} \frac{1}{n} \log \mathcal{E}_i \left(\mathbf{R}_{\mathcal{I},n}^{(\alpha)-1} \right) \overset{a.s.}{=} -2\lambda_{\alpha\mathbf{H},i}. \tag{B.23}$$

By combining (B.22), (B.23), and

$$-\max\{0, -a\} = \min\{0, a\},\ a \in \mathbb{R}, \tag{B.24}$$

the upper bound of (B.21) follows immediately from the following claim (the proof of which is given at the end of Appendix 2).

Claim 4 *The eigenvalues of* $\left(\mathbf{R}_{\mathcal{I},n}^{(\alpha)}\mathbf{R}_{\mathcal{N},n}^{(\alpha)-1}\right)^{-1}$ *are bound in the following way:*

$$\mathcal{E}_i\left(\left(\mathbf{R}_{\mathcal{I},n}^{(\alpha)}\mathbf{R}_{\mathcal{N},n}^{(\alpha)-1}\right)^{-1}\right) \geq \max\left\{\mathcal{E}_i\left(\mathbf{R}_{\mathcal{I},n}^{(\alpha)-1}\right), \mathcal{E}_i\left(\mathbf{R}_{\mathcal{I},1}^{(\alpha)-1}\right)\right\}, \tag{B.25}$$

B.3.1.2 Lower Bound

We will now provide the second part of the proof (constructing the lower bound). To begin, let us introduce the following RDS[1], which will be exploited in a moment:

$$Y_n := \mathbf{M}_1^{(\alpha)} \cdots \mathbf{M}_n^{(\alpha)} \begin{bmatrix} \hat{Y}_0 \\ 1 \end{bmatrix}, \tag{B.26}$$

where

$$\mathbf{M}_i^{(\alpha)} := \begin{bmatrix} \frac{1}{\alpha_i}\mathbf{H}_i^{-1} & \hat{Y}_0 \\ \mathbf{0^T} & \pm 1 \end{bmatrix}. \tag{B.27}$$

To allow us to describe the mechanism by which the sign of ± 1 is chosen in the bottom right corner of (B.27), we must first establish the inner product

[1]Note, (B.26) is a backward RDS as per (5.22).

of Y_n. The inner product of Y_n is given by

$$\begin{aligned}\|Y_n\|^2 =& \overbrace{\hat{Y}_0^\dagger \left(\overline{\mathbf{R}}_{\mathcal{I},n}^{(\alpha)-1} + \sum_{l=1}^{n-1} \overline{\mathbf{R}}_{\mathcal{I},l}^{(\alpha)-1} + \mathbf{I}_d \right)^\dagger \hat{Y}_0}^{\text{First inner product term}} \\ & \overbrace{\pm \hat{Y}_0^\dagger \left(\frac{1}{g_{\alpha,j}} \left(\mathbf{H}_n^{-1}\right)^\dagger \cdots \left(\mathbf{H}_1^{-1}\right)^\dagger \mathbf{H}_1^{-1} \cdots \mathbf{H}_{n-1}^{-1} \prod_{j=1}^{n} \frac{1}{g_{\alpha,j}} \prod_{j=1}^{n-1} \right.}^{\text{Second inner product term}} \\ & \pm \cdots \pm \left(\mathbf{H}_n^{-1}\right)^\dagger \cdots \left(\mathbf{H}_1^{-1}\right)^\dagger \mathbf{H}_1^{-1} \frac{1}{g_{\alpha,1}} \prod_{j=1}^{n} \frac{1}{g_{\alpha,j}} \\ & \left. \pm \cdots \pm \left(\mathbf{H}_1^{-1}\right)^\dagger \frac{1}{g_{\alpha,1}} \right) \hat{Y}_0, \end{aligned} \tag{B.28}$$

where

$$\overline{\mathbf{R}}_{\mathcal{I},i}^{(\alpha)-1} := \mathbf{H}_i^{-1} \cdots \mathbf{H}_1^{-1} \left(\mathbf{H}_1^{-1}\right)^\dagger \cdots \left(\mathbf{H}_i^{-1}\right)^\dagger \prod_{j=1}^{i} \frac{1}{g_{\alpha,j}^2}. \tag{B.29}$$

It is clear that the second inner product term is a real number that, at the moment, may be either positive or negative. However, there is nothing stopping us from ensuring that this is strictly positive by appropriately selecting the sign of ± 1 in (B.27); for, the RDS is permitted to remember the past, and predict the future [6]. This is the mechanism that we will use to select the sign. Furthermore, performing sign selection in this way will not affect the Lyapunov exponents of the system in question (Fact 3). We now have the following upper bound on the first inner product term of (B.28), which will be exploited later on:

$$\|Y_n\|^2 \geq \hat{Y}_0^\dagger \left(\overline{\mathbf{R}}_{\mathcal{I},n}^{(\alpha)-1} + \sum_{l=1}^{n-1} \overline{\mathbf{R}}_{\mathcal{I},l}^{(\alpha)-1} + \mathbf{I}_d \right)^\dagger \hat{Y}_0. \tag{B.30}$$

It can already be seen that (B.20) is remarkably similar to the first

inner product term of (B.28). We will now show that this similarity is not superficial, and that

$$\lim_{n\to\infty}\frac{1}{n}\log\mathcal{E}_i\left(\left(\mathbf{R}_{\mathcal{I},n}^{(\alpha)}\mathbf{R}_{\mathcal{N},n}^{(\alpha)-1}\right)^{-1}\right)\leq\lim_{n\to\infty}\frac{1}{n}\log\mathcal{E}_i\left(\overline{\mathbf{R}}_{\mathcal{I},n}^{(\alpha)-1}+\sum_{l=1}^{n-1}\overline{\mathbf{R}}_{\mathcal{I},l}^{(\alpha)-1}+\mathbf{I}_d\right). \tag{B.31}$$

To do this, note that

$$\mathcal{E}_i\left\{\mathbf{H}_n\cdots\mathbf{H}_l\mathbf{R}_{\mathcal{I},l-1}^{(\alpha)-1}\mathbf{H}_l^{-1}\cdots\mathbf{H}_n^{-1}\right\} \;=\; \mathcal{E}_i\left\{\mathbf{R}_{\mathcal{I},l-1}^{(\alpha)-1}\right\}\overset{d}{=}\mathcal{E}_i\left\{\overline{\mathbf{R}}_{\mathcal{I},l-1}^{(\alpha)-1}\right\}, \tag{B.32}$$

Consequently,

$$\mathcal{E}_i\left(\left(\mathbf{R}_{\mathcal{I},n}^{(\alpha)}\mathbf{R}_{\mathcal{N},n}^{(\alpha)-1}\right)^{-1}\right)\overset{d}{=}\mathcal{E}_i\left(\mathbf{R}_{\mathcal{I},n}^{(\alpha)-1}+\sum_{l=1}^{n-1}\mathbf{R}_{\mathcal{I},l}^{(\alpha)-1}\right) \tag{B.33}$$

$$\overset{d}{=}\mathcal{E}_i\left(\overline{\mathbf{R}}_{\mathcal{I},n,1}^{(\alpha)-1}+\sum_{l=1}^{n-1}\overline{\mathbf{R}}_{\mathcal{I},l}^{(\alpha)-1}\right) \tag{B.34}$$

$$\leq\mathcal{E}_i\left(\overline{\mathbf{R}}_{\mathcal{I},n,1}^{(\alpha)-1}+\sum_{l=1}^{n-1}\overline{\mathbf{R}}_{\mathcal{I},l}^{(\alpha)-1}+\mathbf{I}_d\right), \tag{B.35}$$

where (B.33) follows from the first equality of (B.32), (B.34) follows from the second equality of (B.32), and (B.35) follows trivially from (B.34).

With (B.33) and (B.35), we have shown (B.31). The right hand side of (B.30) is known to be equal to the ith eigenvalue when $\hat{Y}_0$ is an ith unit eigenvector. Combining this fact with (B.35) gives us

$$\lim_{n\to\infty}\frac{1}{n}\log\mathcal{E}_i\left(\left(\mathbf{R}_{\mathcal{I},n}^{(\alpha)}\mathbf{R}_{\mathcal{N},n}^{(\alpha)-1}\right)^{-1}\right)\leq\lim_{n\to\infty}\frac{1}{n}\log\|Y_n\|^2. \tag{B.36}$$

But the limit on the right hand side of (B.36), when Y_n is given by (B.26),

is given by Theorem 1. Thus, (B.36) and Theorem 1 give us

$$\lim_{n\to\infty}\frac{1}{n}\log\mathcal{E}_i\left(\mathbf{R}_{\mathcal{I},n}^{(\alpha)}\mathbf{R}_{\mathcal{N},n}^{(\alpha)-1}\right)\geq-\max\left\{-2\lambda_{\alpha\mathbf{H},i},0\right\}, \tag{B.37}$$

which can then be combined with (B.24) to yield the lower bound.

B.3.2 Second Statement

From the first statement of Theorem 2, we have

$$\mathbb{P}\left[\log\left(e^{n\lambda_{\gamma,i}^{(\alpha)}-o(n)}+1\right)\leq c_{n,i}^{(\alpha)}\leq\log\left(e^{n\lambda_{\gamma,i}^{(\alpha)}+o(n)}+1\right)\right]\rightarrow 1,$$

which gives

$$\begin{aligned}\mathbb{P}\Big[e^{n\lambda_{\gamma,i}^{(\alpha)}-o(n)}+O\left(e^{2n\lambda_{\gamma,i}^{(\alpha)}}\right)\leq c_n^{(\alpha)}\leq e^{n\lambda_{\gamma,i}^{(\alpha)}+o(n)}+O\left(e^{2n\lambda_{\gamma,i}^{(\alpha)}}\right)\Big]&\rightarrow 1\\ \Rightarrow\mathbb{P}\left[e^{n\lambda_{\gamma,i}^{(\alpha)}-o(n)}O\left(1\right)\leq c_n^{(\alpha)}\leq e^{n\lambda_{\gamma,i}^{(\alpha)}+o(n)}O\left(1\right)\right]&\rightarrow 1\\ \Rightarrow\mathbb{P}\left[e^{n\lambda_{\gamma,i}^{(\alpha)}-o(n)}\leq c_n^{(\alpha)}\leq e^{n\lambda_{\gamma,i}^{(\alpha)}+o(n)}\right]&\rightarrow 1\end{aligned}$$

where the first line follows from the Taylor expansion of $\log(1+x)$ about $x=0$ and the second line follows by factoring $e^{n\lambda_{\gamma}^{(\alpha)}\pm o(n)}$ from the left and right sides of the second line, respectively, and noting that $\lambda_{\gamma,i}^{(\alpha)}\leq 0$.

Proof of Claim 4: An immediate consequence of the dual Lidskii inequality [137] is that

$$\mathcal{E}_i\left(\mathbf{A}+\mathbf{B}\right)\geq\mathcal{E}_i\left(\mathbf{A}\right)+\mathcal{E}_d\left(\mathbf{B}\right), \tag{B.38}$$

which applies to $d\times d$ Hermitian matrices $\mathbf{A}$ and $\mathbf{B}$. Combining (B.38) with the fact that the summands in (B.20) are positive definite (i.e., they have

positive eigenvalues), gives us

$$\mathcal{E}_i\left(\left(\mathbf{R}_{\mathcal{I},n}^{(\alpha)}\mathbf{R}_{\mathcal{N},n}^{(\alpha)-1}\right)^{-1}\right) \geq \mathcal{E}_i\left(\mathbf{R}_{\mathcal{I},n}^{(\alpha)-1}\right)$$
$$\text{and} \quad \mathcal{E}_i\left(\left(\mathbf{R}_{\mathcal{I},n}^{(\alpha)}\mathbf{R}_{\mathcal{N},n}^{(\alpha)-1}\right)^{-1}\right) \geq \mathcal{E}_i\left(\mathbf{H}_n\cdots\mathbf{H}_2\mathbf{R}_{\mathcal{I},1}^{(\alpha)-1}\mathbf{H}_2^{-1}\cdots\mathbf{H}_n^{-1}\right). \quad \text{(B.39)}$$

Claim 4 follows immediately from (B.39) after noting that

$$\mathcal{E}_i\left(\mathbf{H}_n\cdots\mathbf{H}_2\mathbf{R}_{\mathcal{I},1}^{(\alpha)-1}\mathbf{H}_2^{-1}\cdots\mathbf{H}_n^{-1}\right) = \mathcal{E}_i\left(\mathbf{R}_{\mathcal{I},1}^{(\alpha)-1}\right).$$

B.4 Proof of Lemma 6

Lemma 6 contains two statements. We prove these separately in the following two subsections.

B.4.1 First Statement

The Lyapunov exponents of the matrix product that describes the progression of $\mathcal{I}_n$, (5.6), follow immediately from [138, Proposition 1]. The Lyapunov exponents of $X_n^{(\alpha)}$, (5.6), then follow immediately from Theorem 1. Combining these with (5.31), we obtain (5.43) and (5.44).

B.4.2 Second Statement

For the second statement, we begin by showing that the limit is greater than or equal to zero for both fixed-gain and variable-gain:

$$\lim_{n\to\infty}\frac{1}{n}\log\frac{p_n}{p_0} \geq \lim_{n\to\infty}\frac{1}{n}\log\frac{g_{\alpha,n}^2 n_0}{p_0} \overset{a.s.}{=} 0, \quad \text{(B.40)}$$

where the *almost sure* equality becomes an equality for fixed-gain. For fixed-gain, the stated result then follows immediately from (B.40) and (B.43). For variable-gain, the stated result then follows immediately from (B.40) and (B.44).

B.5 Proof of Lemma 7

The lower bound follows trivially from (2) and (5.48). By noting that $\lambda_{\alpha\mathbf{H},1} > \lambda_{\alpha\mathbf{H},i} \geq 0 \Leftrightarrow \lambda_{\gamma,1}^{(\alpha)} = \lambda_{\gamma,i}^{(\alpha)} = 0$, we obtain equality of the bound. For the upper bound, we need to prove that

$$a - b \geq \min\{0, a\} - \min\{0, b\} \tag{B.41}$$

for $a \geq b$. To do this, we need to check the following three cases:

1. $a \geq 0,\ b \geq 0,\ a \geq b$;
2. $a \geq 0,\ b \leq 0$;
3. $a \leq 0,\ b \leq 0,\ a \geq b$;

which can be done trivially. Equality of the upper bound occurs when $b \leq a \leq 0$. Finally, to obtain the if and only if statements, we need to show that $a > 0$ and $b < 0$ implies that

$$a - b > \min\{0, a\} - \min\{0, b\} > 0, \tag{B.42}$$

which can be done trivially. The independence of fixed-gain or variable-gain implementation is trivial.

B.6 Lemma 11 and Proof

Lemma 11 *For the fixed-gain network,*

$$\lambda_{g_{FG}\mathbf{H},j} \leq \frac{1}{2}\left(\lim_{n\to\infty}\frac{1}{n}\log\frac{p_n}{p_0} - \log d + \psi(d-j+1)\right), \tag{B.43}$$

For the variable-gain network,

$$\lambda_{g_{VG}\mathbf{H},i} \leq \frac{1}{2}\left(\lim_{n\to\infty}\frac{1}{n}\log\frac{p_n}{p_0} + \log(d) - \psi\left(d^2\right) + \psi\left(d-i+1\right)\right). \tag{B.44}$$

Proof The first equation, (B.43), is obtained from (5.40) by noting that

$$L(g_{FG}^2\mu) \leq \lim_{n\to\infty}\frac{1}{n}\log\frac{p_n}{p_0} - \log d.$$

For the second equation, (B.44), we have

$$\begin{aligned} L(g_{VG}^2\mu) &= \lim_{n\to\infty}\frac{1}{n}\sum_{i=1}^{n}\log\left(\frac{p_i}{\frac{p_{i-1}}{d}\|\mathbf{H}_i\|_F^2 + dn_0}\mu_i\right) \\ &\leq \lim_{n\to\infty}\frac{1}{n}\sum_{i=1}^{n}\log\left(\frac{dp_i}{p_{i-1}\|\mathbf{H}_i\|_F^2}\mu_i\right) \\ &= \lim_{n\to\infty}\frac{1}{n}\log\frac{p_n}{p_0} + \log(d) - \psi(d^2). \end{aligned} \tag{B.45}$$

where the final line follows from $\mathbb{E}\log\|\mathbf{H}_i\|_F^2/\mu_i = \psi(d^2)$. From (5.40), the stated result follows immediately. ■

Bibliography

[1] S. Janson, "Probability Asymptotics: Notes on Notation," *arXiv preprint arXiv:1108.3924*, 2011.

[2] M. Abramowitz and I. A. Stegun, *Handbook of Mathematical Functions: with Formulas, Graphs, and Mathematical Tables*. No. 55, Courier Corporation, 1964.

[3] C. E. Shannon, "A Mathematical Theory of Communication," *ACM SIGMOBILE Mobile Computing and Communications Review*, vol. 5, no. 1, pp. 3–55, 2001.

[4] J. J. Bussgang, "Crosscorrelation Functions of Amplitude-Distorted Gaussian Signals," 1952.

[5] A. M. Tulino and S. Verdú, *Random Matrix Theory and Wireless Communications*, vol. 1. Now Publishers Inc, 2004.

[6] L. Arnold, *Random Dynamical Systems*. Monographs in Mathematics, Springer, 1998.

[7] D. Dardari, V. Tralli, and A. Vaccari, "A Theoretical Characterization of Nonlinear Distortion Effects in OFDM Systems," *IEEE Transactions on Communications*, vol. 48, no. 10, pp. 1755–1764, 2000.

[8] D. E. Simmons and J. P. Coon, "Two-way OFDM-based Nonlinear Amplify-and-forward Relay Systems," *IEEE Transactions on Vehicular Technology*, vol. 65, no. 5, pp. 3808–3812, 2016.

[9] D. E. Simmons and J. P. Coon, "Two-way OFDM-based Nonlinear Amplify-and-forward Relaying: Power Allocation," in *European Conference on Networks and Communications (EuCNC)*, pp. 280–284, IEEE, 2015.

[10] D. Simmons, D. Halls, and J. P. Coon, "OFDM-based Nonlinear Fixed-Gain Amplify-and-Forward Relay Systems: SER Optimization and Experimental Testing," in *European Conference on Networks and Communications (EuCNC)*, pp. 1–5, IEEE, 2014.

[11] D. E. Simmons and J. P. Coon, "Distortion Limited Amplify-and-forward Relay Networks and the ϵ-critical Phase Transition," *arXiv preprint arXiv:1511.08700*, 2015.

[12] D. E. Simmons, J. P. Coon, and N. Warsi, "Capacity and Power Scaling Laws for Finite Antenna MIMO Amplify-and-Forward Relay Networks," *IEEE Transactions on Information Theory*, vol. 62, no. 4, pp. 1993–2008, 2016.

[13] B. Lab, "High-Capacity Mobile Telephone System Technical Report," Dec 1971.

[14] D. E. Noble, "The History of Land-Mobile Radio Communications," *Proceedings of the IRE*, vol. 50, pp. 1405–1414, May 1962.

[15] V. H. Mac Donald, "Advanced Mobile Phone Service: The Cellular Concept," *The Bell System Technical Journal*, vol. 58, no. 1, pp. 15–41, 1979.

[16] T. S. Rappaport *et al.*, *Wireless Communications: Principles and Practice*, vol. 2. Prentice hall PTR New Jersey, 1996.

[17] W. C. Jakes and D. C. Cox, *Microwave Mobile Communications*. Wiley-IEEE Press, 1994.

[18] J. Meurling and R. Jeans, "The Mobile Phone Book," *Communications Week International, London*, 1994.

[19] A. F. Molisch, *Wireless communications*. John Wiley & Sons, 2007.

[20] V. K. Garg and J. E. Wilkes, *Principles and Applications of GSM*. Prentice Hall PTR, 1998.

[21] D. Collins, C. Smith, A. N. Rosenberg, and S. Kemp, *3G Wireless Networks*. McGraw-Hill Professional Publishing, 2001.

[22] S. Glisic and B. Lorenzo, *Advanced Wireless Networks: Cognitive, Cooperative & Opportunistic 4G Technology*. John Wiley & Sons, 2009.

[23] A. Ghosh, R. Ratasuk, B. Mondal, N. Mangalvedhe, and T. Thomas, "LTE-advanced: Next-generation Wireless Broadband Technology [Invited Paper]," *IEEE Wireless Communications*, vol. 17, no. 3, pp. 10–22, 2010.

[24] ITU.Int, "Press release." `http://www.itu.int/net/pressoffice/press_releases/2010/48.aspx#.Vl3HKnrDhC0/`, 2012.

[25] ITU.Int, "Press release." http://www.itu.int/newsroom/press_releases/2009/48.html/, 2012.

[26] E. Dahlman, S. Parkvall, and J. Skold, *4G: LTE/LTE-advanced for Mobile Broadband*. Academic press, 2013.

[27] X. Tao, X. Xu, and Q. Cui, "An Overview of Cooperative Communications," *IEEE Communications Magazine*, vol. 50, no. 6, pp. 65–71, 2012.

[28] R. Pabst, B. H. Walke, D. C. Schultz, P. Herhold, H. Yanikomeroglu, S. Mukherjee, H. Viswanathan, M. Lott, W. Zirwas, M. Dohler, *et al.*, "Relay-based Deployment Concepts for Wireless and Mobile Broadband Radio," *IEEE Communications Magazine*, vol. 42, no. 9, pp. 80–89, 2004.

[29] W. H. Chin, Z. Fan, and R. Haines, "Emerging Technologies and Research Challenges for 5G Wireless Networks," *IEEE Wireless Communications*, vol. 21, no. 2, pp. 106–112, 2014.

[30] X.-H. You and X. Gao, "Development of Beyond 3G Techniques and Experiment System: An Introduction to the Future Project," *ICT Shaping the World: A Scientific View, Wiley*, 2008.

[31] L. Atzori, A. Iera, and G. Morabito, "The Internet of Things: A Survey," *Computer networks*, vol. 54, no. 15, pp. 2787–2805, 2010.

[32] K. Ashton, "That 'Internet of Things' thing," *RFiD Journal*, vol. 22, no. 7, pp. 97–114, 2009.

[33] R. Van Kranenburg, E. Anzelmo, A. Bassi, D. Caprio, S. Dodson, and M. Ratto, "The Internet of things," *A critique of ambient technology and the all-seeing network of RFID, Network Notebooks*, vol. 2, 2011.

[34] J. P. Conti, "The Internet of things," *Communications Engineer*, vol. 4, no. 6, pp. 20–25, 2006.

[35] M. Chui, M. Löffler, and R. Roberts, "The Internet of Things," *McKinsey Quarterly*, vol. 2, no. 2010, pp. 1–9, 2010.

[36] C. E. Perkins, *Ad hoc Networking*. Addison-Wesley Professional, 2008.

[37] C. K. Toh, *Ad hoc Mobile Wireless Networks: Protocols and Systems*. Pearson Education, 2001.

[38] I. F. Akyildiz, W. Su, Y. Sankarasubramaniam, and E. Cayirci, "A Survey on Sensor Networks," *IEEE Communications Magazine*, vol. 40, no. 8, pp. 102–114, 2002.

[39] T. M. Cover and J. A. Thomas, *Elements of Information Theory*. John Wiley & Sons, 2012.

[40] W. W. Peterson and E. J. Weldon, *Error-correcting Codes*. MIT press, 1972.

[41] E. Biglieri, J. Proakis, and S. Shamai, "Fading Channels: Information-theoretic and Communications Aspects," *IEEE Transactions on Information Theory*, vol. 44, no. 6, pp. 2619–2692, 1998.

[42] D. Tse and P. Viswanath, *Fundamentals of Wireless Communication*. Cambridge university press, 2005.

[43] I. E. Telatar *et al.*, "Capacity of Multi-Antenna Gaussian Channels," *European transactions on telecommunications*, vol. 10, no. 6, pp. 585–595, 1999.

[44] D. P. Bertsekas, *Nonlinear Programming.* Athena scientific, 1999.

[45] B. Noble and J. W. Daniel, *Applied Linear Algebra*, vol. 3. Prentice-Hall New Jersey, 1988.

[46] Z. Wang and G. B. Giannakis, "Wireless Multicarrier Communications," *IEEE Signal Processing Magazine*, vol. 17, no. 3, pp. 29–48, 2000.

[47] H. Schneider and G. P. Barker, *Matrices and Linear Algebra.* Courier Corporation, 1973.

[48] C.-P. Liang, J.-h. Jong, W. E. Stark, and J. R. East, "Nonlinear Amplifier Effects in Communications Systems," *IEEE Transactions on Microwave Theory and Techniques*, vol. 47, no. 8, pp. 1461–1466, 1999.

[49] S. Ariyavisitakul and T.-P. Liu, "Characterizing the Effects of Nonlinear Amplifiers on Linear Modulation for Digital Portable Radio Communications," *IEEE Transactions on Vehicular Technology*, vol. 39, no. 4, pp. 383–389, 1990.

[50] K. M. Gharaibeh, *Nonlinear Distortion in Wireless Systems.* John Wiley & Sons,, 2011.

[51] R. Prasad, *OFDM for wireless communications systems.* Artech House, 2004.

[52] K. Mekechuk, W.-J. Kim, S. P. Stapleton, and J. H. Kim, "Linearizing Power Amplifiers Using Digital Predistortion, EDA tools and Test Hardware," *High Frequency Electronics*, vol. 3, no. 4, pp. 18–25, 2004.

[53] H. Rohling, *OFDM: Concepts for Future Communication Systems*. Springer Science & Business Media, 2011.

[54] E. C. Van der Meulen, "A Survey of Multi-way Channels in Information Theory: 1961-1976," *IEEE Transactions on Information Theory*, vol. 23, no. 1, pp. 1–37, 1977.

[55] C. Ng and A. Goldsmith, "Capacity Gain from Transmitter and Receiver Cooperation," in *International Symposium on Information Theory (ISIT). Proceedings.*, pp. 397–401, IEEE, Sept 2005.

[56] H. Bolcskei, R. U. Nabar, O. Oyman, and A. J. Paulraj, "Capacity scaling laws in mimo relay networks," *IEEE Transactions on Wireless Communications*, vol. 5, no. 6, pp. 1433–1444, 2006.

[57] O. Souihli and T. Ohtsuki, "Cooperative Diversity can Mitigate Keyhole Effects in Wireless MIMO Systems," in *Global Telecommunications Conference (GLOBECOM)*, pp. 1–6, IEEE, 2009.

[58] P. Almers, F. Tufvesson, and A. F. Molisch, "Keyhole Effect in MIMO Wireless Channels: Measurements and Theory," *IEEE Transactions on Wireless Communications*, vol. 5, no. 12, pp. 3596–3604, 2006.

[59] S. Mengesha and H. Karl, "Relay Routing and Scheduling for Capacity Improvement in Cellular WLANs," in *WiOpt'03: Modeling and Optimization in Mobile, Ad Hoc and Wireless Networks*, pp. 1–7, 2003.

[60] S. Mengesha, H. Karl, and A. Wolisz, "Capacity Increase of Multi-hop Cellular WLANs Exploiting Data Rate Adaptation and Frequency Recycling," *Proceedings of MedHocNet 2004*, 2004.

[61] V. I. Morgenshtern and H. Bolcskei, "Crystallization in large wireless networks," *IEEE Transactions on Information Theory*, vol. 53, no. 10, pp. 3319–3349, 2007.

[62] L. Zheng and D. N. Tse, "Diversity and Multiplexing: A Fundamental Tradeoff in Multiple-antenna Channels," *IEEE Transactions on Information Theory*, vol. 49, no. 5, pp. 1073–1096, 2003.

[63] J. N. Laneman, G. W. Wornell, and D. N. Tse, "An Efficient Protocol for Realizing Cooperative Diversity in Wireless Networks," in *International Symposium on Information Theory (ISIT). Proceedings*, p. 294, IEEE, 2001.

[64] J. N. Laneman and G. W. Wornell, "Distributed Space-time-coded Protocols for Exploiting Cooperative Diversity in Wireless Networks," *IEEE Transactions on Information Theory*, vol. 49, no. 10, pp. 2415–2425, 2003.

[65] J. N. Laneman, D. N. Tse, and G. W. Wornell, "Cooperative Diversity in Wireless Networks: Efficient Protocols and Outage Behavior," *IEEE Transactions on Information theory*, vol. 50, no. 12, pp. 3062–3080, 2004.

[66] A. Bletsas, A. Khisti, D. P. Reed, and A. Lippman, "A Simple Cooperative Diversity Method Based on Network Path Selection," *IEEE*

journal on Selected Areas in Communications, vol. 24, no. 3, pp. 659–672, 2006.

[67] T. Q. Duong, H. A. Suraweera, T. A. Tsiftsis, H.-J. Zepernick, and A. Nallanathan, "Keyhole Effect in Dual-hop MIMO AF Relay Transmission with Space-time Block Codes," *IEEE Transactions on Communications*, vol. 60, no. 12, pp. 3683–3693, 2012.

[68] J. P. Coon, "A Theorem on the Asymptotic Outage Behavior of Fixed-gain Amplify-and-forward Relay Systems," *IEEE Communications Letters*, vol. 18, no. 9, pp. 1567–1570, 2014.

[69] Y. Zhao, R. Adve, and T. J. Lim, "Improving Amplify-and-forward Relay Networks: Optimal Power Allocation Versus Selection," in *International Symposium on Information Theory (ISIT). Proceedings.*, pp. 1234–1238, IEEE, 2006.

[70] Y. Zhao, R. Adve, and T. J. Lim, "Symbol Error Rate of Selection Amplify-and-forward Relay Systems," *IEEE Communications Letters*, vol. 10, no. 11, pp. 757–759, 2006.

[71] M. O. Hasna and M.-S. Alouini, "A Performance Study of Dual-hop Transmissions with Fixed gain Relays," in *International Conference on Acoustics, Speech, and Signal Processing. Proceedings.(ICASSP'03).*, vol. 4, pp. IV–189, IEEE, 2003.

[72] M. O. Hasna and M.-S. Alouini, "End-to-end Performance of Transmission Systems with Relays over Rayleigh-fading Channels," *IEEE Transactions on Wireless Communications*, vol. 2, no. 6, pp. 1126–1131, 2003.

[73] X. Wu and L.-L. Xie, "On the Optimal Compressions in the Compress-and-forward Relay Schemes," *IEEE Transactions on Information Theory*, vol. 59, no. 5, pp. 2613–2628, 2013.

[74] X. Bao and J. Li, "Efficient Message Relaying for Wireless User Cooperation: Decode-Amplify-Forward (DAF) and Hybrid DAF and Coded-Cooperation," *IEEE Transactions on Wireless Communications*, vol. 6, pp. 3975–3984, November 2007.

[75] Y. Li, B. Vucetic, Z. Chen, and J. Yuan, "An Improved Relay Selection Scheme with Hybrid Relaying Protocols," in *Global Telecommunications Conference (GLOBECOM '07)*, pp. 3704–3708, IEEE, Nov 2007.

[76] S. Zhang, S. C. Liew, and P. P. Lam, "Hot Topic: Physical-Layer Network Coding," in *Proceedings of the 12th annual international conference on Mobile computing and networking*, pp. 358–365, ACM, 2006.

[77] R. H. Louie, Y. Li, and B. Vucetic, "Practical Physical Layer Network Coding for Two-way Relay Channels: Performance Analysis and Comparison," *IEEE Transactions on Wireless Communications*, vol. 9, pp. 764–777, February 2010.

[78] S. Katti, S. Gollakota, and D. Katabi, "Embracing Wireless Interference: Analog Network Coding," in *SIGCOMM Computer Communication Review*, vol. 37, pp. 397–408, ACM, 2007.

[79] S. C. Liew, S. Zhang, and L. Lu, "Physical-layer Network Coding: Tutorial, Survey, and Beyond," *Physical Communication*, vol. 6, pp. 4–42, 2013.

[80] K. Ishibashi and H. Ochiai, "Performance Analysis of Amplify and Forward Cooperation over Peak-Power Limited Channels," in *International Conference on Communications (ICC)*, pp. 1–5, IEEE, June 2011.

[81] C. Alexandre and R. Fernandes, "Outage Performance of Cooperative Amplify-and-Forward OFDM Systems with Nonlinear Power Amplifiers," in *13th International Workshop on Signal Processing Advances in Wireless Communications (SPAWC)*, pp. 459–463, IEEE, 2012.

[82] T. Riihonen, S. Werner, F. Gregorio, R. Wichman, and J. Hamalainen, "BEP Analysis of OFDM Relay Links with Nonlinear Power Amplifiers," in *Wireless Communications and Networking Conference (WCNC)*, pp. 1–6, IEEE, 2010.

[83] V. del Razo, T. Riihonen, F. Gregorio, S. Werner, and R. Wichman, "Nonlinear Amplifier Distortion in Cooperative Amplify-and-Forward OFDM Systems," in *Wireless Communications and Networking Conference (WCNC)*, pp. 1–5, IEEE, 2009.

[84] C. Zhang, Q. Du, Y. Wang, and G. Wei, "Optimal Relay Power Allocation for Amplify-and-forward OFDM Relay Networks with Deliberate Clipping," in *Wireless Communications and Networking Conference (WCNC)*, pp. 381–386, IEEE, 2012.

[85] N. Maletić, M. Čabarkapa, and N. Nešković, "Performance of Fixed-gain Amplify-and-forward Nonlinear Relaying with Hardware Impairments," *International Journal of Communication Systems*, 2015.

[86] V. Erceg, D. Michelson, S. Ghassemzadeh, L. Greenstein, A. Rustako, P. Guerlain, M. Dennison, R. Roman, D. Barnickel, S. Wang, and R. Miller, "A Model for the Multipath Delay Profile of Fixed Wireless Channels," *IEEE Journal on Selected Areas in Communications*, vol. 17, pp. 399–410, Mar 1999.

[87] S. S. Ghassemzadeh, L. J. Greenstein, T. Sveinsson, A. Kavčić, and V. Tarokh, "UWB Delay Profile Models for Residential and Commercial Indoor Environments," *IEEE Transactions on Vehicular Technology*, vol. 54, no. 4, pp. 1235–1244, 2005.

[88] B. Zhou, H. Hu, and H. Wang, "Cyclic Prefix Update for OFDM Amplify-and-Forward Relay Systems," *Wireless Personal Communications: An International Journal*, vol. 72, no. 4, pp. 2281–2294, 2013.

[89] S. Wei, D. L. Goeckel, P. Kelly, *et al.*, "Convergence of the Complex Envelope of Bandlimited OFDM Signals," *IEEE Transactions on Information Theory*, vol. 56, no. 10, pp. 4893–4904, 2010.

[90] N. Moraitis, A. Kanatas, G. Pantos, and P. Constantinou, "Delay Spread Measurements and Characterization in a Special Propagation Environment for PCS Microcells," in *The 13th International Symposium on Personal, Indoor and Mobile Radio Communications (PIMRC).*, vol. 3, pp. 1190–1194 vol.3, IEEE, Sept 2002.

[91] J. Coon, D. Simmons, and M. Renzo, "Approximating the Outage Probability of Parallel Fading Channels," *IEEE Communications Letters*, vol. 19, pp. 2190–2193, Dec 2015.

[92] I. Krikidis, "Relay Selection for Two-Way Relay Channels With MABC DF: A Diversity Perspective," *IEEE Transactions on Vehicular Technology*, vol. 59, pp. 4620–4628, Nov 2010.

[93] J. Lagarias, "EulerâĂŹs Constant: EulerâĂŹs Work and Modern Developments," *Bulletin of the American Mathematical Society*, vol. 50, no. 4, pp. 527–628, 2013.

[94] N. Yang, M. Elkashlan, J. Yuan, and T. Shen, "On the SER of Fixed Gain Amplify-and-Forward Relaying with Beamforming in Nakagamim Fading," *IEEE Communications Letters*, vol. 14, pp. 942–944, October 2010.

[95] A. P. Prudnikov, I. A. Brychkov, and O. I. Marichev, *Integrals and Series: Special Functions*, vol. 2. CRC Press, 1986.

[96] T. Riihonen and R. Wichman, "Power Allocation for a Single-Frequency Fixed-Gain Relay Network," in *18th International Symposium on Personal, Indoor and Mobile Radio Communications (PIMRC)*, pp. 1–5, IEEE, Sept 2007.

[97] Ettus Research, "N200/N210 product overview." `https://www.ettus.com/content/files/07495_Ettus_N200-210_DS_Flyer_HR_1.pdf`.

[98] GNURadio, "GNURadio overview." `http://gnuradio.org/redmine/projects/gnuradio`.

[99] T. Schmidl and D. Cox, "Robust Frequency and Timing Synchronization for OFDM," *IEEE Transactions on Communications*, vol. 45, no. 12, pp. 1613–1621, 1997.

[100] J. Wagner and A. Wittneben, "On Capacity Scaling of (Long) MIMO Amplify-and-Forward Multihop Networks," in *42nd Asilomar Conference on Signals, Systems and Computers*, pp. 346–350, Oct 2008.

[101] J. Wagner and A. Wittneben, "On Capacity Scaling of Multi-Antenna Multi-Hop Networks: The Significance of the Relaying Strategy in the "Long Network Limit"," *IEEE Transactions on Information Theory*, vol. 58, pp. 2107–2133, April 2012.

[102] N. Fawaz, K. Zarifi, M. Debbah, and D. Gesbert, "Asymptotic Capacity and Optimal Precoding in MIMO Multi-Hop Relay Networks," *IEEE Transactions on Information Theory*, vol. 57, no. 4, pp. 2050–2069, 2011.

[103] M. A. Girnyk, M. Vehkaperä, and L. K. Rasmussen, "Asymptotic Performance Analysis of a K-Hop Amplify-and-Forward Relay MIMO Channel," *IEEE Transactions on Information Theory*, vol. 62, no. 6, pp. 3532–3546, 2016.

[104] R. Muller, "On the Asymptotic Eigenvalue Distribution of Concatenated Vector-Valued Fading Channels," *IEEE Transactions on Information Theory*, vol. 48, pp. 2086–2091, Jul 2002.

[105] S. p. Yeh and O. Leveque, "Asymptotic Capacity of Multi-Level Amplify-and-Forward Relay Networks," in *International Symposium on Information Theory (ISIT)*, pp. 1436–1440, IEEE, June 2007.

[106] D. Gunduz, M. Khojastepour, A. Goldsmith, and H. Poor, "Multi-hop MIMO Relay Networks: Diversity-Multiplexing Trade-Off Analysis," *IEEE Transactions on Wireless Communications*, vol. 9, pp. 1738–1747, May 2010.

[107] G. Farhadi and N. Beaulieu, "On the Ergodic Capacity of Multi-hop Wireless Relaying Systems," *IEEE Transactions on Wireless Communications*, vol. 8, pp. 2286–2291, May 2009.

[108] L.-L. Xie and P. R. Kumar, "An achievable rate for the multiple level relay channel," in *International Symposium on Information Theory (ISIT). Proceedings.*, p. 3, IEEE, 2004.

[109] G. Levin and S. Loyka, "Amplify-and-Forward Versus Decode-and-Forward Relaying: Which is Better?," in *International Zurich Seminar on Communications*, p. 123, 2012.

[110] M. Sikora, J. N. Laneman, M. Haenggi, D. J. Costello, and T. Fuja, "On the Optimum Number of Hops in Linear Wireless Networks," in *Information Theory Workshop (ITW)*, pp. 165–169, IEEE, 2004.

[111] E. L. Lawler, *Combinatorial optimization: networks and matroids*. Courier Corporation, 2001.

[112] T. Cover and A. E. Gamal, "Capacity Theorems for the Relay Channel," *IEEE Transactions on Information Theory*, vol. 25, no. 5, pp. 572–584, 1979.

[113] A. Khina, O. Ordentlich, U. Erez, Y. Kochman, and G. W. Wornell, "Decode-and-forward for the Gaussian Relay Channel via Stan-

dard AWGN Coding and Decoding," in *Information Theory Workshop (ITW).*, pp. 457–461, IEEE, 2012.

[114] S. Borade, L. Zheng, and R. Gallager, "Amplify-and-Forward in Wireless Relay Networks: Rate, Diversity, and Network Size," *IEEE Transactions on Information Theory*, vol. 53, pp. 3302–3318, Oct 2007.

[115] S. Yang and J.-C. Belfiore, "Diversity of MIMO Multihop Relay Channels," *arXiv preprint arXiv:0708.0386*, 2007.

[116] K. Sreeram, S. Birenjith, and P. Vijay Kumar, "DMT of Multi-hop Cooperative Networks-Part II: Layered and Multi-Antenna Networks," in *International Symposium on Information Theory (ISIT). Proceedings.*, pp. 2081–2085, IEEE, 2008.

[117] I. Maric, A. Goldsmith, and M. Medard, "Multihop Analog Network Coding via Amplify-and-Forward: The High SNR Regime," *IEEE Transactions on Information Theory*, vol. 58, pp. 793–803, Feb 2012.

[118] S. Jin, M. R. McKay, C. Zhong, and K.-K. Wong, "Ergodic Capacity Analysis of Amplify-and-forward MIMO Dual-hop Systems," *IEEE Transactions on Information Theory*, vol. 56, no. 5, pp. 2204–2224, 2010.

[119] Y. Q. Yin, "Limiting Spectral Distribution for a Class of Random Matrices," *Journal of multivariate analysis*, vol. 20, no. 1, pp. 50–68, 1986.

[120] J. W. Silverstein, "Strong Convergence of the Empirical Distribution of Eigenvalues of Large Dimensional Random Matrices," *Journal of Multivariate Analysis*, vol. 55, no. 2, pp. 331–339, 1995.

[121] V. A. Marčenko and L. A. Pastur, "Distribution of Eigenvalues for some Sets of Random Matrices," *Sbornik: Mathematics*, vol. 1, no. 4, pp. 457–483, 1967.

[122] A. Guionnet, "Large Random Matrices: Lectures on Macroscopic Asymptotics," 2008.

[123] R. Bhattacharya and M. Majumdar, *Random Dynamical Systems: Theory and Applications*. Cambridge University Press, 2007.

[124] H. Weinberger, "Long-Time Behavior of a Class of Biological Models," *SIAM journal on Mathematical Analysis*, vol. 13, no. 3, pp. 353–396, 1982.

[125] S. H. Strogatz, "Nonlinear Dynamics and Chaos: With Applications to Physics, Biology, Chemistry, and Engineering (Studies in Nonlinearity)," 2001.

[126] L. Yu, E. Ott, and Q. Chen, "Transition to Chaos for Random Dynamical Systems," *Physical review letters*, vol. 65, no. 24, p. 2935, 1990.

[127] M. S. Raghunathan, "A Proof of Oseledec's Multiplicative Ergodic Theorem," *Israel Journal of Mathematics*, vol. 32, no. 4, pp. 356–362, 1979.

[128] V. I. Oseledets, "A Multiplicative Ergodic Theorem. Characteristic Lyapunov, Exponents of Dynamical Systems," *Trudy Moskovskogo Matematicheskogo Obshchestva*, vol. 19, pp. 179–210, 1968.

[129] N. Levy, O. Zeitouni, and S. Shamai, "Central Limit Theorem and Large Deviations of the Fading Wyner Cellular Model via Product of Random Matrices Theory," *Problems of Information Transmission*, vol. 45, no. 1, pp. 5–22, 2009.

[130] N. Levy, O. Zeitouni, and S. Shamai, "On Information Rates of the Fading Wyner Cellular Model via the Thouless Formula for the Strip," *IEEE Transactions on Information Theory*, vol. 56, pp. 5495–5514, Nov 2010.

[131] A. Goldsmith, *Wireless Communications*. Cambridge University Press, 2005.

[132] R. H. Louie, Y. Li, H. Suraweera, and B. Vucetic, "Performance Analysis of Beamforming in Two Hop Amplify and Forward Relay Networks with Antenna Correlation," *IEEE Transactions on Wireless Communications*, vol. 8, pp. 3132–3141, June 2009.

[133] E. S. Key, "Lyapunov Exponents for Matrices with Invariant Subspaces," *The Annals of Probability*, pp. 1721–1728, 1988.

[134] A. Özgür, O. Lévêque, and D. N. Tse, "Hierarchical Cooperation Achieves Optimal Capacity Scaling in Ad hoc Networks," *IEEE Transactions on Information Theory*, vol. 53, no. 10, pp. 3549–3572, 2007.

[135] D. Simmons and J. Coon, "Strictly Positive and Continuous Random Fibonacci Sequences and Network Theory Applications," *arXiv preprint arXiv:1602.07225*, 2016.

[136] A. Jeffrey and D. Zwillinger, *Table of Integrals, Series, and Products*. Academic Press, 2007.

[137] T. Tao, *Topics in Random Matrix Theory*, vol. 132. American Mathematical Society, 2012.

[138] P. Forrester, "Lyapunov Exponents for Products of Complex Gaussian Random Matrices," *Journal of Statistical Physics*, vol. 151, no. 5, pp. 796–808, 2013.